NASA TN D-1566

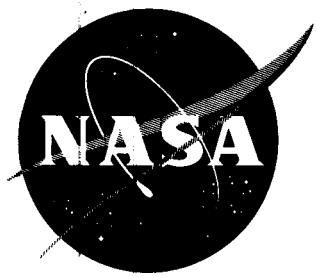

TECHNICAL NOTE

D-1566

BASE HEAT TRANSFER, PRESSURE RATIOS, AND CONFIGURATION EFFECTS OBTAINED ON A 1/27 SCALE SATURN (C-1) MODEL AT MACH NUMBERS FROM 0.1 TO 2.0

By John L. Allen and Robert A. Wasko

Lewis Research Center
Cleveland, Ohio

NATIONAL AERONAUTICS AND SPACE ADMINISTRATION
WASHINGTON

May 1963

NATIONAL AERONAUTICS AND SPACE ADMINISTRATION

TECHNICAL NOTE D-1566

BASE HEAT TRANSFER, PRESSURE RATIOS, AND CONFIGURATION EFFECTS OBTAINED ON A 1/27 SCALE SATURN (C-1) MODEL AT MACH NUMBERS FROM 0.1 TO 2.0

By John L. Allen and Robert A. Wasko

SUMMARY

Base heat transfer and pressures were measured over a range of stream Mach numbers from 0.1 to 2.0 on a 1/27 scale Saturn (C-1) booster stage having scale-model rocket engines that use liquid oxygen and JP-4 fuel as propellants.

The turbopump exhaust from the inboard engines was simulated by discharging hydrogen through stacks in the shroud or afterbody surface. This discharge resulted in very high heat-flux rates to the base plate (located at the plane of the nozzle throats) with stack heights less than about one-third of the height of the local boundary layer. Simulated turbopump exhaust (hydrogen) for the outboard engines discharged through exhausterators around the nozzle-exit perimeters severely increased base heat flux.

The use of cooling air scoops and external flow deflectors produced significant decreases in base heating. One configuration that had a recessed base and appreciable base bleed reduced the heat flux to values below 5 Btu per square foot per second for Mach numbers from 0.8 to 2.0 compared with values without base bleed varying from 80 at Mach 0.8 to 20 Btu per square foot per second at Mach 2.0 (all values for a wall temperature of 100° F).

Comparatively minor changes in base heat flux were found when the outboard engines were gimbaled or one outboard engine was inoperative. With an inboard engine inoperative, local increases in base heating occurred at some Mach numbers.

A flame shield or center star located at the plane of the nozzle exits and bounded by the inner perimeters of the inboard nozzles had a heat flux (at 100° F) that increased from a value of about 40 Btu per square foot per second at Mach 0.1 to between 300 and 400 Btu per square foot per second at Mach 2.0, the corresponding recovery temperature varying from about 1000° to 2800° R. The center-star pressure exceeded that of the base region by as much as 48 percent (depending on configuration) at Mach 2.0, which indicated appreciable backflow toward the center star from the mutual impingement of the inner jets.

INTRODUCTION

Rocket-missile base heating is primarily caused by (1) radiation from the exhaust, (2) recirculation of the hot exhaust gases into the base region, and (3) burning of combustibles that have been recirculated into the base from the rockets and/or turbopump exhausts. Various aspects of this problem are reported in references 1 to 5 for single as well as clustered nozzles. Because of the complex arrangements of multirocket assemblies, experimental heat-transfer results obtained on scale models having hot rocket flow can be of value to the missile designer. As discussed in detail in reference 6, however, such tests are necessarily limited by the following general qualifications:

(1) Base heating is influenced by a large number of factors, and it is not possible to simulate them all simultaneously with a small scale model.

(2) Several factors that influence base heating cannot be scaled properly (e.g., base-burning and radiant-heating effects).

(3) There are instrumentation difficulties in obtaining heating rates because of variations in flow angularity and nonisothermal wall effects (ref. 7).

In spite of these limitations accurate base pressure data can be obtained in addition to quantitative heating data of a relative nature showing effects of configuration variables.

Accordingly, a 1/27 scale model of the base of the complex eight-rocket Saturn booster was investigated over a range of Mach numbers up to 2.0. Relatively high efficiency, scale rocket engines that burn liquid oxygen and JP-4 fuel were used. Various configurations of the afterbody shroud were investigated; included were two having base-bleed as cooling and two different arrangements of aerodynamic stabilizing surfaces. In order to evaluate five turbine-exhaust-stack configurations, hydrogen was used to simulate the turbopump exhaust gases from the inboard engines while exhausterators were used on the outboard rockets. The effects of both an inoperative engine and gimbal angle of the outboard engines were determined.

SYMBOLS

C^* characteristic velocity, ft/sec

D diameter

h coefficient of heat transfer

L^* characteristic chamber length, in.

l length

M Mach number

O/F oxidant-fuel weight ratio, oxygen/JP-4

P total pressure

p static pressure

$\dot{Q}$ heat flux, Btu/(sq ft)(sec)

Re Reynolds number

T temperature

δ boundary-layer height

η efficiency

Subscripts:

b base

c combustion chamber

cs center star

e nozzle exit

R recovery

r radiation

th theoretical

w disk (wall)

0 free stream

Superscript:

$\bar{}$ average

MODEL, ENGINE, AND INSTRUMENTATION DETAILS

General Description of Model

A drawing of the essential features of the model test installation is shown in figure 1(a). During some of the exploratory testing, the entire C-1 booster stage including the scalloped propellant tank region was simulated. However, for all the data presented with the exceptions of the boundary-layer survey data, only the rear $7\frac{1}{2}$ inches or 0.8 diameter were representative of the Saturn (C-1)

afterbody, whereas the conical-tipped, cylindrical forebody was simply the minimum envelope for the required structure, plumbing, and instrumentation. The thin, short-cord strut was located as far forward as practical in order to reduce disturbances in the base region. The simulated part of the Saturn (C-1) afterbody is shown in greater detail in figure 1(b). The centers of the four inboard engines were spaced 0.416 nozzle-exit diameter (where D_e = 1.70 in.) from the center of the base and were axially alined because of internal space limits rather than radially canted outward 3° as in the C-1 prototype. The outboard engines were canted radially outward 6° and were 2.25 exit diameters from the base center for the normal gimbal position. The shroud surrounding the engine assembly was fabricated from 1/8-inch steel and consisted of two general regions: (1) the flared part with skirts that extended over a portion of each outboard or control engine (trailing edge of skirt is at station 0.8) in order to reduce air loads on the nozzle and permit gimbaling and (2) a boattail region that ends at the plane of the nozzle throats, station 2.08, which forms a notch or cutout over each inboard engine. The resultant shape of the heat shield or base plate at the plane of the nozzle throats resembled a four-leaf clover. A flame shield, referred to as the center star, was located at station 0.09 between the inner perimeters of the inboard engines. The joints between shroud and heat shield and center star and nozzle walls were carefully sealed with a steel-filled epoxy polymer so that inadvertent base bleed could not occur.

Engines, Starting Procedure, and Simulated Turbopump Exhaust Systems

Propellants for the water-cooled, scale rocket engines were liquid oxygen and JP-4 fuel in a nominal mixture ratio O/F of 2.4. At a chamber pressure P_c of 650 pounds per square inch absolute, the engine produced a thrust of about 270 pounds and a specific impulse of 265 seconds. The chamber pressure was measured at the face of the injector and was not corrected for heat-addition effects (probably less than 5 percent). Fabrication and design details of the rockets are given in reference 8. Two slightly different rockets were used during the test program and are referred to as the Mark I and the Mark II (improved version of Mark I). The bell-shaped nozzle contour and exit angle for the Mark II design (coordinates given in fig. 1(c)) were in good agreement with those for the full-scale H-1 rocket since the chamber and nozzle were fully machined, whereas the dimensions of the Mark I were not as precise since a casting was used. Detailed differences are listed in the following table:

	Mark I	Mark II
Nozzle area ratio	7.8	8
Nozzle-exit diameter, D_e, in.	1.69	1.70
Throat diameter, in.	0.605	0.602
Characteristic chamber length, L*, in.	14	18
Characteristic velocity[a], C*	5200 to 5400	5300 to 5500
Combustion efficiency, $\eta = (C^*/C^*_{th})^2$	0.81 to 0.874	0.842 to 0.906

[a]At chamber pressure of 650 lb/sq in. and mixture ratio of 2.4 ft/sec.

Nozzle-exit static pressure, which was measured on a test stand with a zero-secondary-flow ejector attached in order to assure full flow, was established as 0.027 P_c. Both the nozzle-exit pressure and the internal pressure distribution were in good agreement with those for a 150,000-pound-thrust rocket with the same nozzle shape.

Since the eight engines were manifolded to common propellant systems, all engines were started simultaneously by injecting TEA (triethylaluminum, a hypergolic compound) into each chamber with a small oxygen flow to build a pilot flame that was subsequently enriched by JP-4 fuel. Oxygen and fuel flows were then increased to give a chamber pressure of about 80 pounds per square inch absolute. Then, if all the engines were burning, the chamber pressures and mixture ratios were increased to and automatically controlled at the desired values. The starting sequence lasted about 17 seconds and included 5 seconds of operation at rated conditions prior to data recording. Data recording consumed about 15 seconds. The long starting cycle was necessary because of the fragile nature of the soldered, wire wrapping that formed the engine water coolant chamber.

For a large majority of the data presented, the rocket operating conditions were as follows:

Average chamber pressure, $\bar{P}_c$, lb/sq in.	650±10
Mixture ratio O/F	2.4±0.1
Maximum deviation in chamber pressure among the eight rockets, lb/sq in.	±20

After all engines were carefully static tested, those with relatively high efficiency and the necessary injector flow characteristics were selected for installation in the model. However, because the propellant supplies of all eight engines were manifolded, the individual engine performance in the model could not be evaluated. Therefore, a periodic program of flow checking and ultrasonic cleaning of the injectors was maintained.

Turbopump exhaust gas was simulated by discharging hydrogen through ejectors (called exhausterators) around the exit of each outboard engine (fig. 1(c)) and through stacks (referred to as turbine-exhaust stacks) protruding through the shroud for each inboard engine. The variety of turbine-exhaust-stack configurations investigated are illustrated in figure 1(d). The hydrogen weight flow was selected to be the scale equivalent of the stoichiometric heat content of the unburned turbopump fuel. Data were obtained at half-rated flow rates also. The exit momentum per unit area of the turbine-exhaust stacks was approximately equal to that for the prototype Saturn at full-rated flows but decreased with weight flow since the exit area was not changed.

Because of the transport and mixing phenomena involved as the discharged turbopump gases encounter the external flow field and rocket jets, the use of the exact gas species at the proper temperature is highly desirable but was not possible on the small, complex Saturn model. Even though the molecular weight of hydrogen is much less than that for the real turbopump gas, it was selected

because of its wide ignition and flammability limits. The reason for this selection is the inherent difference between an actual rocket, which flies at varying flight conditions from launch to burnout, and a rocket fired in a wind tunnel, at essentially steady flight conditions. For example, in the actual launching the turbopump exhaust may recirculate into the base, ignite at launch, and continue to burn throughout the flight path until some quenching or flameout condition is encountered. The alternative of firing the rockets at wind-tunnel conditions, such as a free-stream Mach number M_0 of 2.0 at a 35,000-foot altitude, may not provide the necessary ignition source for a gas with narrow flammability limits, although combustion may be possible. In addition, the problem of duplicating the scaled heat released in the base depends on successfully duplicating the complex base-entrainment mechanism.

Configurations

The configurations investigated and the figures in which they are pictured are as follows:

(1) Basic Saturn without base cooling, but with 3/8-inch turbine-exhaust stacks (fig. 2(a))

(2) Basic Saturn with four cooling air scoops per shroud, valley flow deflectors, and 3/8-inch turbine exhaust stacks (fig. 2(b))

(3) Basic Saturn with three cooling air scoops per shroud, valley flow deflectors, and curved turbine-exhaust pipes (SA-1) (fig. 3)

(4) Basic Saturn with three cooling air scoops per shroud, valley flow deflectors, and streamlined turbine-exhaust stacks (fig. 4(a))

(5) Basic Saturn without base cooling or outboard engine shrouds, but with 3/8-inch turbine-exhaust stacks (flush base) (fig. 4(b))

(6) Recessed-base configuration with shroud and valley cooling air scoops and 5/8-inch turbine-exhaust stacks (fig. 5)

(7) Circular-base configuration with four-fin, four-stub stabilizer arrangement, streamlined turbine-exhaust stacks, and streamlined upper-stage hydrogen vents on stubs (fig. 6(a))

(8) Circular-base configuration with eight-stub stabilizer arrangement, streamlined turbine-exhaust stacks, and streamlined upper-stage hydrogen vents on stubs (fig. 6(b))

Details of the various cooling-air bleed scoops are shown in figure 7.

Heat-Transfer Instrumentation

Twelve total calorimeters and one radiation calorimeter were located in the base plate (heat shield), station 2.08; the general locations and designations are shown in figure 8(a). The actual locations varied somewhat because of installation problems and configuration changes (see figs. 2(a), 3(a), and 6(b)). Results from calorimeters from approximately symmetric regions A1 to A4, B1 to B4, or C1 to C4 were averaged because of small differences in rocket-engine performance, in location relative to cooling scoops, and other minor asymmetries. Total calorimeters were also located in the center-star flame shield and for some configurations on the side of the exhausterator of one of the outboard engines that faced into the center-star point (i.e., at position X).

Construction details of the base and center-star calorimeters are shown in figure 8(b). All calorimeters, with the exception of the one in the center star, were 1/10-inch-thick copper with a blackened surface. The copper disk was suspended within a sealed stainless-steel cup by twin pairs of Chromel-Alumel thermocouple wires (26 gage) in order to reduce conduction losses. A nitrogen purge cooling annulus kept the disk from becoming saturated with heat during the rocket starting cycle. When the calorimeter was calibrated by means of a radiant heat source and using a master control calorimeter for comparison, the resultant heat loss was less than 5 percent for a heat flux of 20 Btu per square foot per second and a temperature difference of 400° F between the disk and the case. The radiation calorimeter was nearly identical to the base calorimeters but had a sapphire window with a view angle of 120°, a calibrated efficiency of 52 percent compared with the base calorimeter, and an annular nitrogen purge directed across the window to keep it as clean as possible during the starting and shutdown cycles.

Data Recording and Reduction Technique

The voltages generated by the thermocouple junctions in the calorimeter disks were amplified, recorded on a 14-channel FM tape recorder, and at a later time played back through an appropriate analog circuit and a calibrated x-y plotter (fig. 8(c)). Thus, a continuous trace of heat flux $\dot{Q}$ as a function of disk temperature was obtained. A typical plot is shown in figure 9. The slope of the curve of heat flux as a function of temperature $d\dot{Q}/dT_w$ is equal to the heat-transfer coefficient h, and the intercept at $\dot{Q} = 0$ is the approximate recovery temperature T_R. As shown in figure 9, peak heat fluxes for the three calorimeters occurred at disk temperatures from 140° to 240° F; furthermore, disk A has a heat flux of nearly zero when disk C is at peak heat flux. For disk C in particular the RC time constant of the analog circuit has caused a roll-off in the peak response. Therefore, the slopes were extrapolated to an arbitrary disk temperature of 100° F so that a uniform comparison could be obtained. As such, the results presented represent the response of the model (mass) to the applied heat load if the wall temperature had been 100° F.

As a backup system the output from the second thermocouple junction in each disk was connected to an automatic digital recording system and read at intervals

of 1.23 seconds. The FM-analog system was vastly superior to the digital technique, since a continuous trace was obtained that was capable of displaying changes in heat transfer during the firing, such as base burning.

The film or heat-transfer coefficients $d\dot{Q}/dT_w$ are essentially equal to the convective coefficients. Figure 9 shows that, if the total heat flux were reduced by the magnitude of the radiation heat flux $\dot{Q}_r$, the slope $d\dot{Q}/dT_w = h$ would be unchanged except for the very small effect of the change in reradiation over the range of disk temperatures. If this correction is made, the recovery temperature for convection only would be reduced.

During the purge-off heating cycle of the disks, the temperature rise of the disks intercepted that of the base plate. Thus, at this instant the heat capacity of the disk does not alter the convective flow, and a heat flux representative of isothermal conditions (for the model) is recorded (ref. 7). On the other hand, the quenching effect of the model structure on the recirculating gas prior to contacting the heat-transfer disk cannot be controlled, except by operating the base plate and external surfaces of the engines at flight conditions that are generally not practical for wind-tunnel models.

A limited amount of data was obtained with two heating cycles of the disks (by purging the calorimeters during the firing) that resulted in two heat values at two different points where disk and base plate temperatures were equal. The heat-transfer coefficients were in good agreement. In fact, the variation of heat flux with disk temperature was generally linear (except when sporadic base burning occurred); hence, the heat-transfer coefficient appeared independent of disk or wall temperature within the ranges covered herein.

Operating Procedure

In a continuous-flow wind tunnel the model and instrumentation must withstand repeated firings without damage or contamination effects. The major problems occurred during the required slow-starting cycle. Fundamentally, the rocket jet pressures during start were not high enough to overcome the recirculation of external air. Hence, significant amounts of rocket flow were entrained in the base region, as is the case in the flow field behind a blunt-base body without jet flow or in some base bleed situations (ref. 9). Consequently, very hot gases and particles of carbon and aluminum oxide from the combustion of TEA formed deposits on the calorimeter surfaces. The following measures were taken in order to reduce these effects during the starting and shutdown cycles:

(1) The rocket mixture ratios were carefully controlled in order to reduce carbon formation.

(2) A nitrogen purge delayed the response of the calorimeters until the proper operating conditions had been established and kept the disks relatively free from deposits or coatings, except for the center-star calorimeter at some conditions (see RESULTS AND DISCUSSION).

(3) A very strong nitrogen purge directed across the base plate from four symmetrical locations near the valley regions provided an inert atmosphere and cooled the base instrumentation. This effect was supplemented by nitrogen flow through the turbine-exhaust and exhausterator systems prior to the change to hydrogen for the rated operating conditions.

Comparison of Prototype and Tunnel-Model Operating Conditions

A comparison of the schedule of altitude and nozzle-exit pressure ratio with free-stream Mach number for the prototype Saturn (SA-1) (P_c = 565 lb/sq in.) and the tunnel model is shown in figure 10. The effect of the difference in Reynolds number between the prototype and the model is also shown in figure 10 in terms of the ratio of boundary-layer thickness at the base of the prototype to that of the model by using a flat-plate turbulent analysis. The ratio varies from about 15 to 17 between Mach numbers of 0.8 and 2.0 compared with the linear scale factor of 26.8. Since the linear scale factor was used for the 3/8-inch, curved, and streamlined turbine-exhaust stacks and for the SA-1 cooling scoop heights, the heat-transfer results presented are probably more severe than for the full-scale booster because the stacks discharge into and the cooling scoops capture a lower energy portion of the boundary layer.

Measurements of the model boundary-layer profiles for the turbine-exhaust stack and cooling scoop locations are shown in figure 11 in terms of indicated local-pitot- to free-stream-total-pressure ratio for Mach numbers of 2.0 and 0.8. These results were obtained on an earlier version of the model that included the scalloped-propellant-tank arrangement rather than the cylindrical shape shown in figure 1.

The profiles indicate supersonic boundary-layer heights of about 1.3 and 0.8 inch for the turbine-exhaust and scoop locations, respectively. Flow disturbances and a varying Mach number field associated with the complex shape of the afterbody also are evident.

RESULTS AND DISCUSSION

Thermal Boundary Layer of the Base

In order to provide some insight into the amount of rocket exhaust recirculated into the base and the quenching effect of the model, temperature was measured at the general positions A, B, and C perpendicular to the base at 5/32-inch intervals out to a distance of 5/8 inch by using bayonet-type thermocouple rakes. Results are presented in figure 12 in terms of the temperature-difference ratio $(T_b - T_0)/T_c - T_0)$, which can be interpreted as the mole fraction of combustion-chamber gases. At positions A and B, maximum values of $(T_b - T_0)/(T_c - T_0)$ generally occurred at heights greater than 5/16 inch or a distance ratio of 0.5. At position C, the values were relatively constant for distance ratios greater than 0.25.

Corresponding temperature-difference ratios obtained for the center star 1/2 inch from the center and about 1/4 inch from the surface by using a platinum - platinum-13-percent-rhodium thermocouple were near 0.5 at supersonic speeds, as shown in the following table:

Free-stream Mach number, M_0	$\frac{T_{cs} - T_0}{T_c - T_0}$
2.0	0.55
1.6	0.45 to 0.49

Heat Transfer and Pressure Ratios

Heat flux $\dot{Q}$ has been selected as the basis of comparison for the various configurations and effects of model variables (such as turbine-exhaust or exhausterator flow), although heat-transfer coefficients or recovery temperatures also could have been used. Therefore, the average base heat fluxes for positions A, B, and C and pertinent base pressure ratios are compared in figures 13 to 21 for the configurations and effects investigated. A limited amount of data for the center-star region is presented in figure 22. In figures 23 to 40, the maximum, average, and minimum values of heat flux, heat-transfer or film coefficient, and the approximate recovery temperature are plotted for each of the general locations A, B, and C as functions of free-stream Mach number for each configuration.

Performance of Basic Saturn and General Observations

The variation of the average heat flux for positions A, B, and C with free-stream Mach number is shown in figure 13(a) for the so-called basic Saturn configurations with and without cooling scoops. The peak heat flux occurred at Mach 0.8 and was about twice the values at Mach numbers of 1.6 and 2.0. Position B had the highest heat flux; position A had the lowest. These trends, which are typical of all configurations, except the flush base and recessed base, can only be explained in general terms, since most of the flow phenomena are of a circulating, unsteady type. Position B is sheltered from direct influence of external flow and is exposed to a recirculation of jet flow caused by the interaction of the inboard and outboard jets. Position C is primarily influenced by the interaction of the external stream from the valley (boattail) region with the inboard jet. The base region around the outboard engines (A) is strongly affected by external flow, probably because of a pumping action established by the overhanging shroud (vortex formed between the shroud and valley flows). The flow of external (stream) air into the base generally has a cooling effect, but under the proper conditions can furnish the oxygen necessary for combustion of unburned fuel that has been recirculated into the base. Most of the "base burning" that was observed (photographically) occurred in the B and C regions as sporadic flashes of short duration traveling toward the base plate.

Effect of Adding Cooling Scoops

The addition of cooling scoops (four semicircular cups in the shroud over each outboard engine plus venetian-blind-type flow deflectors in the valley region centered over the inboard engine) reduced the base heat flux at positions B and C, but were not effective at A (on the average) at Mach 0.8 (fig. 13(a)).

Effect of Turbine-Exhaust Flow on Basic Saturn Without Cooling Scoops

The effect of full- and half-rated flow (hydrogen) through the 3/8-inch-high turbine-exhaust stacks is presented in figure 13(b) for the basic Saturn without cooling scoops. The average base heat flux was increased by half-rated turbine-exhaust flow (approx. 0.003 lb/sec per stack), particularly at position B. Full-rated flow (approx. 0.0055 lb/sec per stack) caused additional heat-flux increases only at Mach 0.8 at positions B and C. Hydrogen discharged into this low-energy portion of the boundary layer by the turbine exhaust was entrained in the base region and burned. This effect is shown in greater detail in the following section.

Comparison of Turbine-Exhaust Configurations and Effect of Exhausterator Flow

The effect of discharging the turbine-exhaust flow at heights of 1/16 and 3/8 inch (above the shroud) for the configuration with four scoops per shroud and external flow deflectors is presented in figure 14 and compared with the no-flow heat fluxes. Appreciable increases are shown for the nearly flush, 1/16-inch, discharge height at all positions and Mach numbers. For the 3/8-inch height the major effect, which occurred at Mach 0.8 for positions B and C, was only about half as severe as for the nearly flush discharge.

In order to prevent the exhausterator lips from burning off while data were obtained without exhausterator flow for all the preceding configurations, special exhausterators having the same cylindrical shape around the nozzle and lips flush with the nozzle exit were installed. Consequently, the base flow patterns were not altered, and nitrogen could be used in the exhausterator during the starting cycle. Once the overhanging exhausterators were installed for the following configurations, however, data could only be obtained with exhausterator or exhausterator-plus-turbine-exhaust flows. Therefore, the performance obtained with the SA-1 (curved) and streamlined turbine exhausts (fig. 11(b)) cannot be compared directly with that for the 1/16- and 3/8-inch turbine exhausts. Also, only three scoops per shroud could be used on the curved and streamlined turbine-exhaust configurations because of the revised location on the shroud.

For both the SA-1 and streamlined turbine-exhaust configurations half-rated exhausterator flow significantly increased the average base heat flux at positions B and C except at a Mach number of 0.1, where configuration effects were generally small. Full-rated exhausterator flow resulted in additional increases, particularly at position B for SA-1. Adding either half- or full-rated turbine-

exhaust flow to the corresponding exhausterator flow condition resulted in negligible or small increases in the average base heat flux. Either there was no excess air in the base for combustion of the turbine-exhaust flows, or, more likely, the turbine-exhaust flows were discharged high enough in the external stream to prevent any appreciable entrainment in the base region. The streamlined exhaust stack was nearly three times the height of the 3/8-inch stack, and the curved SA-1 stack discharged behind the trailing edge of the shroud at a height of 5/8 inch directed outward 45°.

Comparison of Various Base Configurations

A comparison of the following configurations is shown in figure 15(a): recessed base with bleed, shroud flush with base, SA-1, and basic Saturn without cooling. The uncooled flush base (with half-rated turbine-exhaust and exhausterator flows) had appreciably higher heat fluxes at base positions A and C compared with the basic Saturn (half-rated turbine exhaust only) or SA-1 (full-rated turbine-exhaust and exhausterator flows, with cooling scoops). Some reduction in heat fluxes for the flush base was noted for exhausterator flow alone (fig. 36). Apparently removal of the shrouds overhanging the outboard engines decreased the pumping effect previously described, increased the base pressure (fig. 17), and increased the base entrainment of turbopump exhaust gases.

The recessed base had an average base heat flux at all positions of less than 5 Btu per square foot per second, even at a Mach number of 0.8. This configuration also had the shroud over the outboard engines cut back to the plane of the nozzle throats (station 2.08); however, the very large cooling scoops, which were located in regions of high pressure rise on the shroud, significantly increased the base pressure ratio (fig. 17) to values above 0.93 within the range tested. Some part of the reduction in heat fluxes may be associated with increased quenching because of the greater amount of cool model metal exposed by recessing the base plate to station 5.08 (compared with station 2.08 for all other configurations). Compared with the SA-1 scoops, a larger amount of bleed air is provided at higher pressures, and better mixing and distribution is attained within the engine compartment so that all areas of the base are more uniformly cooled. Also, the higher pressures reduce the recirculation of rocket gases (refs. 5 and 9). At higher flight Mach numbers aerodynamic heating of the bleed air may require protection of critical hardware located in the engine compartment provided that the pressure level in the engine compartment is high enough to cause appreciable heat transfer.

Radiation Heat Flux

A comparison of radiation heat flux $\dot{Q}_r$ measured at position C, is presented in figure 15(b) for several configurations. These measurements are for a disk temperature of about 200° F and could not be extrapolated, accurately, to the 100° F disk temperature previously used for the total calorimeters. For most configurations the general level of radiation heat flux varied from a maximum of about 7 Btu per square foot per second at Mach 0.8 to 3 at other Mach numbers. The radiation level for the flush-base configuration was approximately doubled with combined turbine and exhausterator flow; furthermore, this configuration had

the greatest amount of base burning (as confirmed photographically).

The general trend of the radiation-heat-flux curve depends on the interacting effects of the increasing view or form factor of a particular base area and the decreasing jet static temperature and hence on radiation from carbon molecules, as the expansion of the jets increases with altitude. Additional factors are afterburning in the jets and burning of the turbopump exhausts.

Circular Base with Stabilizing Surfaces

Tests were also made of some Saturn configurations with aerodynamic stabilizing surfaces intended to reduce the gimbal requirements of the outboard control engines. A cylindrical shroud was used to carry the loads from these surfaces and, hence, the base heat shield was also circular. The shroud or flair over each outboard engine was also revised (shroud angle changed from 8° to 30°). One configuration had four large fins with a height above the shroud surface of 6.8 inches and four stub fins with a height of $1\frac{1}{2}$ inches (see fig. 6). The other configurations had eight $1\frac{1}{2}$-inch stub fins. Neither configuration had base bleed or cooling. Both configurations had 1-inch streamlined stacks (vent) located on the top of each stub fin, which were used to simulate the boiloff and chill cycle of upper-stage engines. Hydrogen was discharged through the vents at the rate of 0.001 and 0.002 pound per second per vent for the boiloff simulation and the chill cycle, respectively.

As shown in figure 16, both circular-base configurations without cooling scoops had substantially higher heat fluxes than the SA-1 configuration at subsonic Mach numbers, particularly at $M_0 = 0.8$; however, there was little difference at Mach numbers of 1.6 and 2.0. The only significant difference between the two circular-base configurations was the lower heat flux at Mach 0.8 at position C for the eight-stub version. Discharging hydrogen through the vents had no significant effect on base heating.

Summary of Base Pressure Ratios

The average base pressure ratio comparison presented in figure 17 shows that the minimum value in each case occurred at a Mach number of 1.6. The recessed-base configuration had the highest base pressure ratio and experienced a slight ram effect ($p_b > p_0$) at Mach number 2.0. The lowest pressure ratios were found for the circular-base configurations, probably because the boattail region was made cylindrical and the flair angle of the shield over the outboard engines was increased from 8° to 30°. For the basic Saturn configurations the average base pressure did not vary at subsonic Mach numbers, but was increased at supersonic Mach numbers by bleed and removal of the shield over the outboard engines.

Base pressure distributions are presented for several operating variations of the SA-1 configuration and for the recessed- and circular-base configurations in figure 18. Some insight into the base flow patterns can be gained by inspect-

ing these plots; however, the exact location of the pressure tube orifices varies because of installation problems and for SA-1 may be very close to a cooling scoop and may result in $p_b/p_0 > 1.0$ for some locations.

Heat Fluxes on Side of Exhausterator

The total calorimeter at station 0.09 mounted on the side of the exhausterator that faced the point of the center star could not be mounted flush with the exhausterator surface. Consequently, the calorimeter housing or cup was supported by the instrumentation lines only and may have acted as a flameholder. In fact, it was frequently destroyed by the starting heat input because the effectiveness of the base purge did not extend that far from the base plate. At supersonic Mach numbers the results obtained (fig. 19) were generally of the same level as those for base positions A, B, and C. No pronounced increase in heat flux with Mach number was noted as might be expected due to increased outflow of hot center-star gas. At Mach 0.8 the streamlined turbine-exhaust configuration had appreciably higher heat fluxes for both half- and full-flow rates. Data at Mach 0.8 for other configurations with turbine-exhaust and exhausterator flow were not obtained.

Effect of Inoperative and Gimbaling Engines

Heat fluxes for each of the 12 calorimeter locations with an outboard or inboard engine inoperative are compared with the eight engine averages in figure 20 for the SA-1 and circular-base configurations. With the outboard engine in quadrant 3 inoperative, the most pronounced increase in base heat flux occurred in quadrant 2 at positions B and C for supersonic Mach numbers. The quadrant containing the inoperative engine had the lowest heat flux except for position A. In general, the effects of an inoperative outboard engine were not severe.

With an inoperative inboard engine (located between quadrants 1 and 4), the variations in heat flux were more significant and for SA-1 occurred primarily in quadrants 1 and 3 for position A and in quadrants 2 and 3 for position B at a Mach number of 0.8; at $M_0 = 1.6$ and 2.0, quadrants 2 and 4 were primarily affected. The quadrants affected were not necessarily adjacent to the inoperative engine. The recessed-base configuration with inboard engine 4 inoperative showed no effective change in base heat flux at the only Mach number tested, 0.8. For the circular-base configuration a marked reduction in heat flux occurred with inboard engine 4 inoperative at Mach 0.8 for all quadrants except the fourth. At supersonic Mach numbers quadrant 1 generally had higher heat fluxes than the eight engine averages, as did position C in quadrant 4.

Two variations from the nominal gimbal position of the outboard engines were investigated, and the results are presented in figure 21. The first variation was a simple pitch correction with all outboard engines gimbaled downward 5° relative to the nominal 6° radial angle (see middle sketch in fig. 21). The second variation represents the necessary gimbal angles if engine 8 were inoperative during maximum dynamic pressure and wind shear. For these cases the effects on base heat flux were again rather random. For the pitch correction, quadrant 3 at

positions A and C showed the most effect. The only significant effect for the inoperative engine gimbal occurs at position A, quadrant 1, for a Mach number of 1.6.

Center-Star Heat Transfer and Pressure Ratios

Great difficulty was experienced in measuring center-star heat transfer because coatings of some form of aluminum oxide (from the TEA ignitor fluid) and carbon collected on the calorimeter surface during the starting cycle. This coating problem was prevalent at supersonic Mach numbers and particularly at a Mach number of 2.0, probably because of the lower base pressures and because the coating thickness becomes more effective at higher applied heat fluxes. The most consistent data were obtained by cycling the center-star purge several times during a firing. This procedure seemed to burn off the coating during the first heating cycle since higher heat fluxes were measured on succeeding heating cycles. An example of this effect is shown in figure 22(a); however, in this case the rockets were fired without the center-star purge on during the starting cycle, and two cycles of low heat transfer were obtained before the disk surface became clean. Perhaps the purge-on temperature of the first cycle was not high enough to allow the coating to dislodge or melt. Duplicate thermocouples were installed in the center-star calorimeter and the results were averaged. An analogous result is reported in reference 10 wherein aluminum oxide deposits on the nozzle wall (from a solid propellant rocket) caused a temperature difference between the gas side and the nozzle surface of the order of 1000° to 2000° F.

As flight Mach number increased, the center-star pressure eventually exceeded that of the outer base (fig. 22(b)); this indicates appreciable backflow from the impingement of the inner jets toward the center star, between the jet boundaries upstream of the impingement point, and into the outer-base region. The center-star to outer-base pressure ratios increased to values no greater than 1.5 at a Mach number of 2.0. This value is considerably below the choking pressure ratio that would have been attained if the center-star pressure had increased or outer-base pressure had decreased enough for the outflow areas to become choked. If the choking condition had been reached, the pressure ratio and heat transfer would have remained constant. With an inboard engine inoperative, the center-star pressure was essentially equal to that of the outer base region over the Mach number range tested because the outflow area was greatly enlarged and the number of jet impingements reduced.

The center-star heat flux increased rapidly with flight Mach number generally in accordance with the pressure-ratio trends from a value of about 40 Btu per square foot per second at a Mach number of 0.1 and a recovery temperature of about 1000° R to a value between 300 and 400 Btu per square foot per second at a Mach number of 2.0 and a recovery temperature between 2500° and 2800° R (fig. 22(c)). With an inboard engine inoperative the heat flux at supersonic Mach numbers was reduced to values of about 50 Btu per square foot per second. At Mach 0.8 the heat flux was highest for the circular-base configurations.

CONCLUDING REMARKS

The general randomness of the heat-transfer data is displayed in figures 23 to 40, where the maximum and minimum values are shown as well as the average. This scatter is related to (1) base burning, which was generally present but occurred in sporadic flashes, (2) differences in efficiency among the eight engines, (3) alinement and aerodynamic asymmetries, and (4) compromises associated with the small size of the model, which was restricted by the tunnel thermal choking limit. When a low-efficiency engine ($C^* < 5200$) was shifted to a new location, the hot-spot on the base shifted with the engine. This is attributed to the unburned fuel recirculating into the base region and then burning. However, extremely fuel-rich operation of all eight engines ($O/F < 2.0$) generally quenched whatever base burning was present and reduced temperatures appreciably.

SUMMARY OF RESULTS

Base heat-transfer and pressure were measured on a 1/27 scale Saturn booster stage using hot, scale-model rockets over a range of stream Mach numbers from 0.1 to 2.0. Various configurations of the afterbody shroud were investigated including two with base bleed or cooling and two different arrangements of aerodynamic stabilizing surfaces. Five turbine-exhaust stack configurations were evaluated by using hydrogen to simulate the turbopump-exhaust gases from the inboard engines while exhausterators were used on the outboard rockets. The effects of an inoperative inboard or outboard engine as well as two gimbal angles of the outboard engine were determined. The following results were obtained:

1. For nearly all configurations the base heat flux peaked sharply at a Mach number of 0.8.

2. Simulated turbopump gases (hydrogen) were entrained in the base and caused severe increases in base heat flux from either exhausterator flow (outboard engines) or turbine-exhaust stacks (inboard engines) that were shorter than one-third of the height of the local shroud boundary layer.

3. The use of cooling air scoops and flow deflectors produced significant decreases in base heating. One configuration that had a recessed base and appreciable base bleed reduced the base heat flux to values less than 5 Btu per square foot per second (at a wall temperature of 100° F) for Mach numbers ranging from 0.8 to 2.0 as compared with values varying from 80 to 20 Btu per square foot per second without base bleed.

4. Removing the shield or shroud "ears" from over the outboard engines so that the shroud was flush with the base plate at the plane of the nozzle throats resulted in very high heat-flux rates except for the base area between the inner and outer engines.

5. Only minor changes in base heat flux were found when the outboard engines were gimbaled or one outboard engine was inoperative. With an inboard engine inoperative, local increases in base heating occurred at some Mach numbers.

6. The center-star heat flux (at a wall temperature of 100° F) increased from a value of about 40 Btu per square foot per second at a Mach number of 0.1 to between 300 and 400 Btu per square foot per second at a Mach number of 2.0, and the recovery temperature increased from about 1000° to 2800° R.

Lewis Research Center
National Aeronautics and Space Administration
Cleveland, Ohio, October 17, 1962

REFERENCES

1. Nettles, J. Cary: Experimental Study of Ballistic-Missile Base Heating with Operating Rocket. NACA RM E58G17, 1958.

2. Chiccine, Bruce G., Valerino, Alfred S., and Shinn, Arthur M.: Experimental Investigation of Base Heating and Rocket Hinge Moments for a Simulated Missile through a Mach Number Range of 0.8 to 2.0. NASA TM X-82, 1959.

3. Geothert, B. H.: Base Flow Characteristics of Missiles with Cluster-Rocket Exhaust. Paper 60-89, Inst. Aero. Sci., 1960.

4. Kennedy, T. L., and Lowry, J. F.: An Investigation of Base Heating on a 5.47-Percent Scale Model of the Saturn S-1 Booster at Transonic Mach Numbers. TN 61-106, Arnold Eng. Dev. Center, Aug. 1961.

5. Allen, John L.: Base-Flow Aerodynamics of a Saturn-Type Booster Stage at Mach Numbers 0.1 to 2.0. NASA TN D-593, 1962.

6. Beheim, Milton A., and Obery, Leonard J.: Wind Tunnel Studies of Booster Base Heating. Paper 62-166, Inst. Aero. Sci., 1962.

7. Rubesin, Morris W.: The Effect of an Arbitrary Surface-Temperature Variation Along a Flat Plate on the Convective Heat Transfer in an Incompressible Turbulent Boundary Layer. NACA TN 2345, 1951.

8. Stein, Samuel: A High-Performance 250-Pound-Thrust Rocket Engine Utilizing Coaxial-Flow Injection of JP-4 Fuel and Liquid Oxygen. NASA TN D-126, 1959.

9. Beheim, Milton A., Klann, John L., and Yeager, Richard A.: Jet Effects on Annular Base Pressure and Temperature in a Supersonic Stream. NASA TR-125, 1962.

10. Ungar, E. W.: Heat Transfer to a Solid-Propellant Rocket-Motor Nozzle. Battelle Memorial Inst., Dec. 30, 1961.

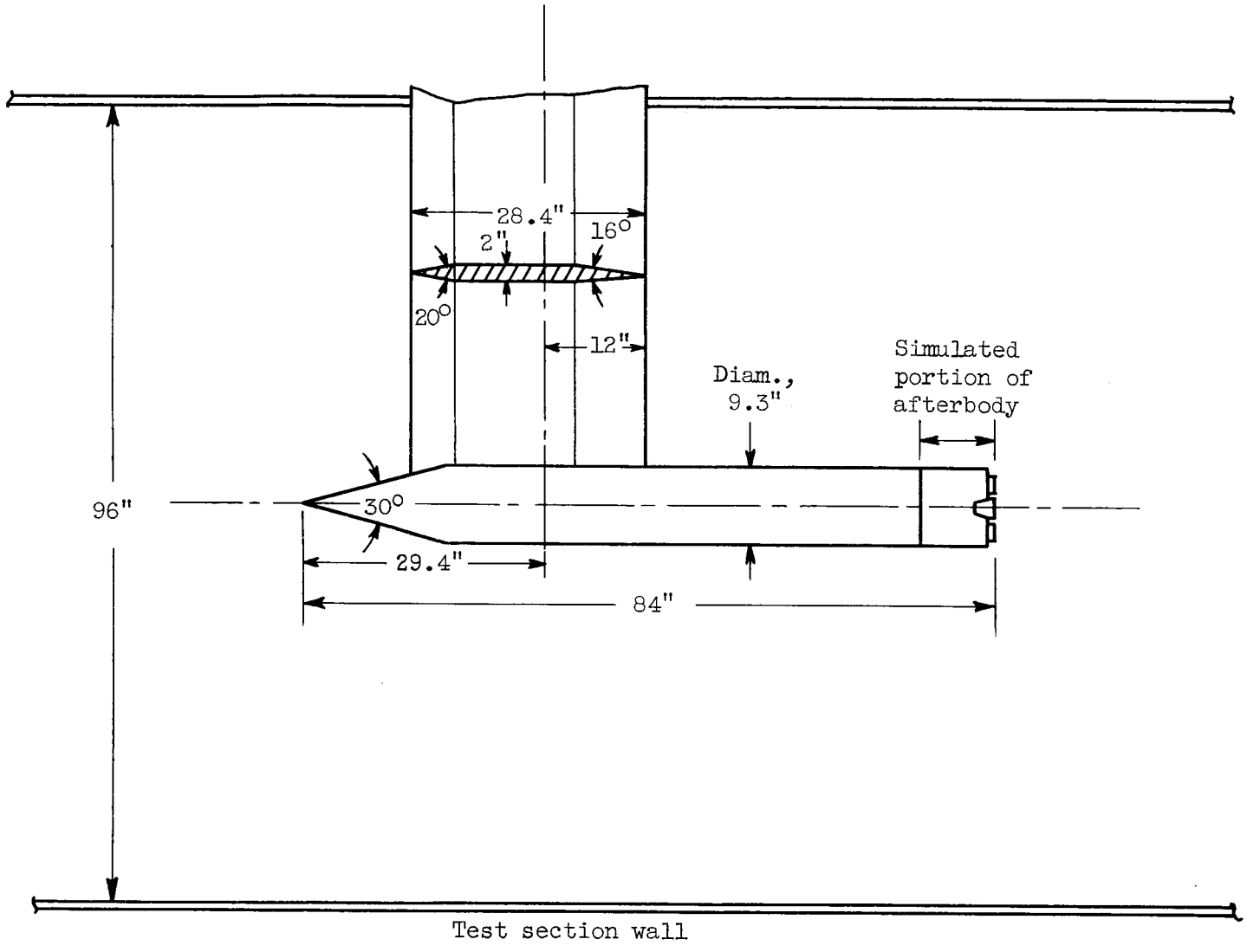

(a) Model test installation.

Figure 1. - General model arrangement.

Detail (see fig. 1(d))	Height, f, in.	α, deg	Distance from stack to edge of shroud, x, in.
A	3/8	19	1.75
B	1/16	19	1.75
C	5/8	27.5	.75+
D	1	27.5	2.0+
E	---	27.5	---

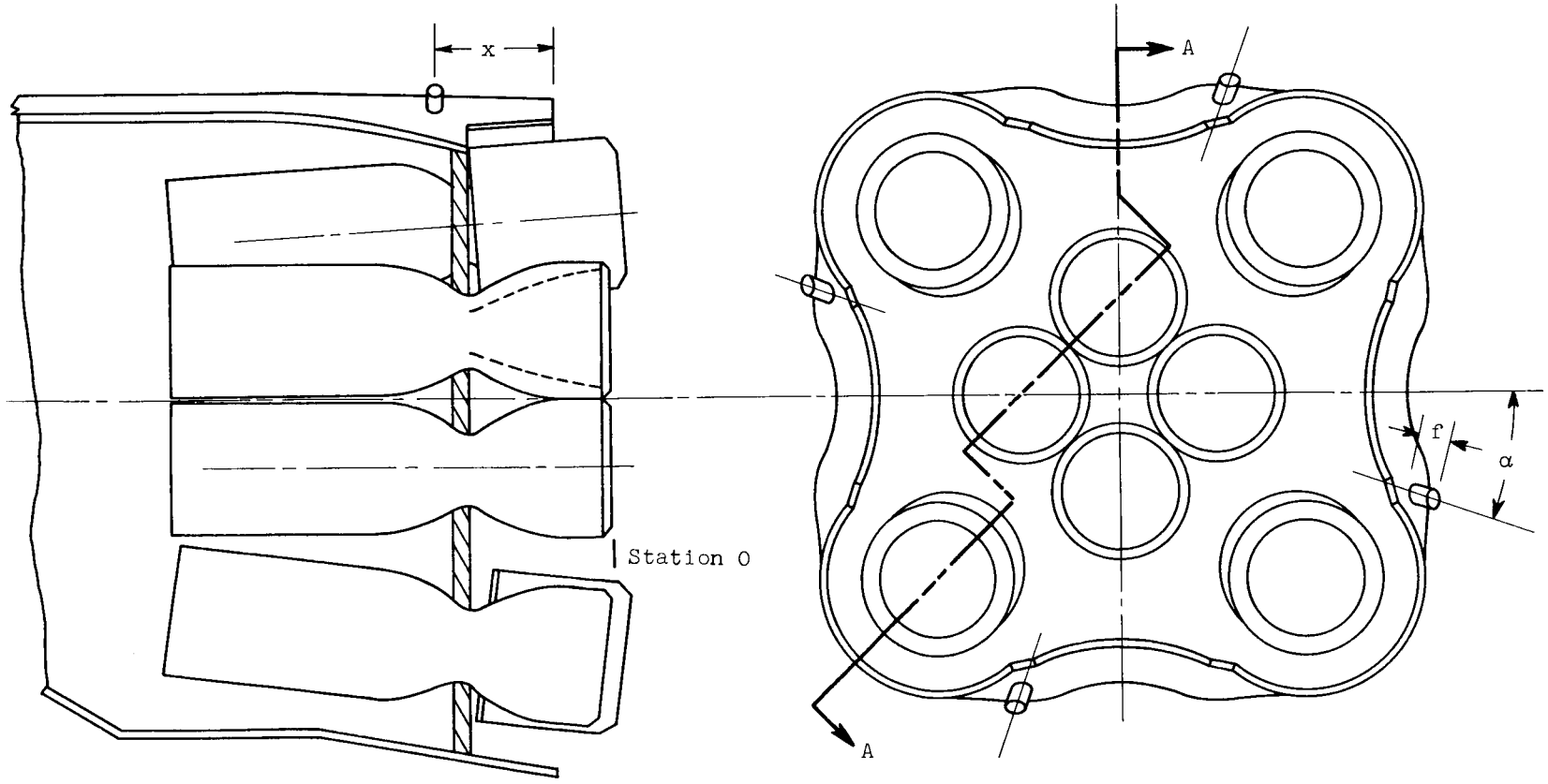

(b) General base arrangement.

Figure 1. - Continued. General model arrangement.

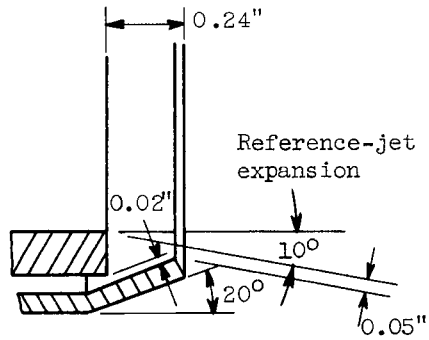

Mark I exhausterator

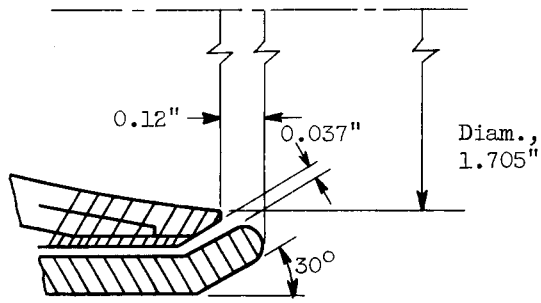

Mark II exhausterator

Distance from nozzle exit, l, in.	Nozzle diameter, D, in.	Distance from nozzle exit, l, in.	Nozzle diameter, D, in.
0	1.705	0.900	1.448
.063	1.702	1.000	1.391
.081	1.701	1.100	1.334
.100	1.698	1.200	1.270
.150	1.693	1.300	1.203
.200	1.685	1.400	1.136
.250	1.677	1.500	1.062
.300	1.699	1.600	.985
.400	1.646	1.700	.904
.500	1.617	1.800	.821
.600	1.583	1.900	.732
.700	1.546	2.000	.651
.800	1.500	2.100	.603

Internal nozzle coordinates, Mark II motor

(c) Exhausterator details and nozzle coordinates.

Figure 1. - Continued. General model arrangement.

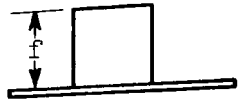

Details A and B

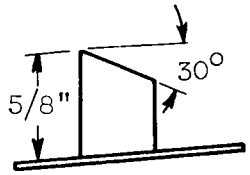

Detail C

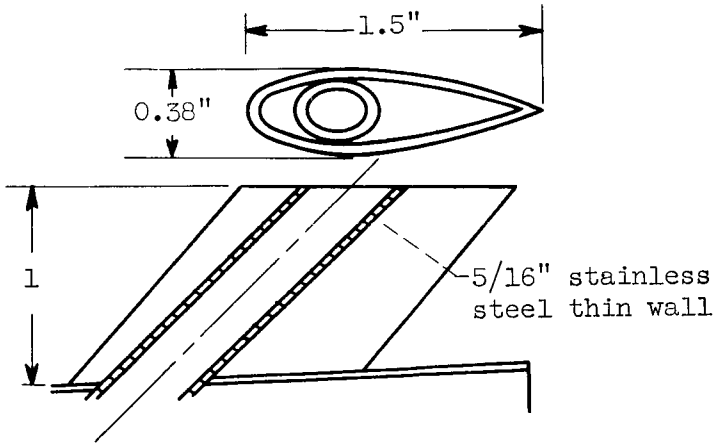

Detail D

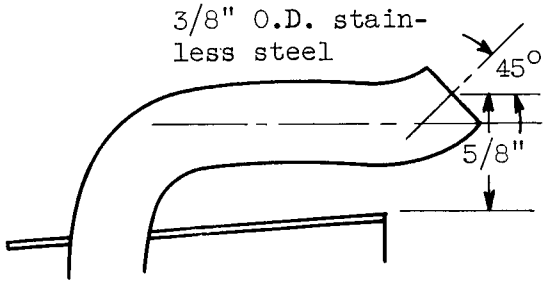

Detail E

(d) Details of various turbine-exhaust stacks.

Figure 1. - Concluded. General model arrangement.

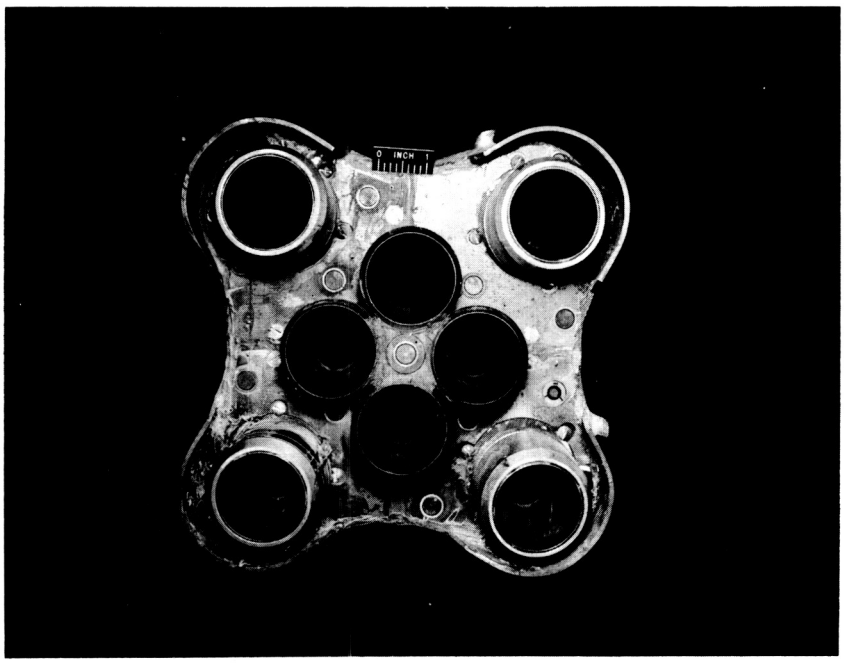

C-57906

(a) Base instrumentation details.

C-56217

(b) Afterbody details (four scoops per shroud and valley flow deflectors).

Figure 2. - Basic Saturn configurations with 3/8-inch turbine-exhaust stacks.

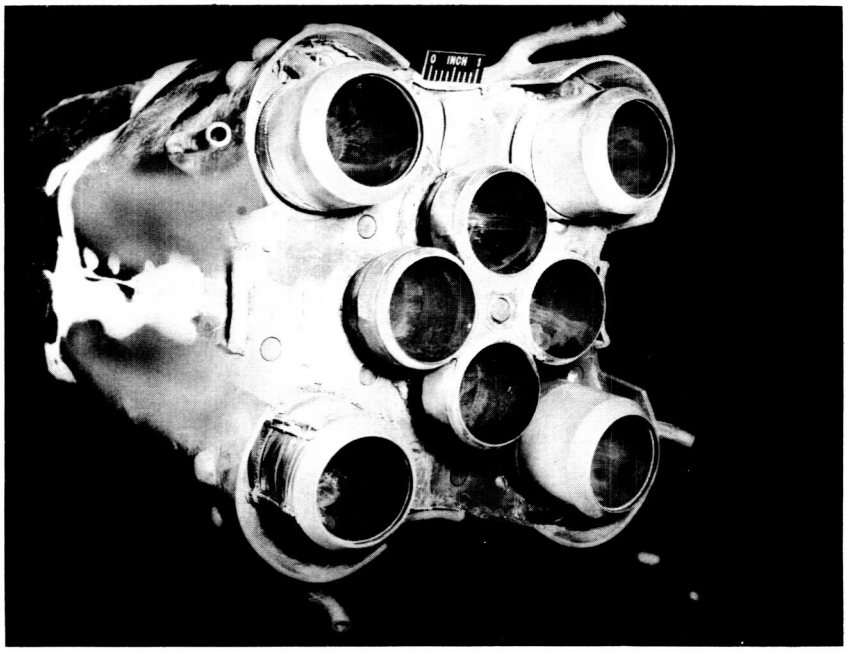

C-57646

(a) Base view.

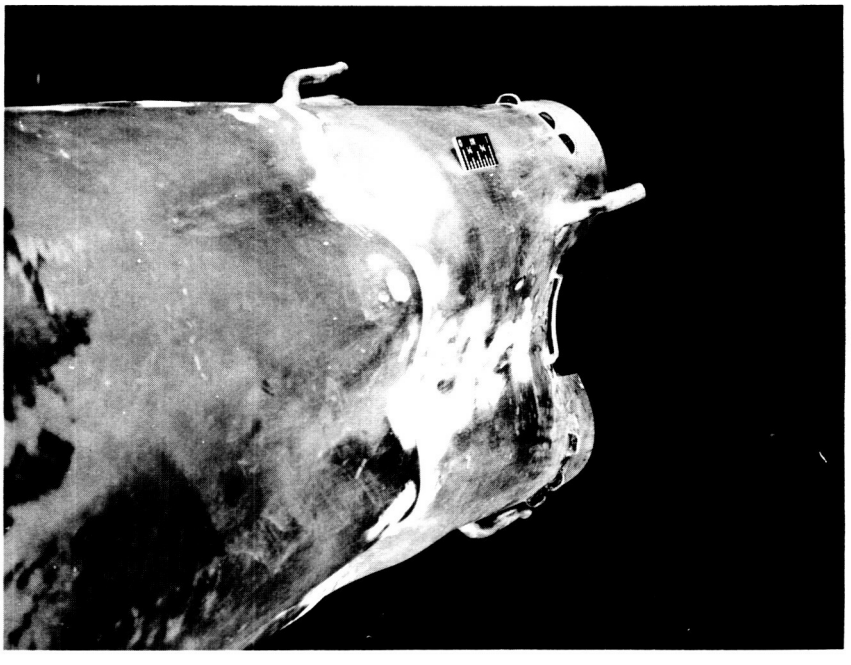

C-56941

(b) Afterbody detail.

Figure 3. - Basic Saturn configuration with curved turbine-exhaust pipes, three scoops per shroud, and valley flow deflectors (SA-1).

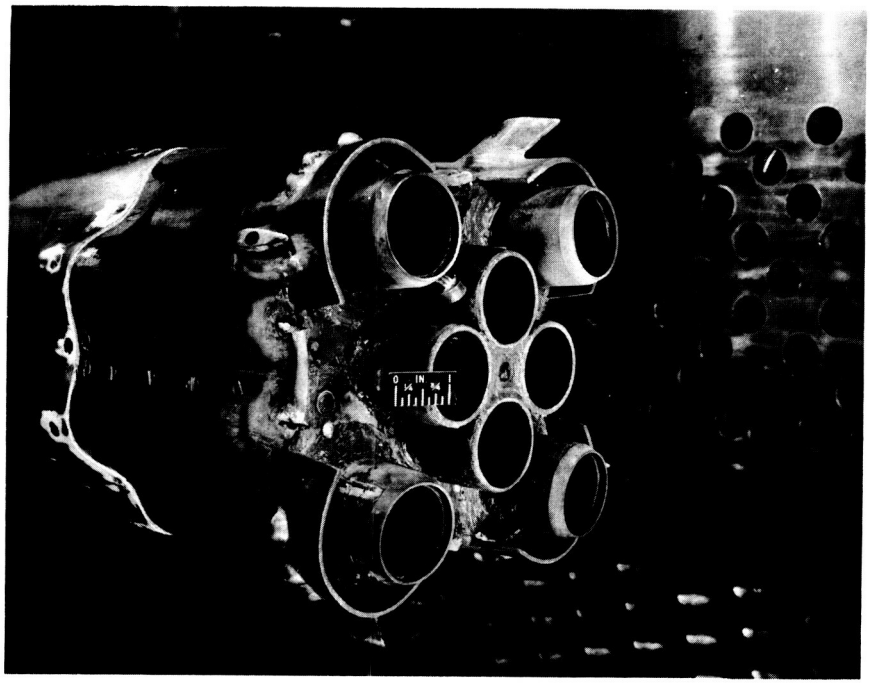

C-56982

(a) With three scoops per shroud, valley flow deflectors, and streamlined turbine-exhaust stacks.

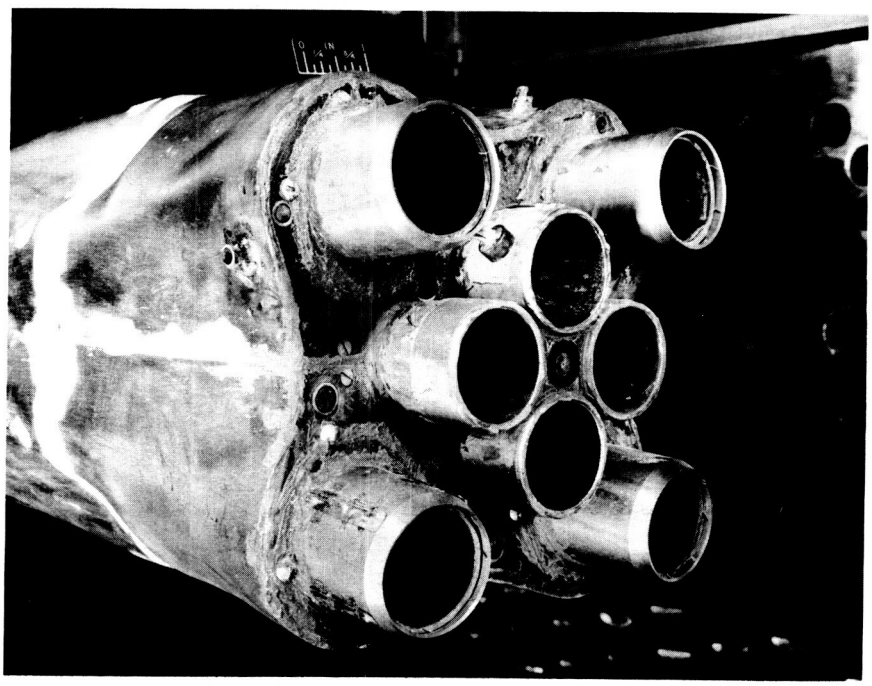

C-56848

(b) Without engine shrouds but with 3/8-inch turbine-exhaust stacks (flush base).

Figure 4. - Basic Saturn configurations.

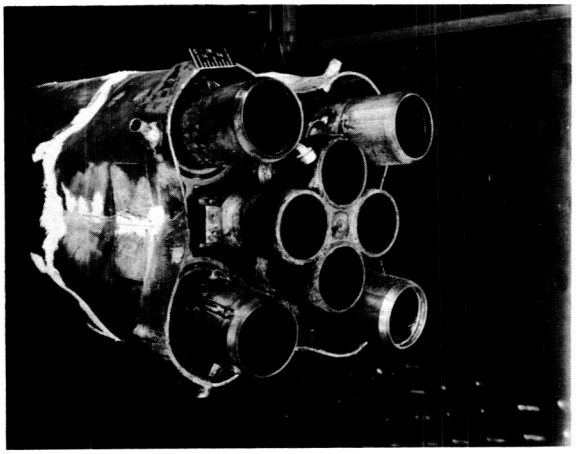

C-57144

(a) Base view.

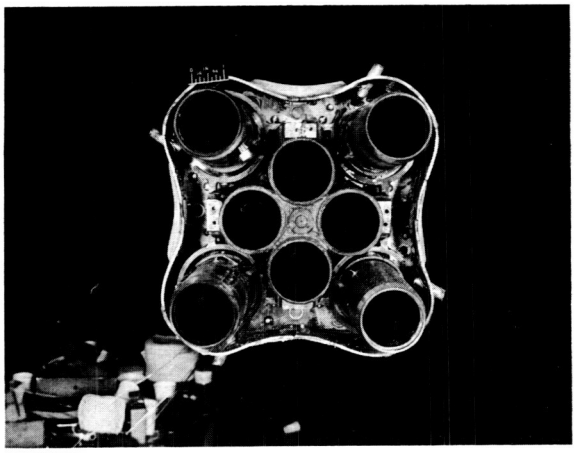

C-57145

(b) Base details.

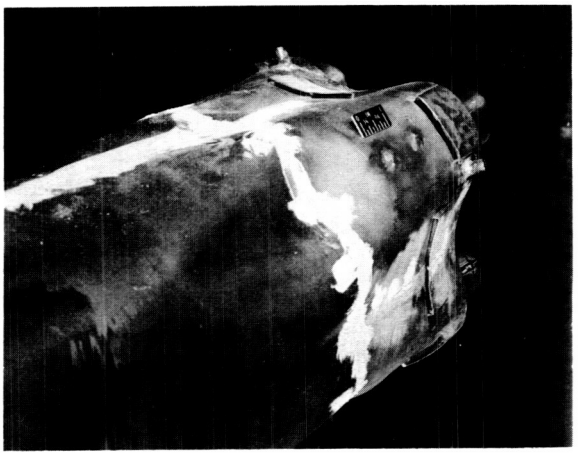

C-57146

(c) Afterbody details.

Figure 5. - Recessed-base configuration with shroud, valley scoops, and 5/8-inch turbine-exhaust stacks.

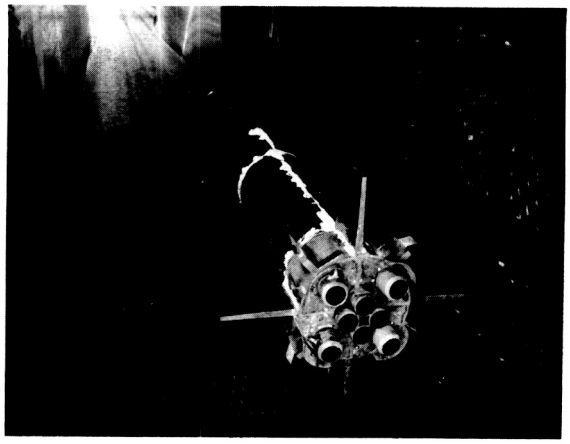

C-57822

(a) Four-fin and four-stub configuration; streamlined turbine-exhaust stacks and streamlined hydrogen vents on stubs.

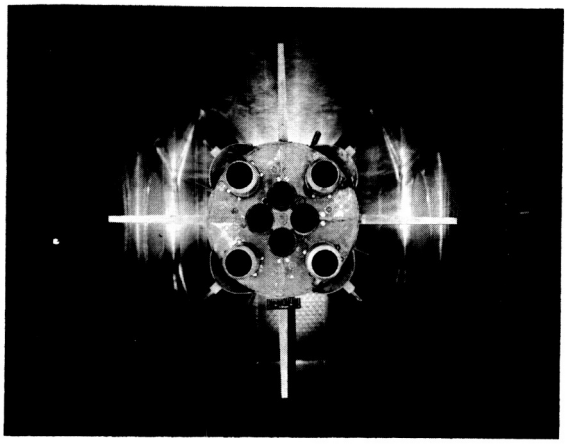

C-57825

(b) Instrumentation details.

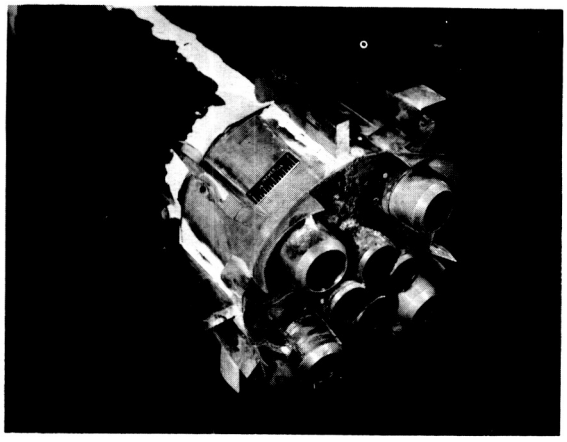

C-57774

(c) Eight-stub configuration; streamlined turbine-exhaust stacks and streamlined hydrogen vents on stubs.

Figure 6. - Circular-base configurations.

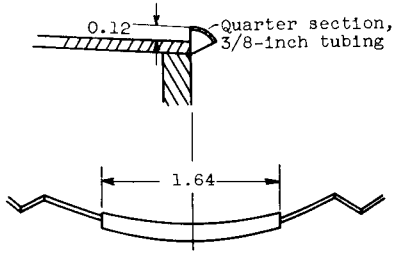

(a) Valley flow deflectors.

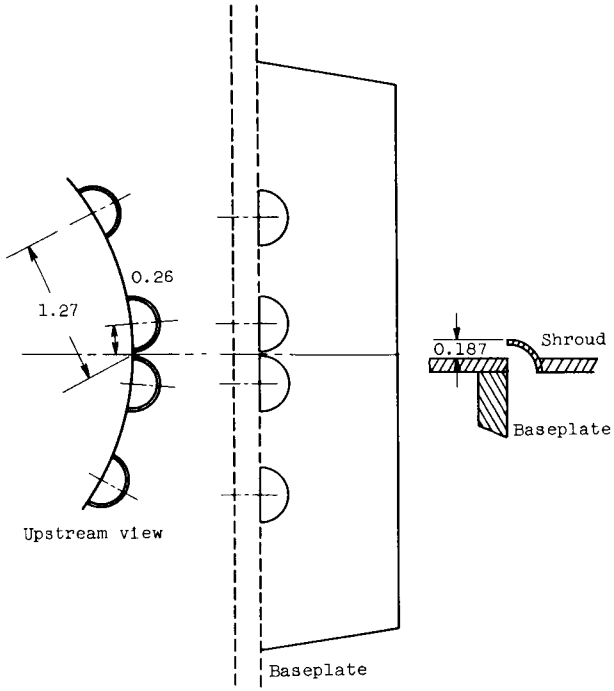

(b) Shroud scoops.

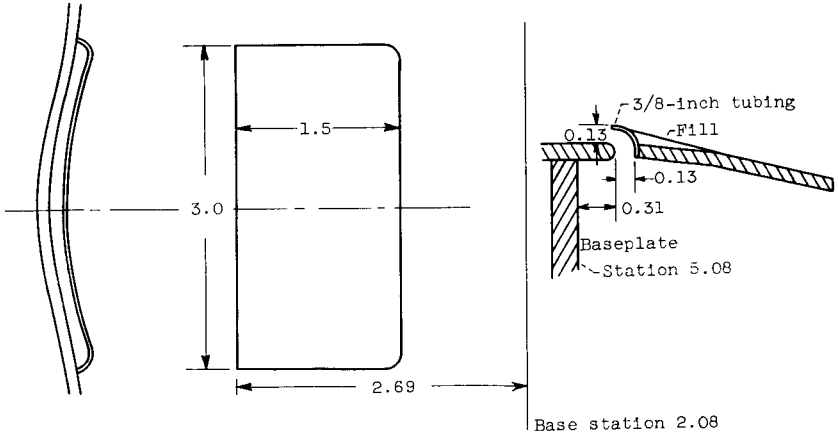

(c) Valley scoops for recessed-base configuration.

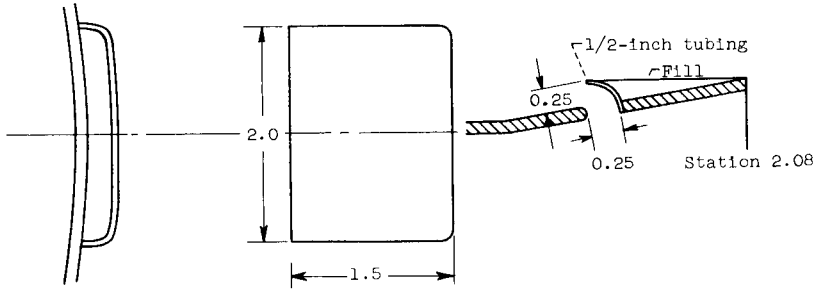

(d) Shroud scoops for recessed-base configuration.

Figure 7. - Details of various cooling scoops. (All dimensions in inches.)

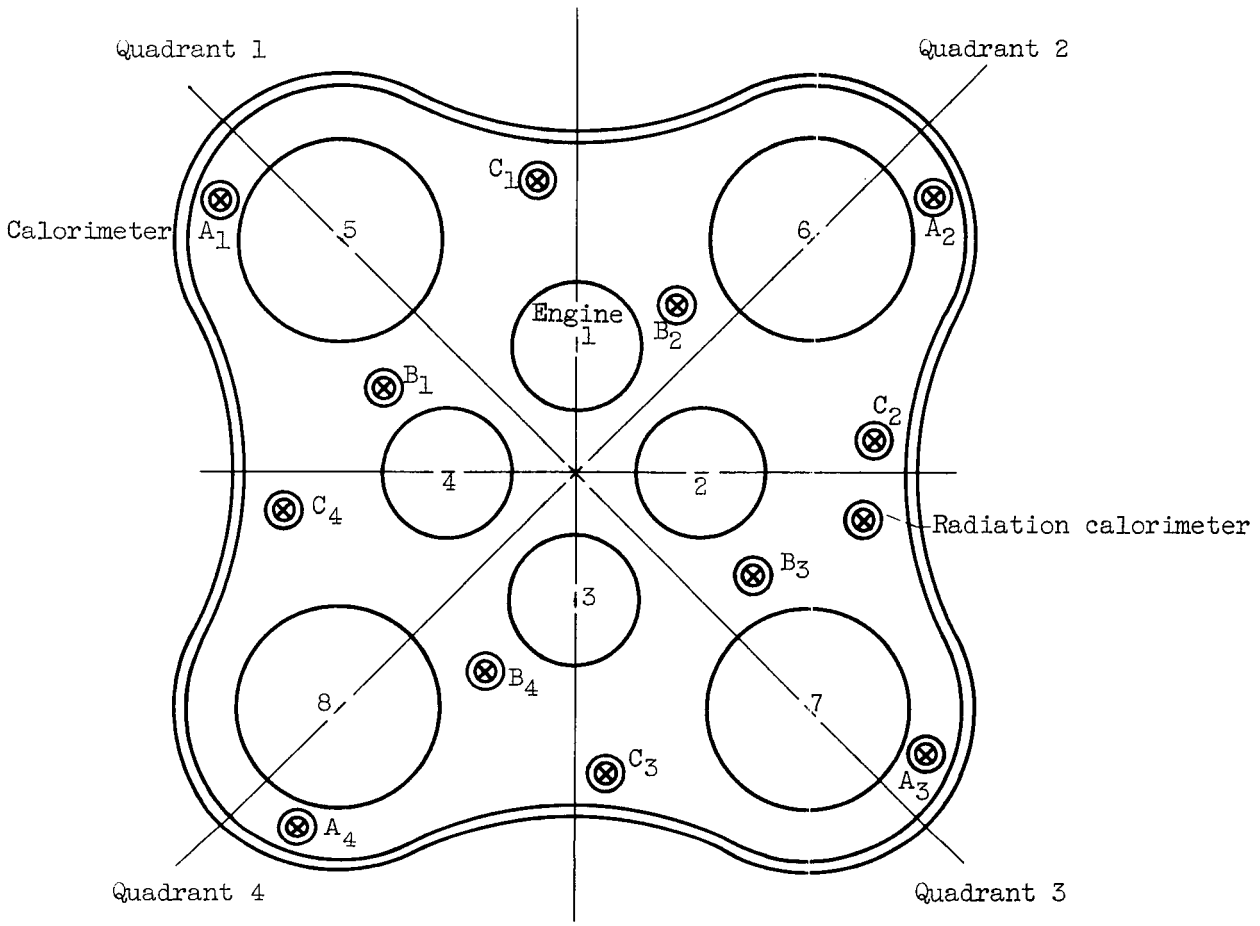

(a) General baseplate calorimeter locations.

Figure 8. - Instrumentation details.

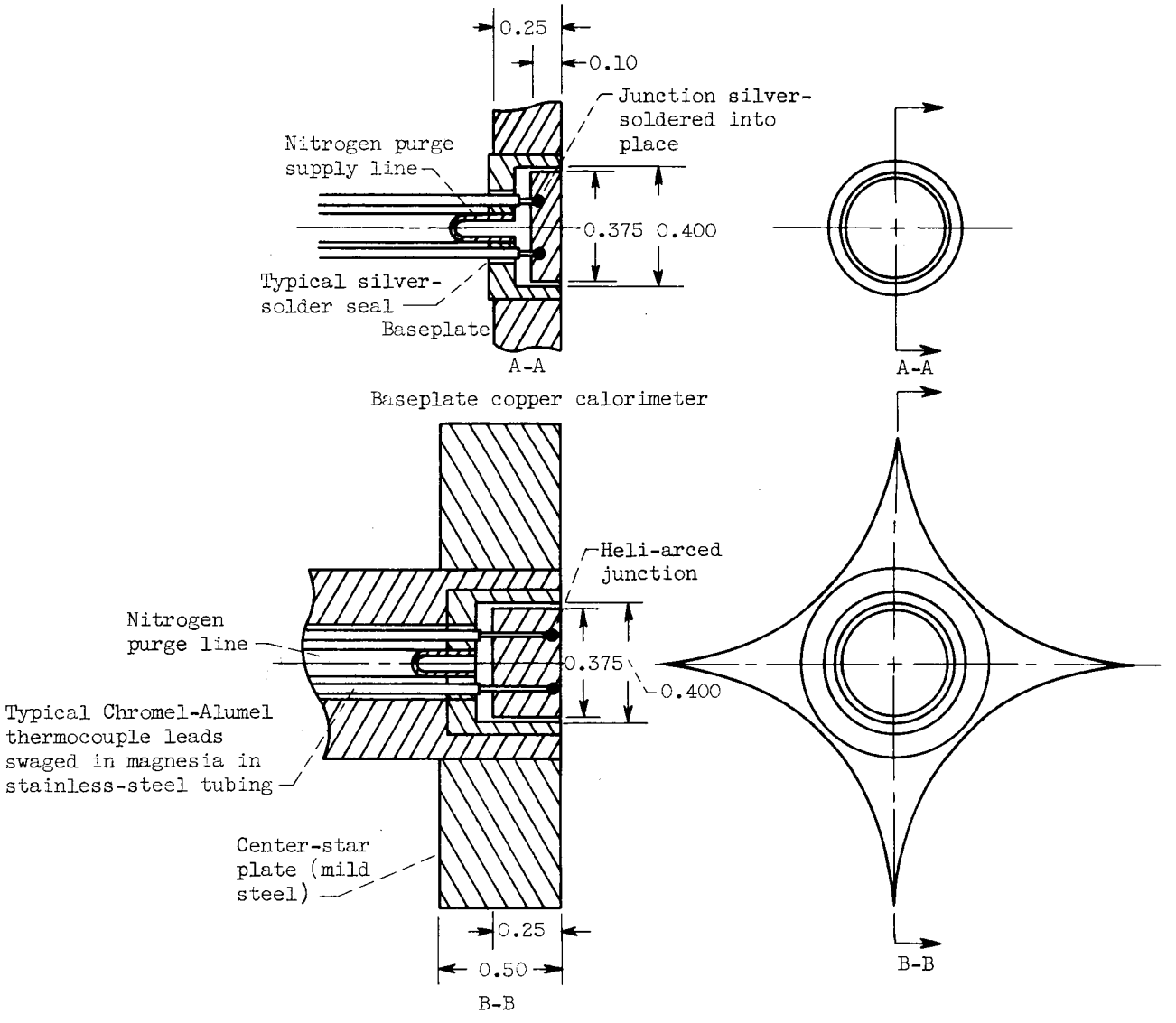

(b) Calorimeter details. (All dimensions in inches.)

Figure 8. - Continued. Instrumentation details.

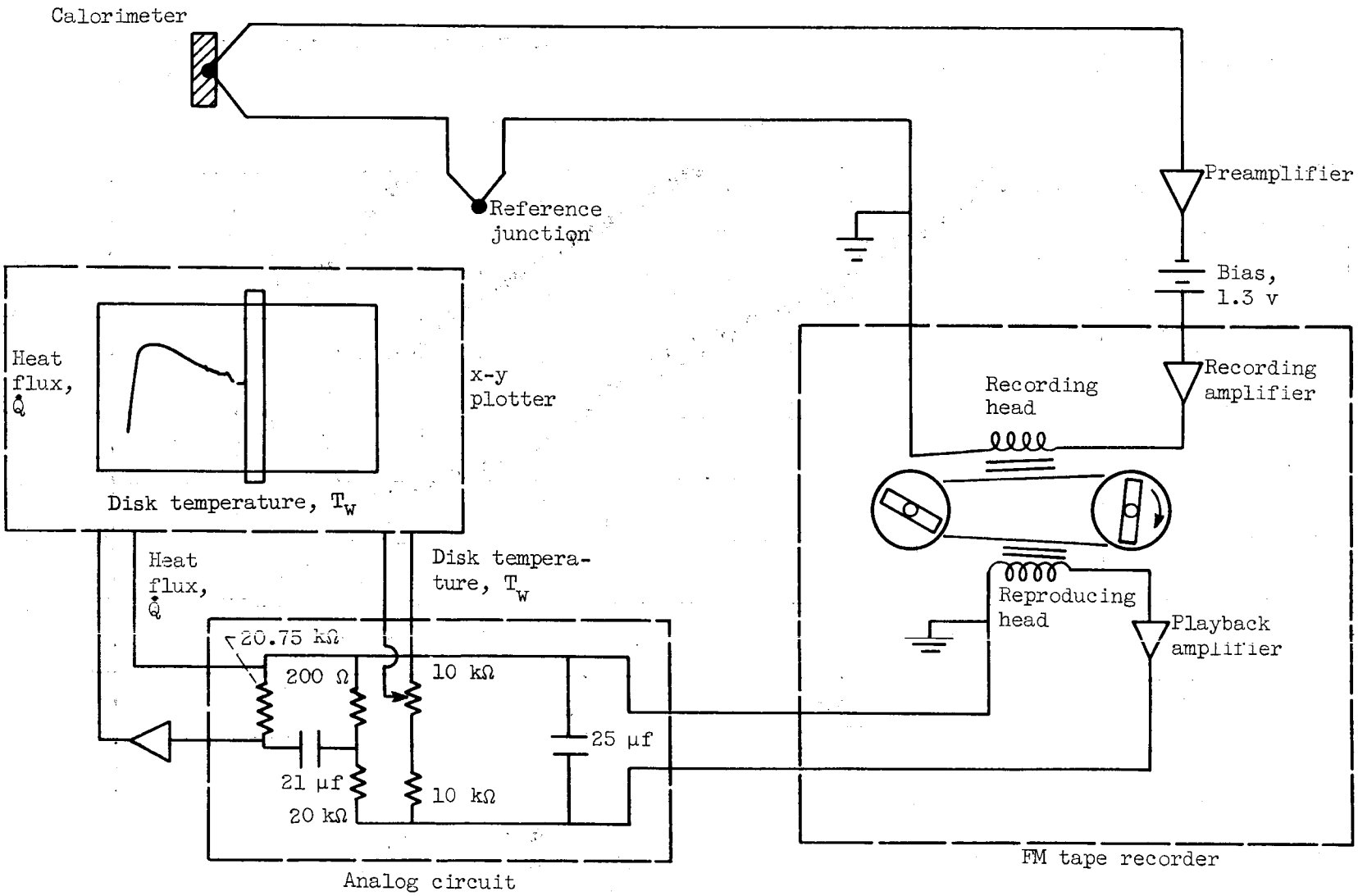

(c) Schematic of recording, analog, and plotting system.

Figure 8. - Concluded. Instrumentation details.

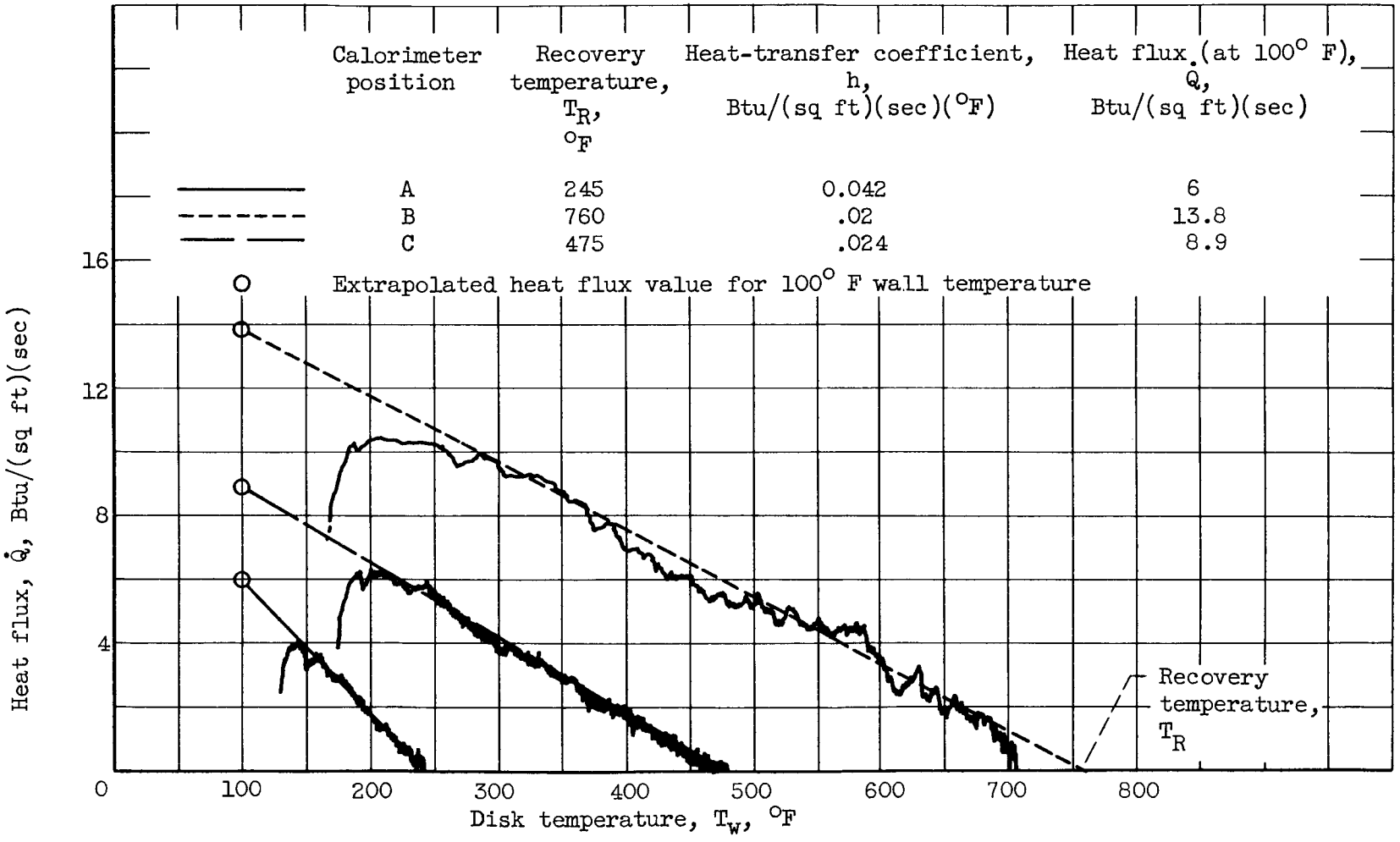

Figure 9. - Typical traces of heat flux as function of disk (wall) temperature obtained by using analog circuit. Heat-transfer coefficient $h = d\dot{Q}/dT$.

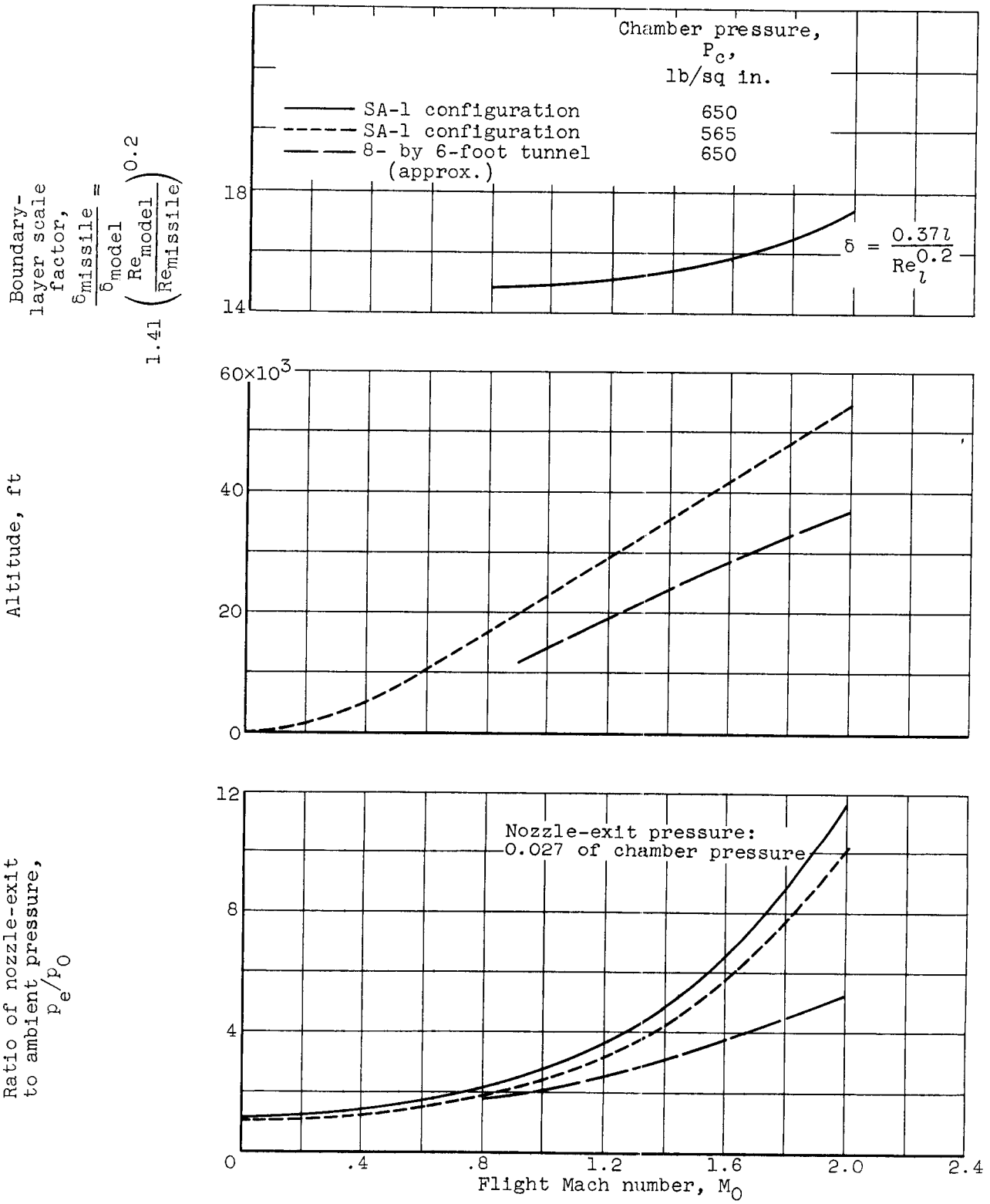

Figure 10. - Schedules of altitude, nozzle-exit pressure ratio, and boundary-layer scale factor with Mach number.

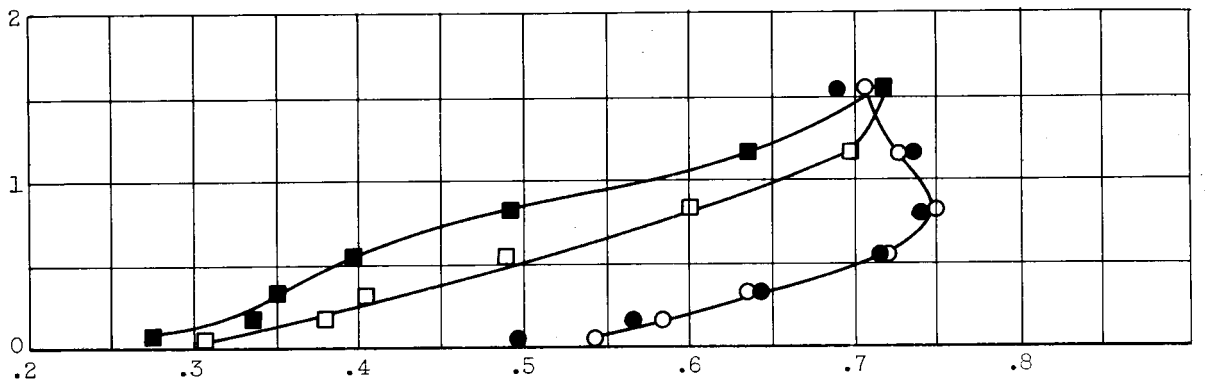

(a) Free-stream Mach number, 2.0; ratio of Reynolds number to length, 4.8×10^6.

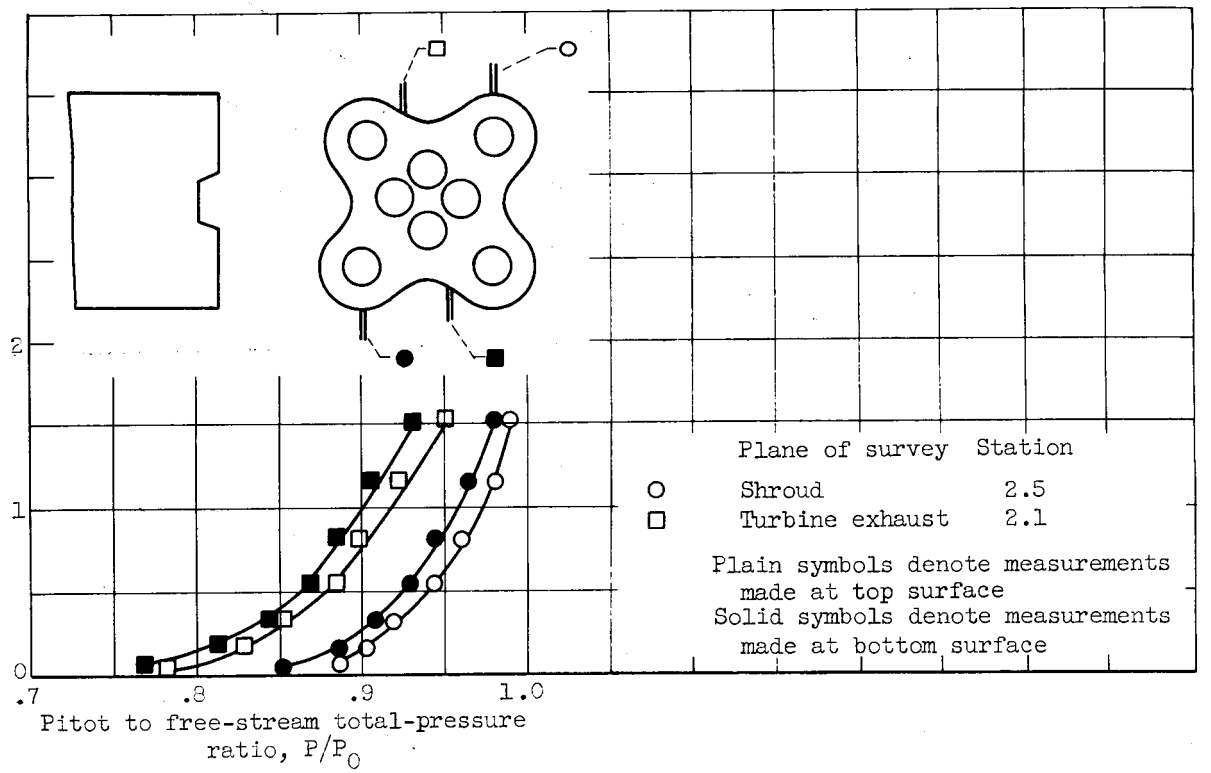

(b) Free-stream Mach number, 0.8; ratio of Reynolds number to length, 4.2×10^6.

Figure 11. - Boundary-layer measurements on shroud. Scalloped-propellant-tank configuration.

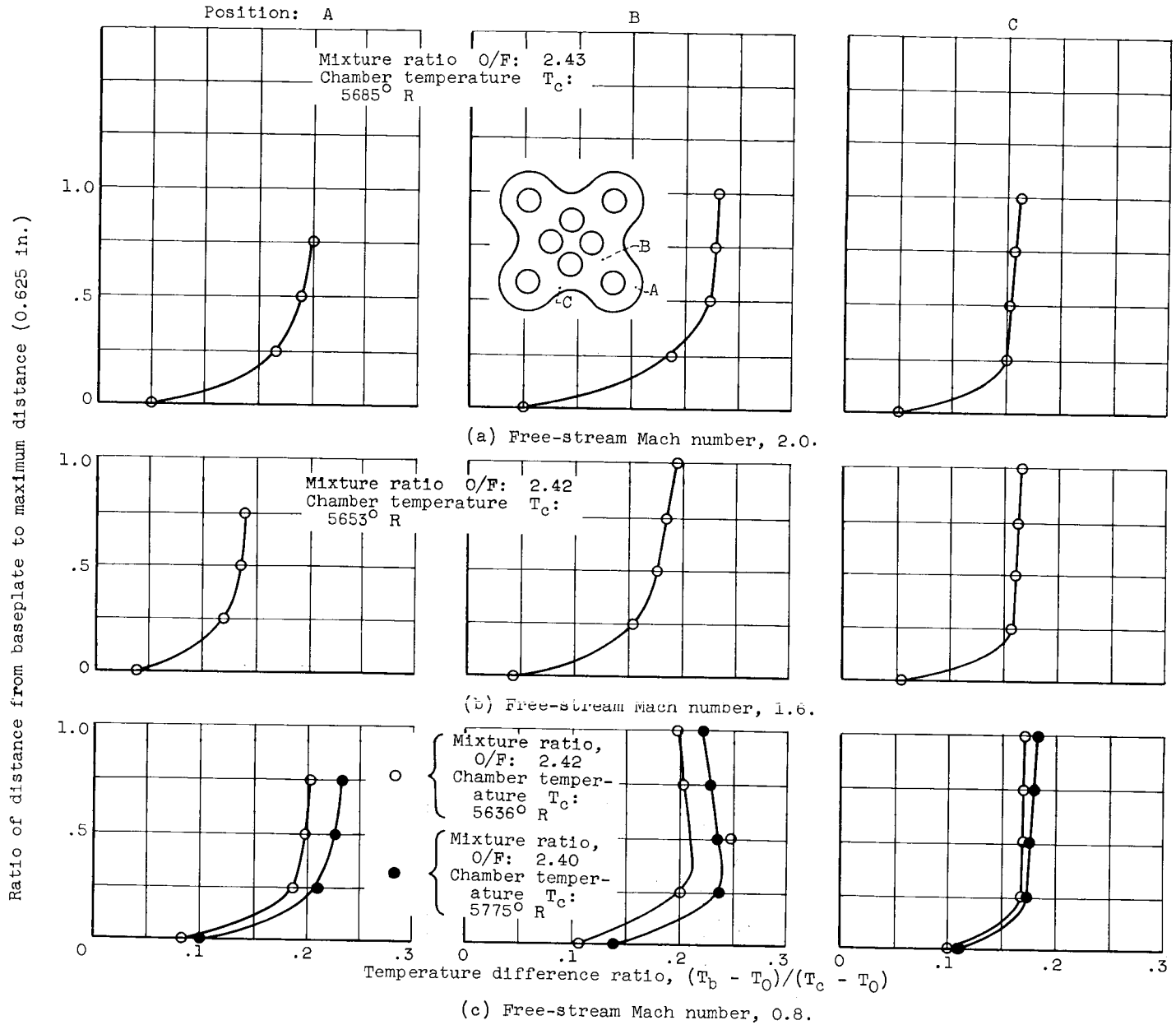

Figure 12. - Profiles of base temperature difference ratio at three positions for basic Saturn configuration without cooling scoops, turbine-exhaust flow or exhausterator flow.

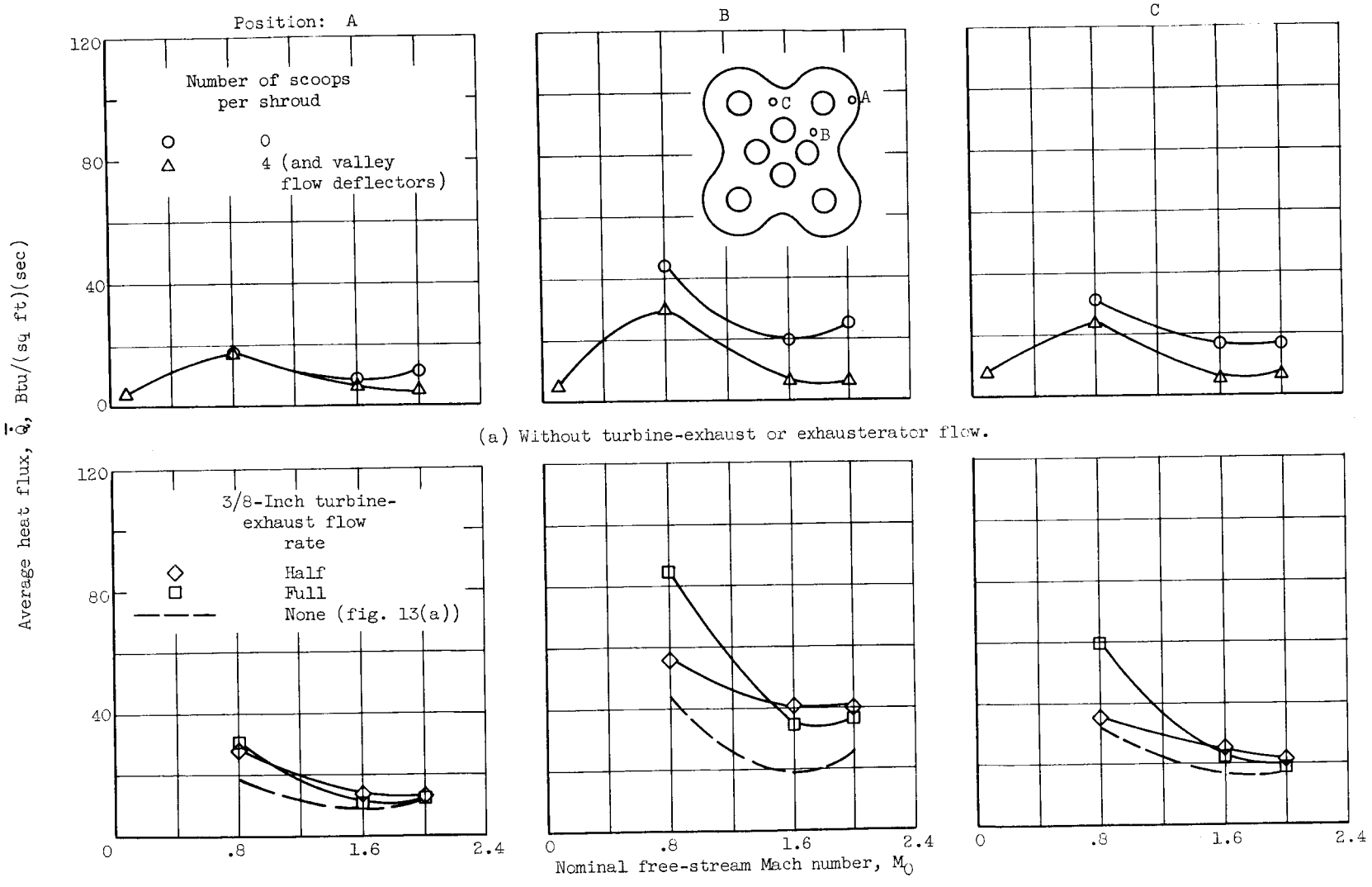

(a) Without turbine-exhaust or exhausterator flow.

(b) Without cooling air scoops, but with turbine-exhaust flow.

Figure 13. - Effects of turbine-exhaust flow and cooling scoops on basic Saturn average base heat flux.

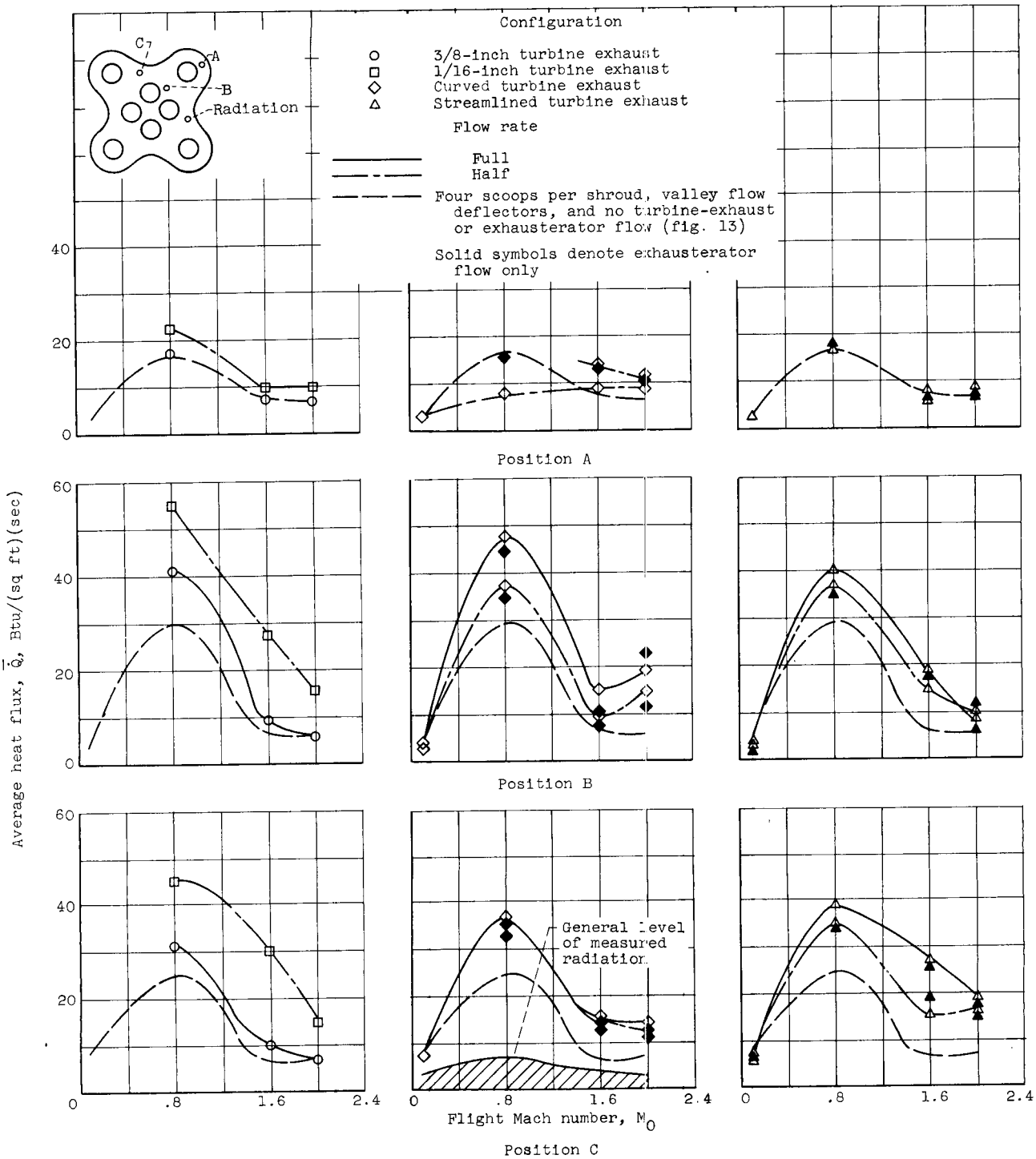

(a) Four scoops per shroud, valley flow deflectors, and half-rated turbine-exhaust flow.

(b) Three scoops per shroud, valley flow deflectors, and SA-1 (curved) turbine exhaust and exhausterators.

(c) Three scoops per shroud, valley flow deflectors, and streamlined turbine exhaust and exhausterators.

Figure 14. - Effect of turbine-exhaust configuration and exhausterator flow on average base heat flux at three positions.

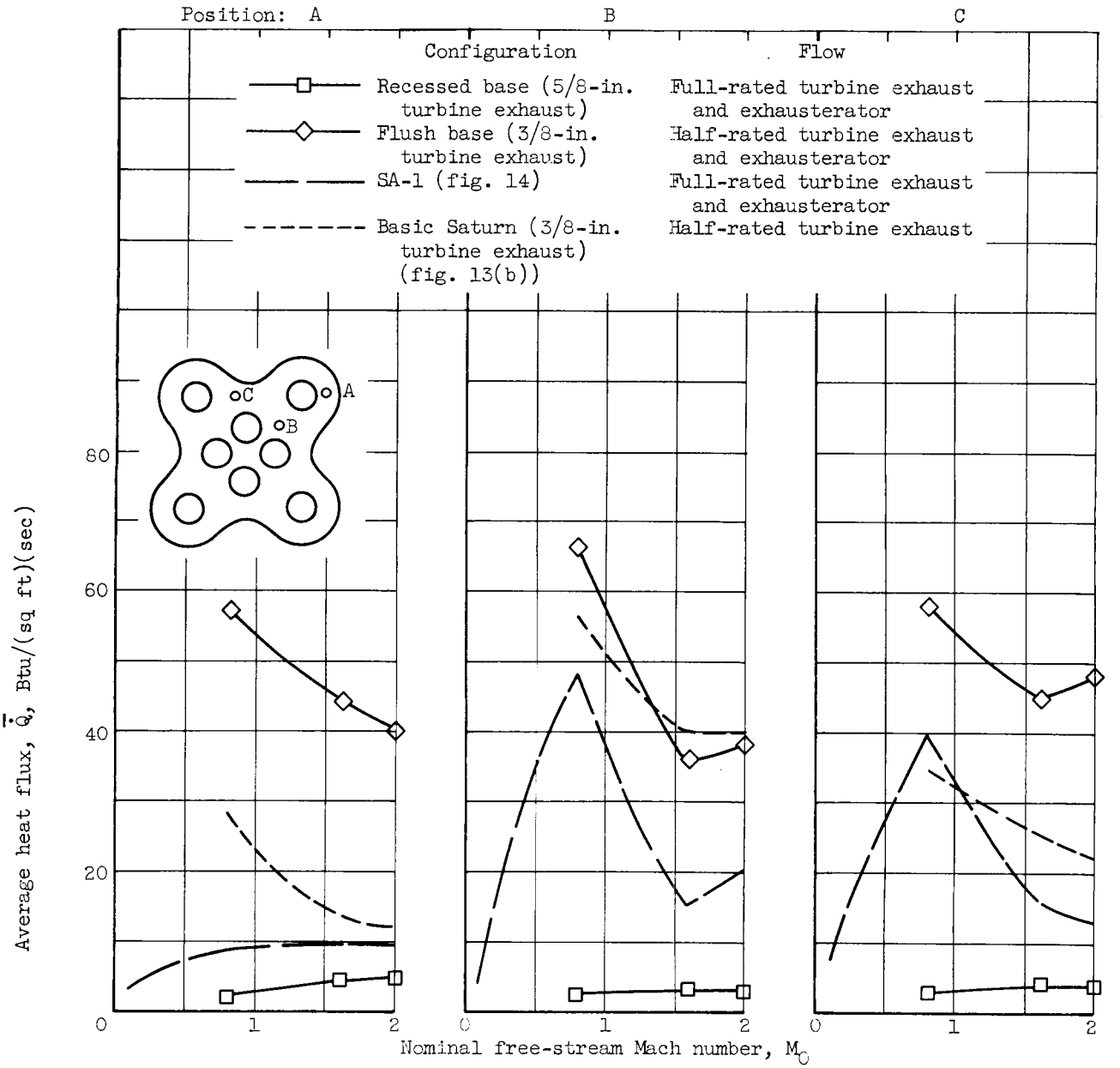

(a) Average heat flux.

Figure 15. - Comparison of various base configurations.

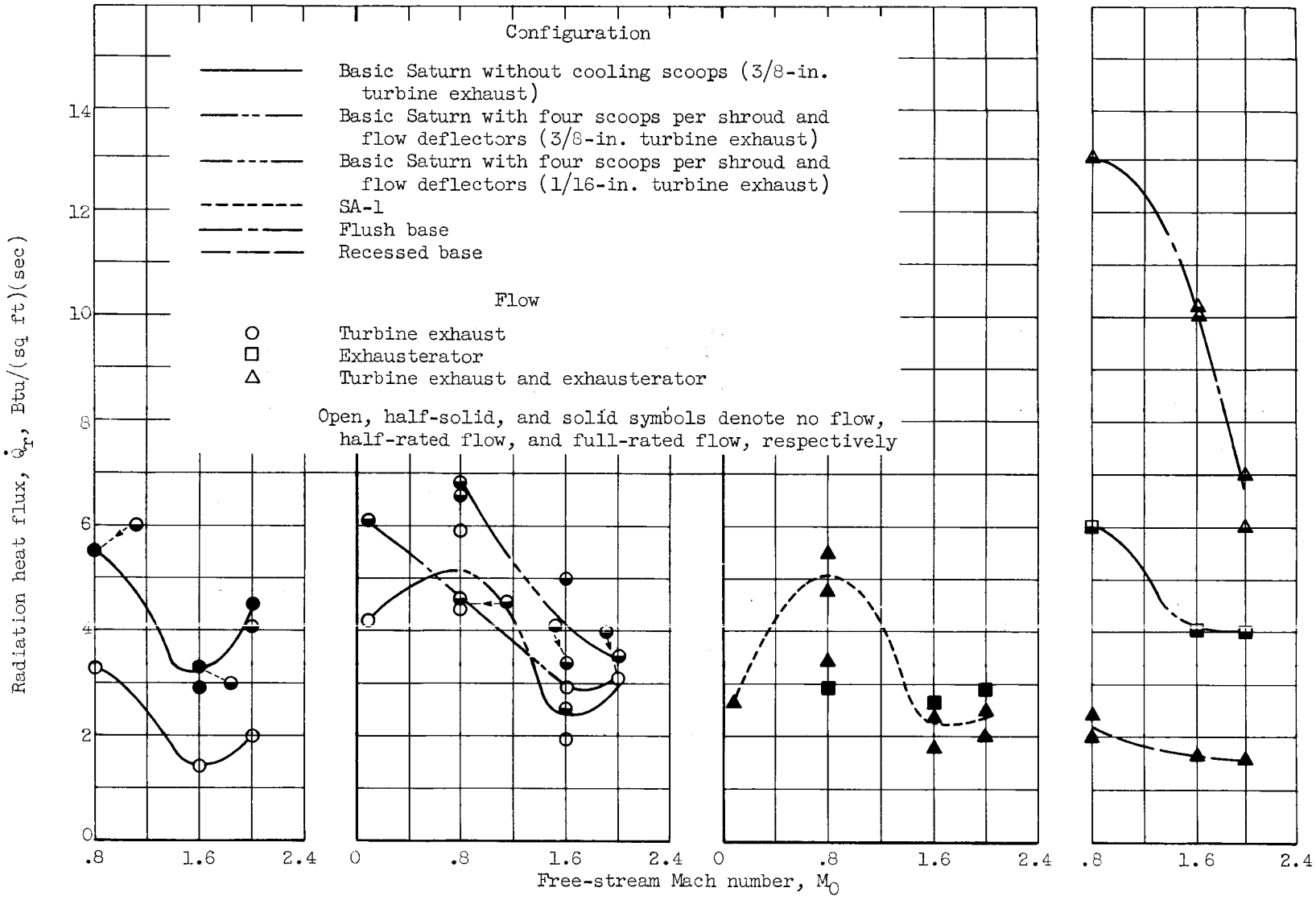

(b) Nominal radiation heat flux at position C.

Figure 15. - Concluded. Comparison of various base configurations.

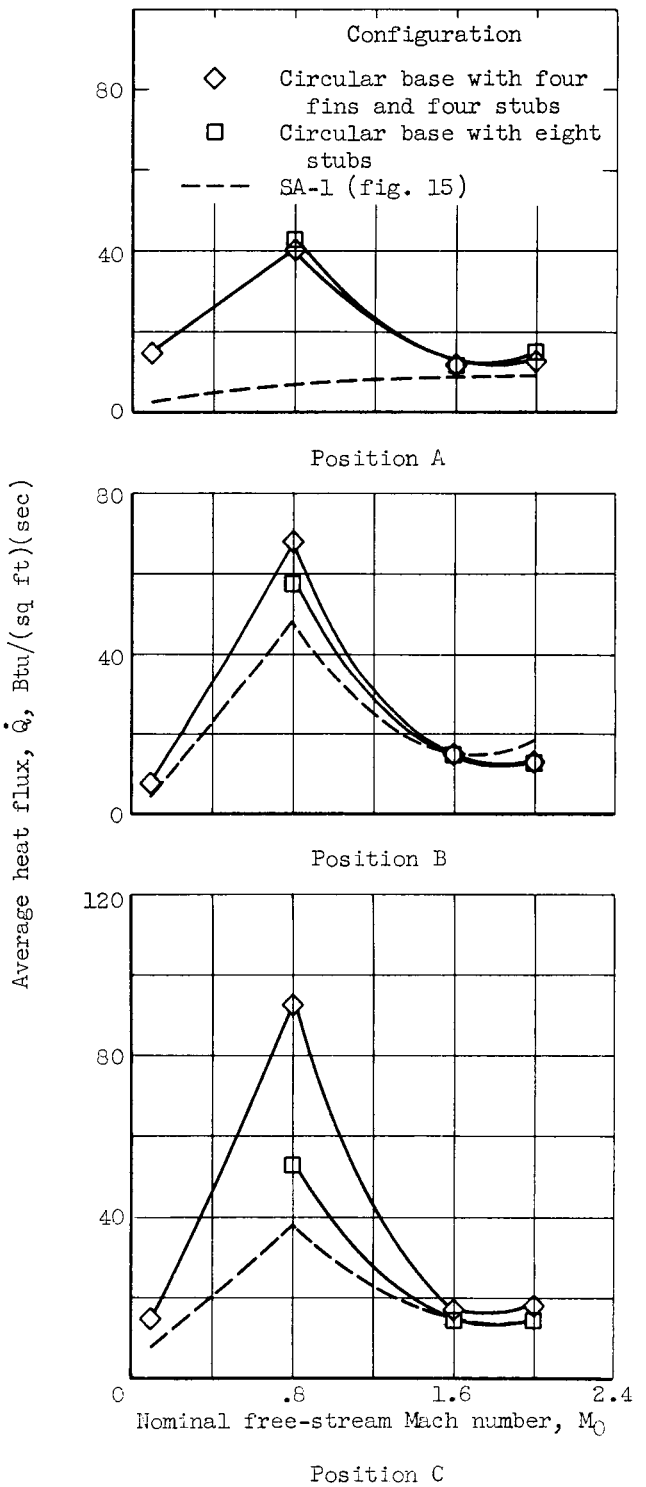

Figure 16. - Comparison of SA-1 and circular-base configurations with stabilizing surfaces, full-rated turbine-exhaust and exhausterator flow, and boiloff vent flow.

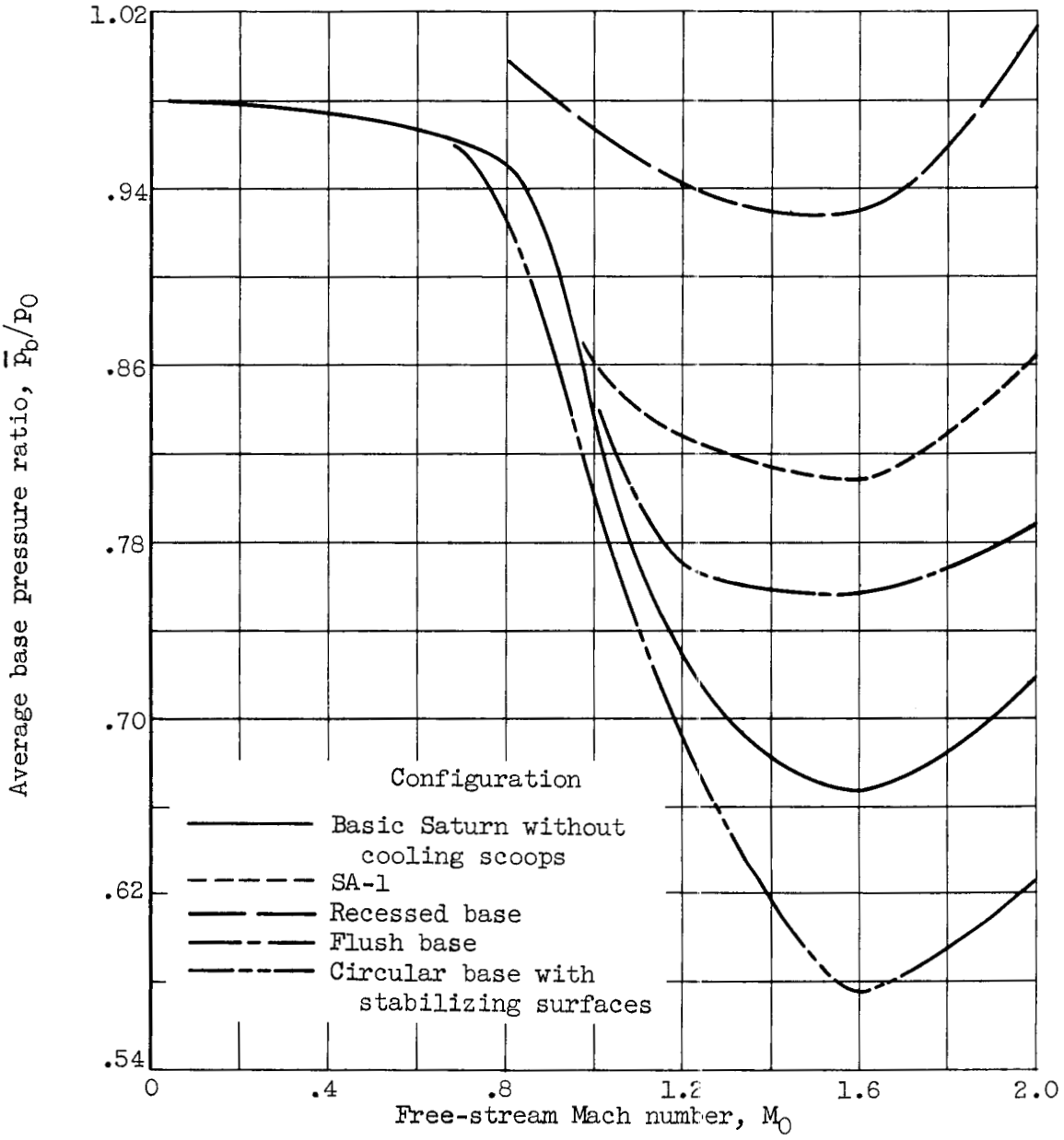

Figure 17. - Comparison of base pressure ratio for various configurations.

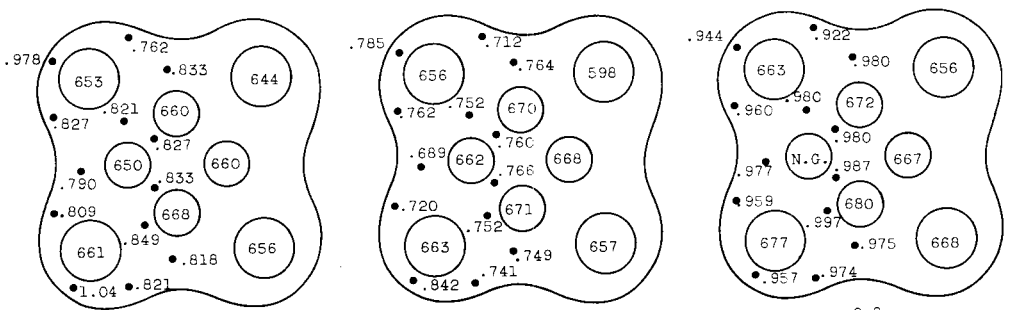

Free-stream Mach number M_0: 2.0
Average chamber pressure $\bar{P}_c$: 656
Average base pressure ratio $\bar{P}_b/P_0$: 0.84

2.0
656
0.84

1.6
656
0.74

0.8
669
0.969

All engines operative

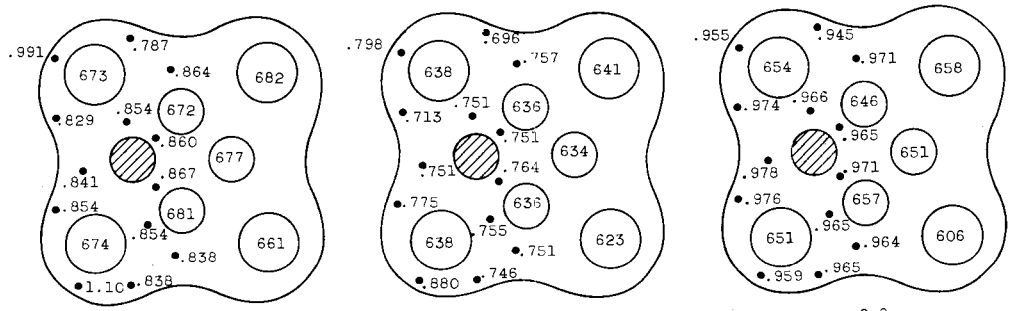

2.0
674
0.873

1.6
635
0.760

0.8
646
0.967

Inboard engine 4 inoperative

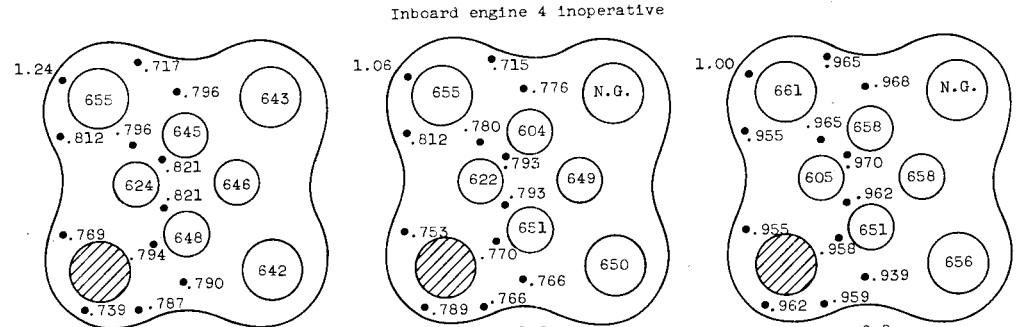

2.0
643
0.824

1.6
639
0.798

0.8
648
0.963

Outboard engine 8 inoperative (maximum corrective gimbal)

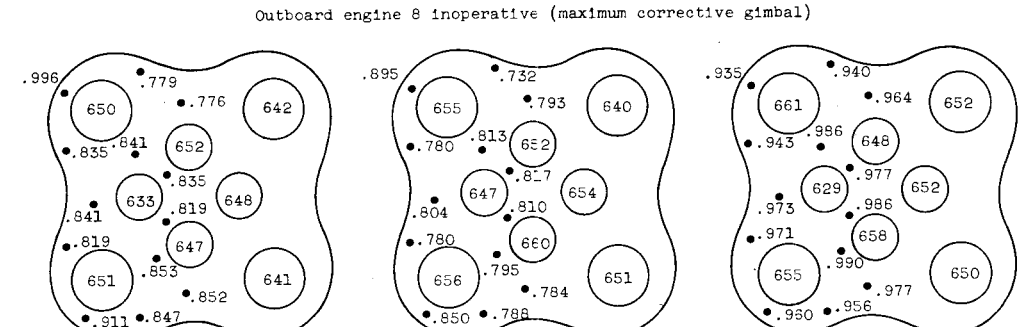

2.0
646
0.846

1.6
652
0.803

0.8
651
0.967

Maximum downward gimbal

(a) SA-1 configuration.

Figure 18. - Base pressure distributions.

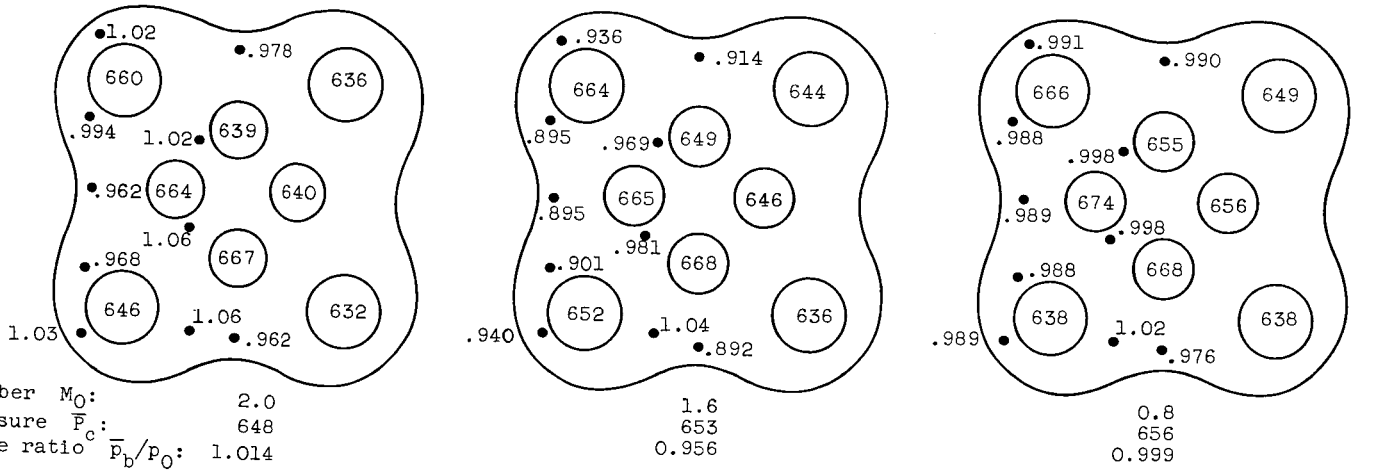

Free-stream Mach number M_0: 2.0
Average chamber pressure $\bar{P}_c$: 648
Average base pressure ratio $\bar{p}_b/p_0$: 1.014

1.6
653
0.956

0.8
656
0.999

Recessed base

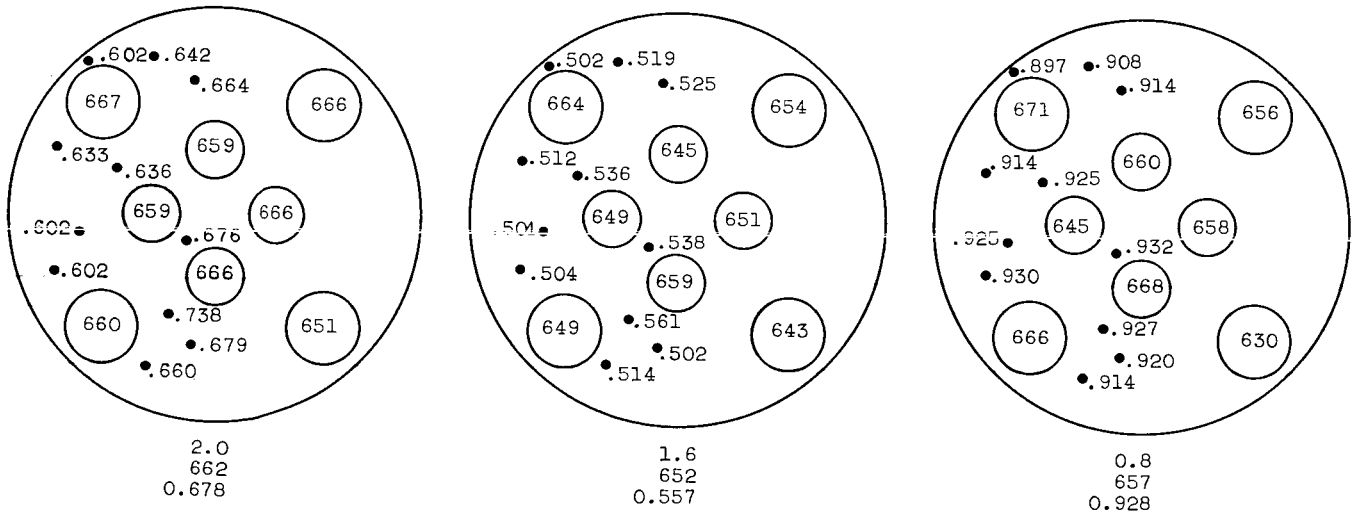

2.0
662
0.678

1.6
652
0.557

0.8
657
0.928

Circular base with four fins and four stubs

(b) Recessed-base and circular-base configurations.

Figure 18. - Concluded. Base pressure distributions.

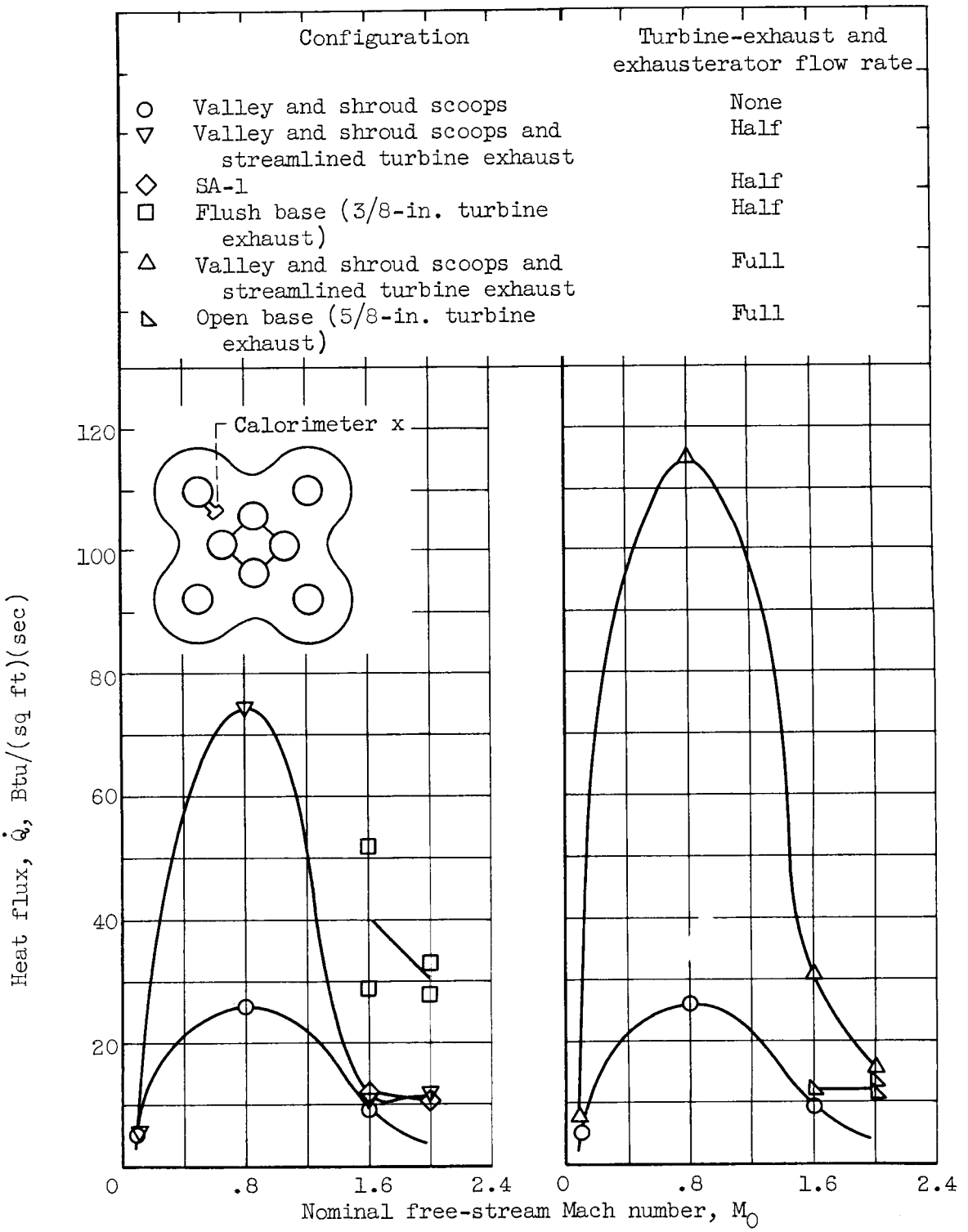

Figure 19. - Effect of turbine-exhaust and exhausterator flow on heat flux measured by exhausterator calorimeter (X).

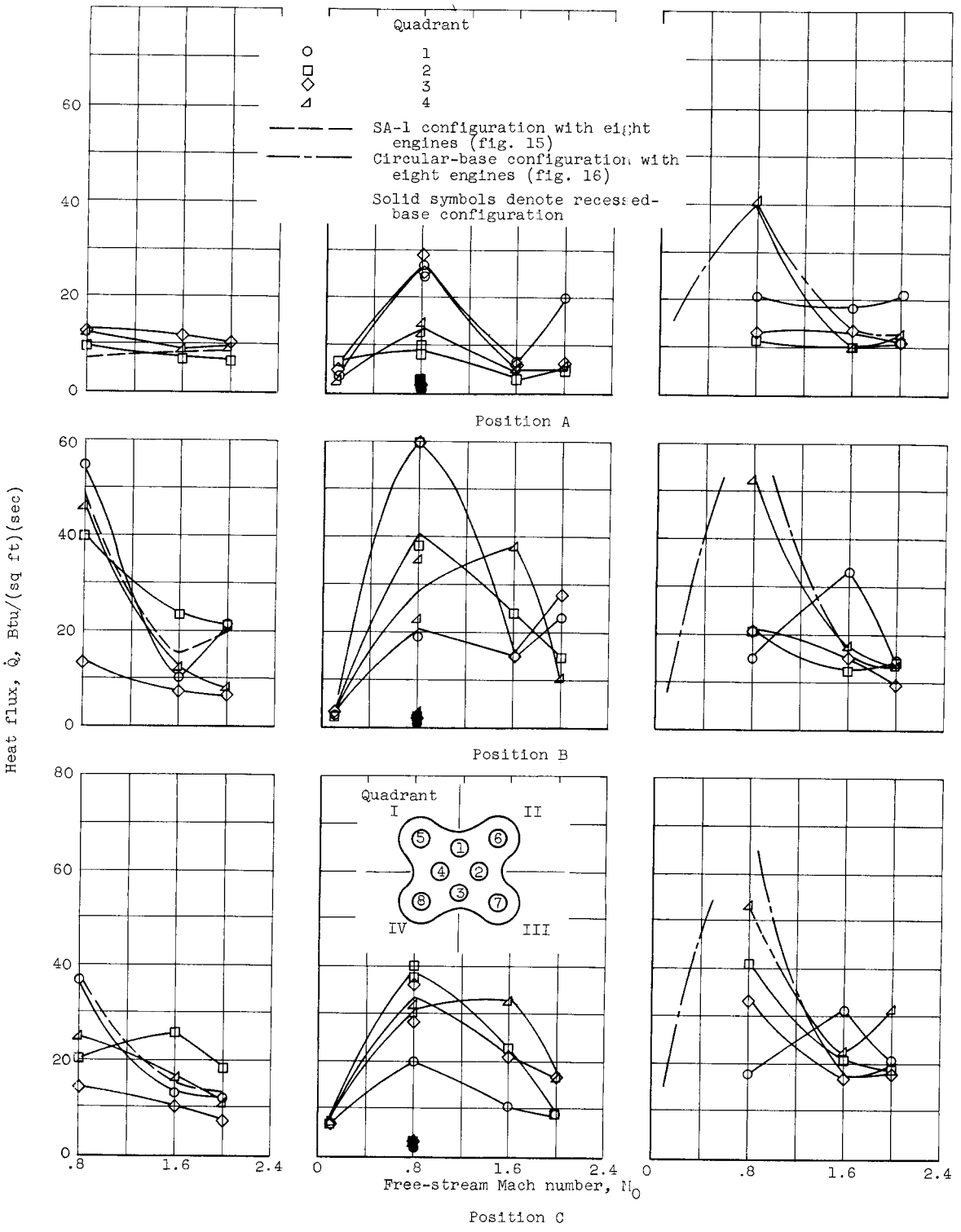

(a) SA-1 configuration; outboard engine 7 operative.

(b) SA-1 configuration; inboard engine 4 inoperative.

(c) Circular-base configuration with four fins and four stubs; inboard engine 4 inoperative.

Figure 20. - Effect of inoperative engine on base heat flux distribution for SA-1 and circular-base configurations with full-rated turbine-exhaust and exhausterator flow.

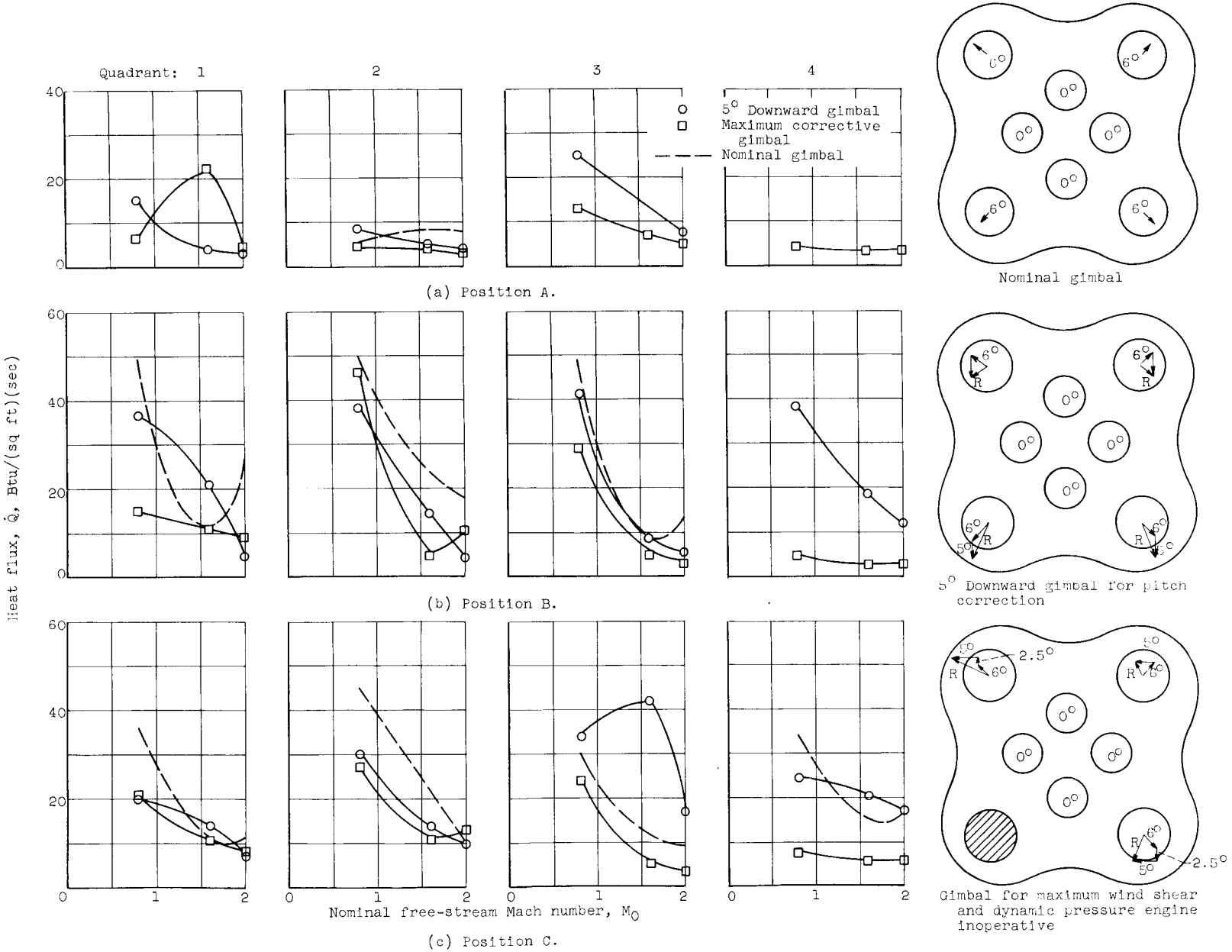

Figure 21. - Effect of downward and inoperative engine corrective gimbal for SA-1 configurations with full-rated turbine-exhaust and exhausterator flows.

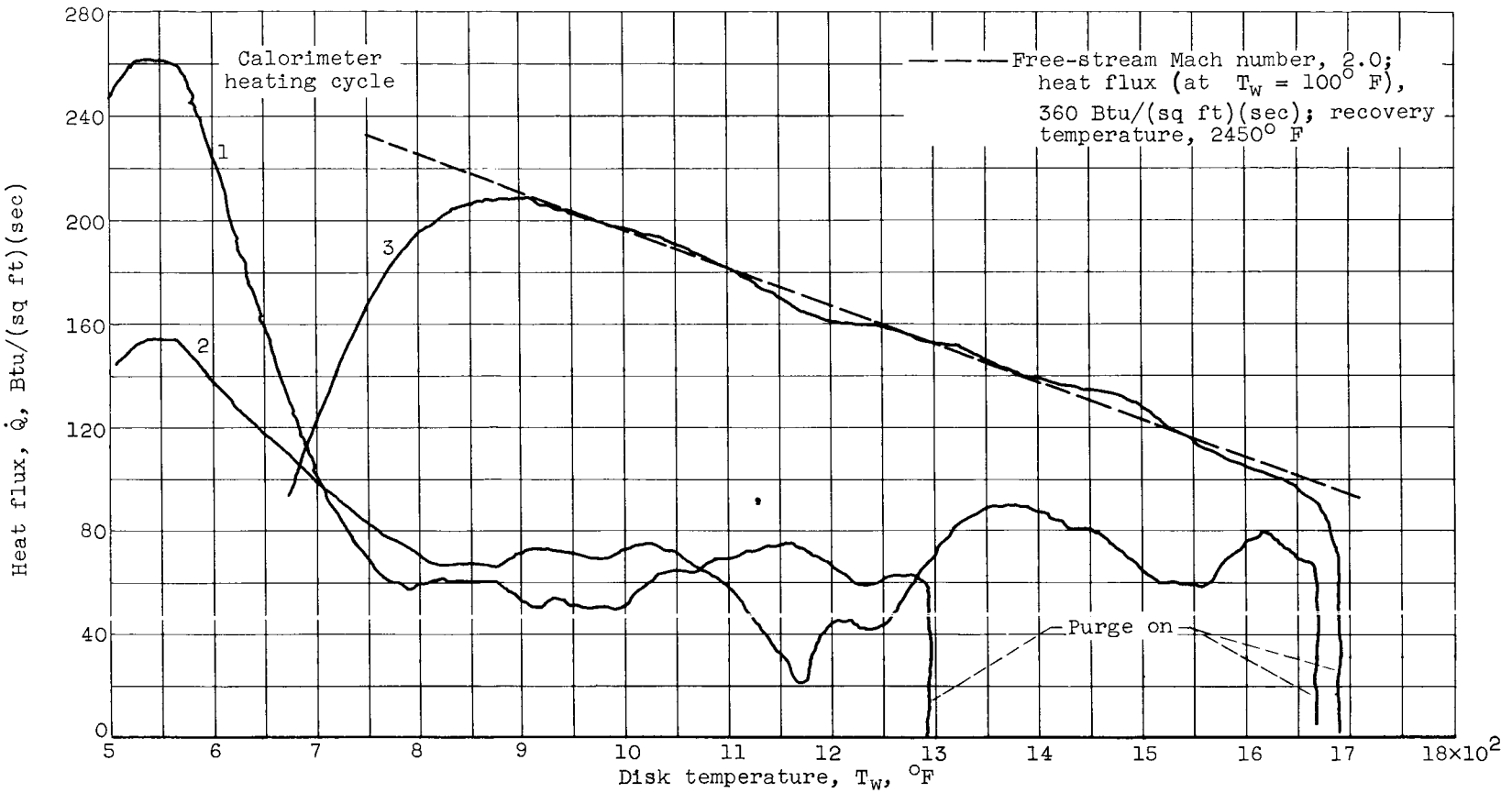

(a) Example of change in center-star calorimeter response with repeated heating cycles during same rocket firing.

Figure 22. - Center-star pressure ratio and heat transfer.

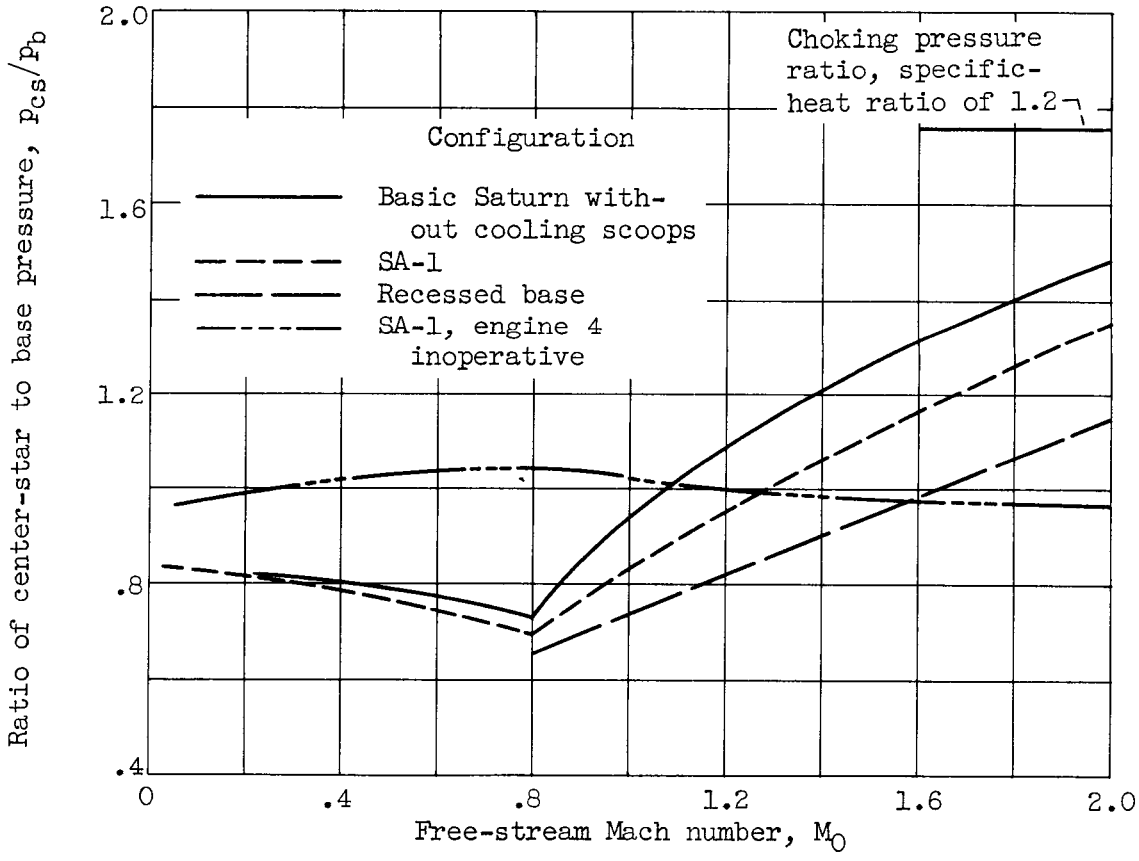

(b) Ratio of center-star to base pressure.

Figure 22. - Center-star pressure ratio and heat transfer.

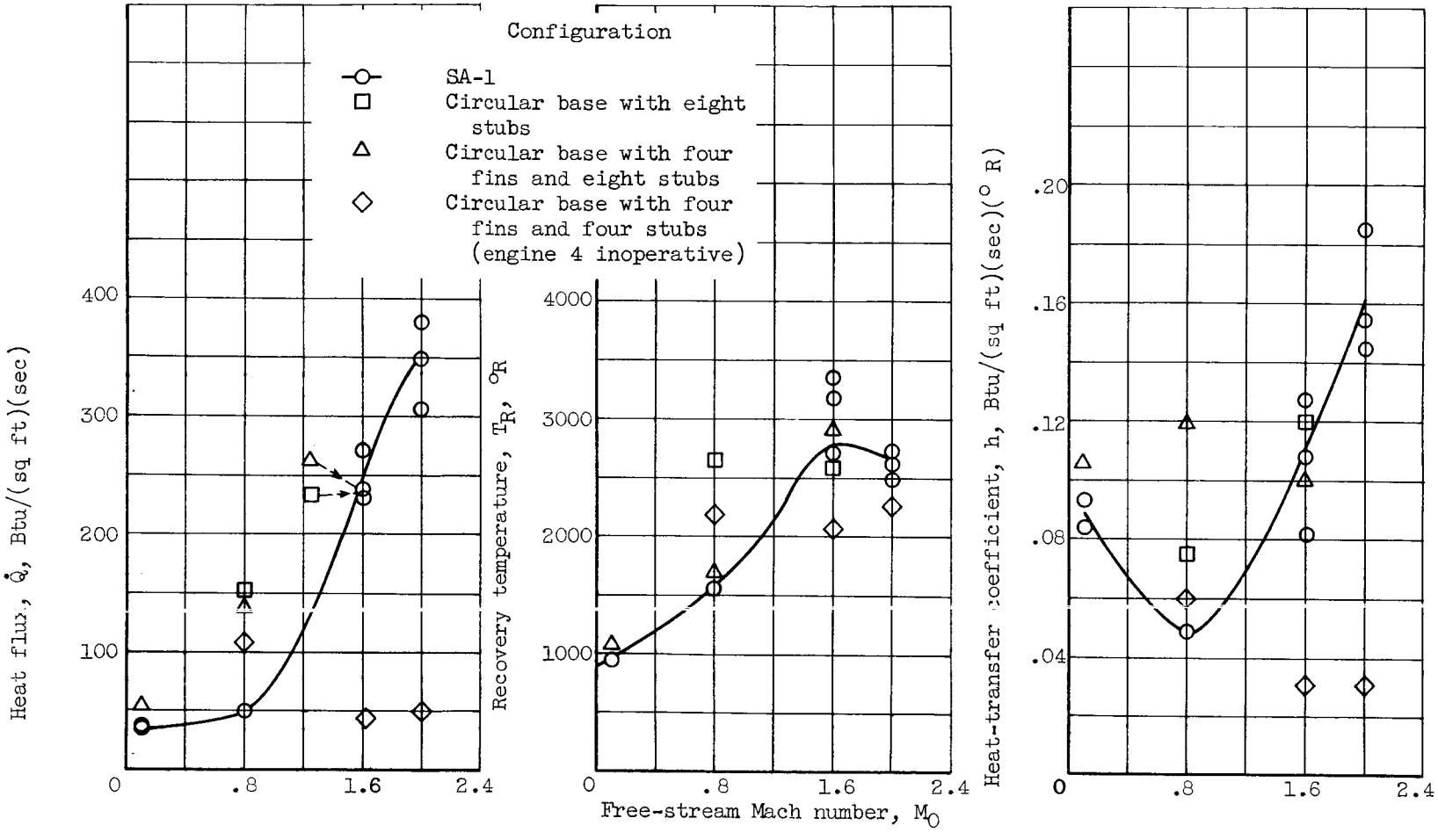

(c) Center-star heat-transfer results. Full-rated turbine-exhaust and exhausterator flow.

Figure 22. - Concluded. Center-star pressure ratio and heat transfer.

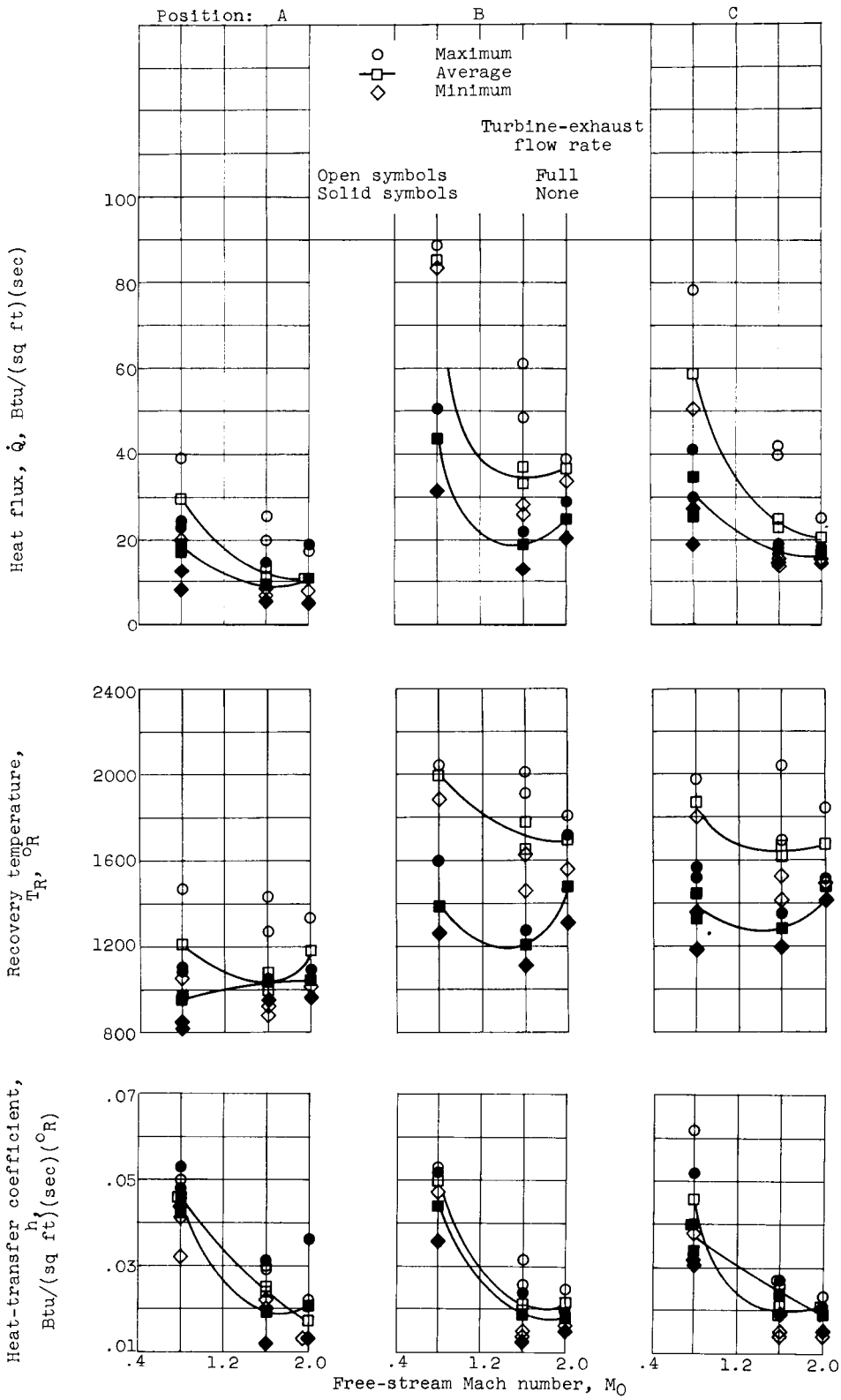

Figure 23. - Basic Saturn configuration without base cooling but with 3/8-inch turbine-exhaust stacks.

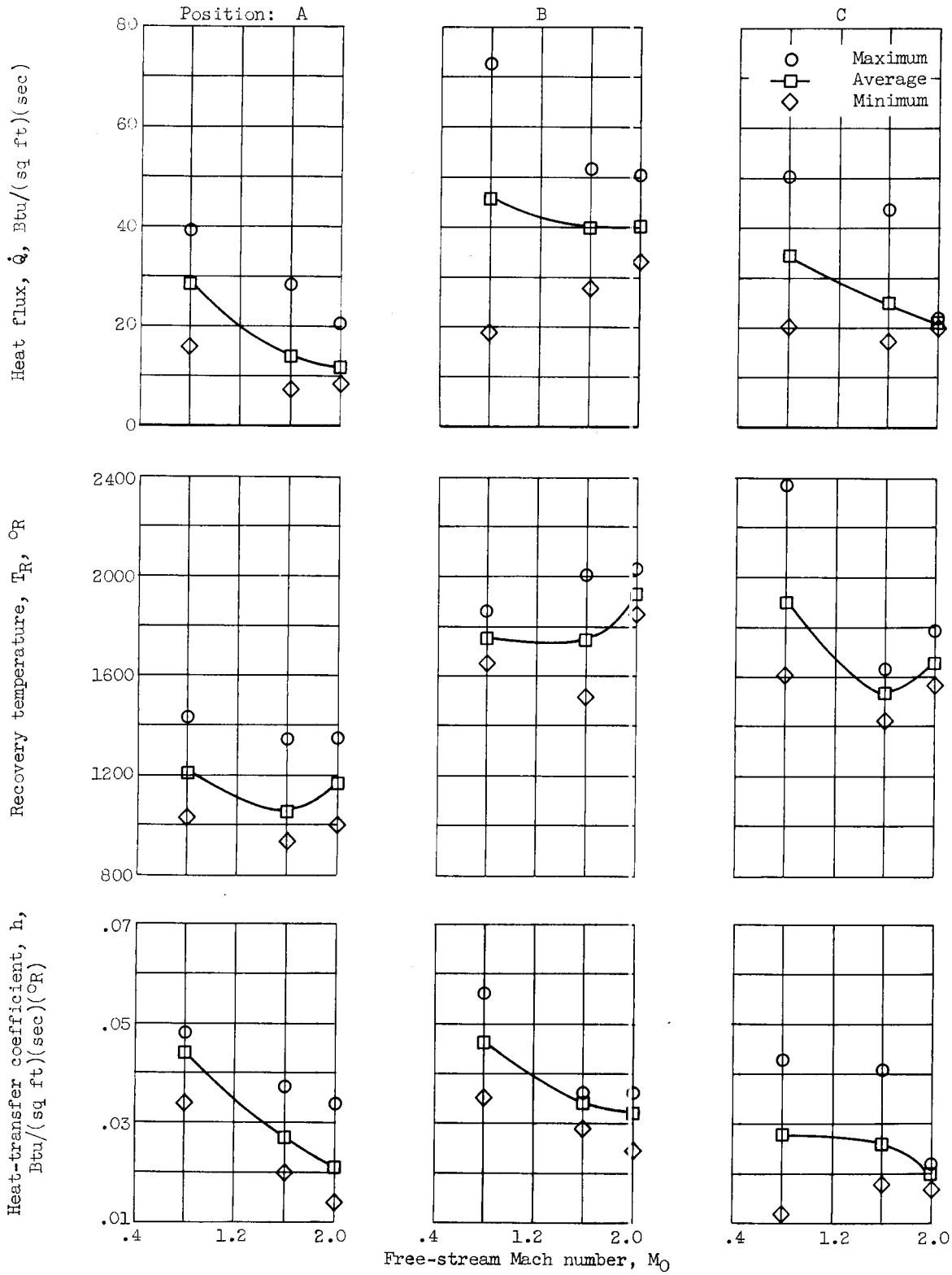

Figure 24. - Basic Saturn configuration without base cooling but with 3/8-inch turbine-exhaust stacks and half-rated turbine-exhaust flow.

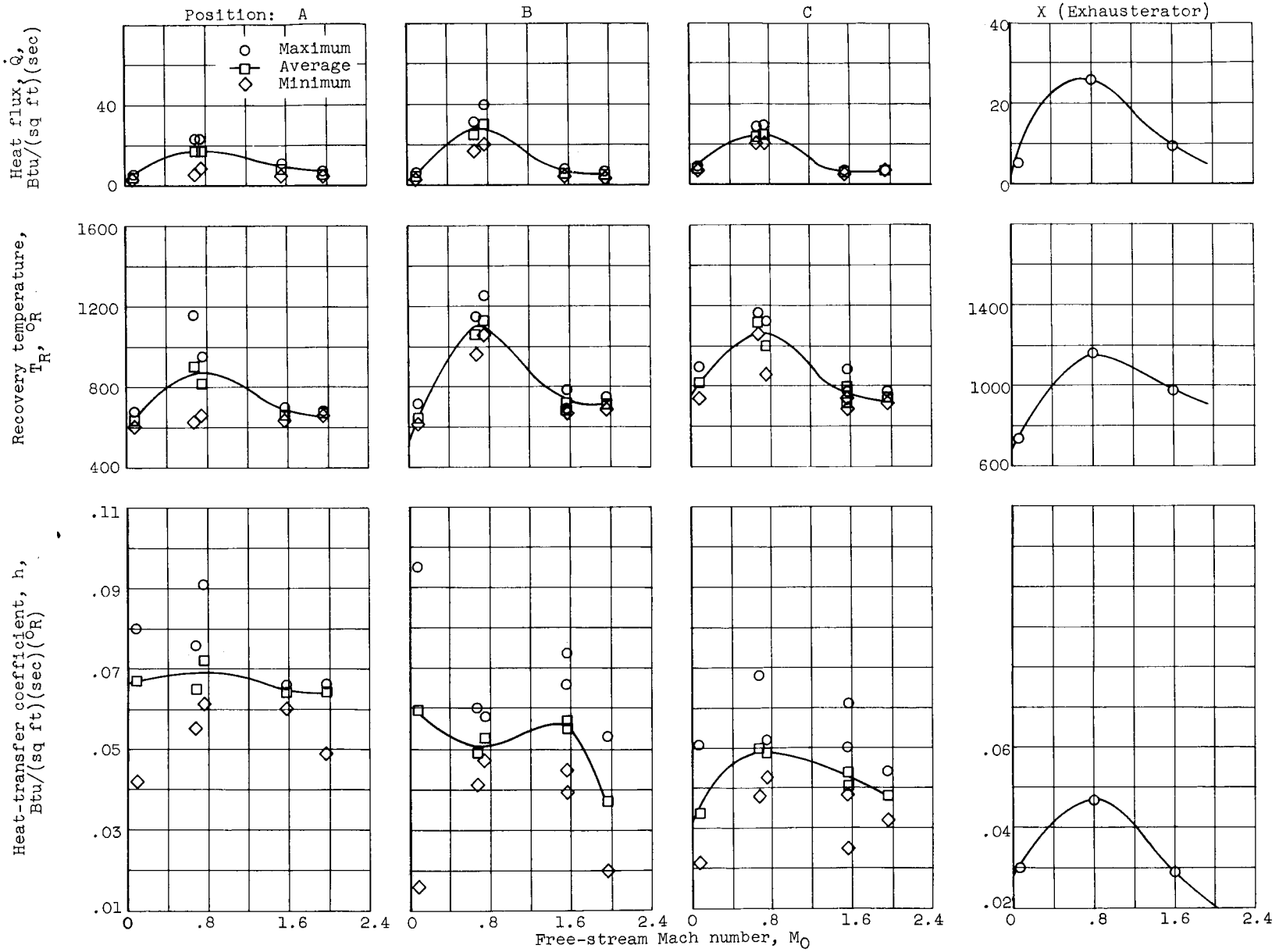

Figure 25. - Basic Saturn configuration with four cooling scoops per shroud, valley flow deflectors, 3/8-inch turbine-exhaust stacks, and no turbine-exhaust flow.

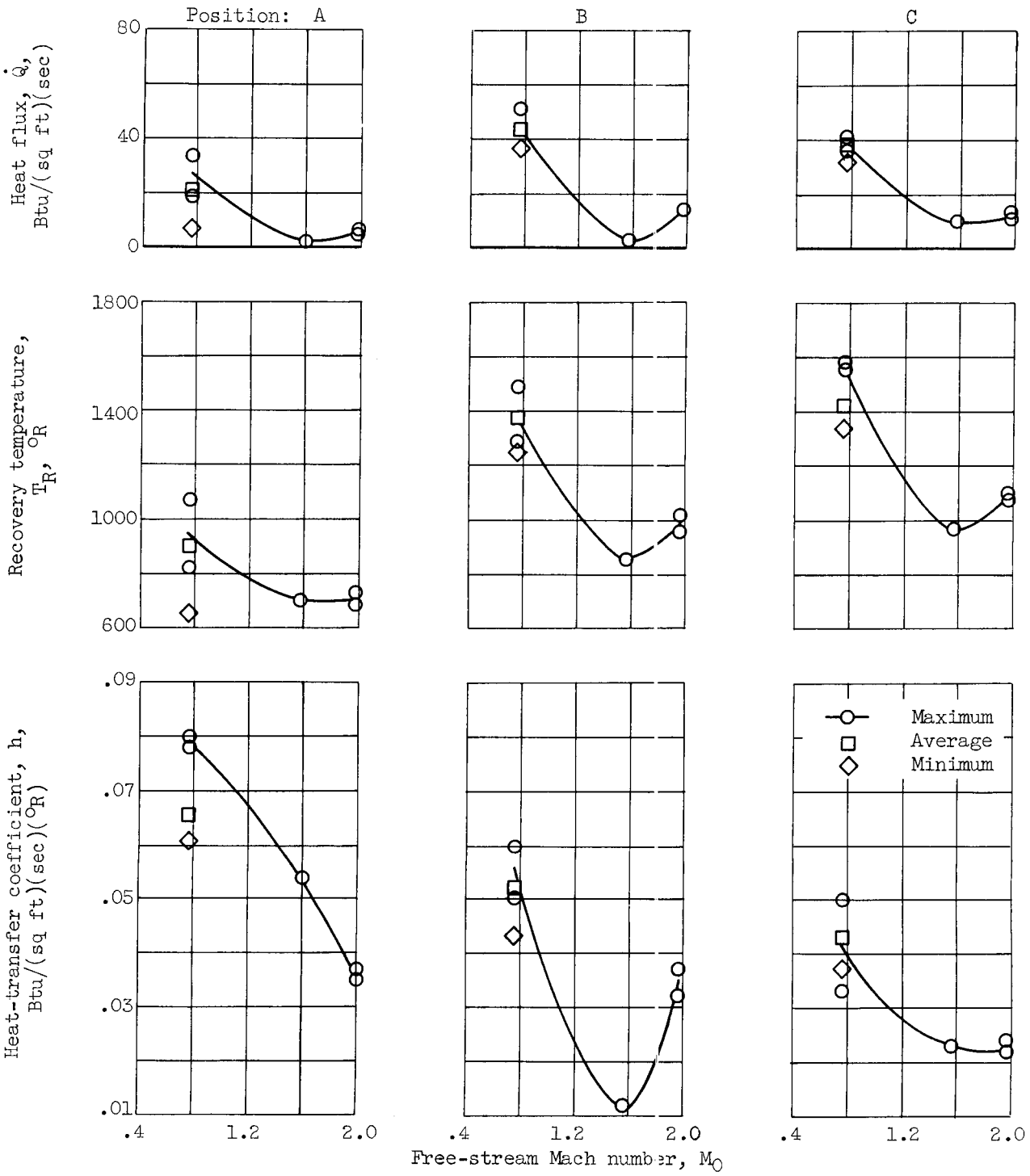

Figure 26. - Basic Saturn configuration with four cooling scoops per shroud, valley flow deflectors, 3/8-inch turbine-exhaust stacks, and half-rated turbine-exhaust flow.

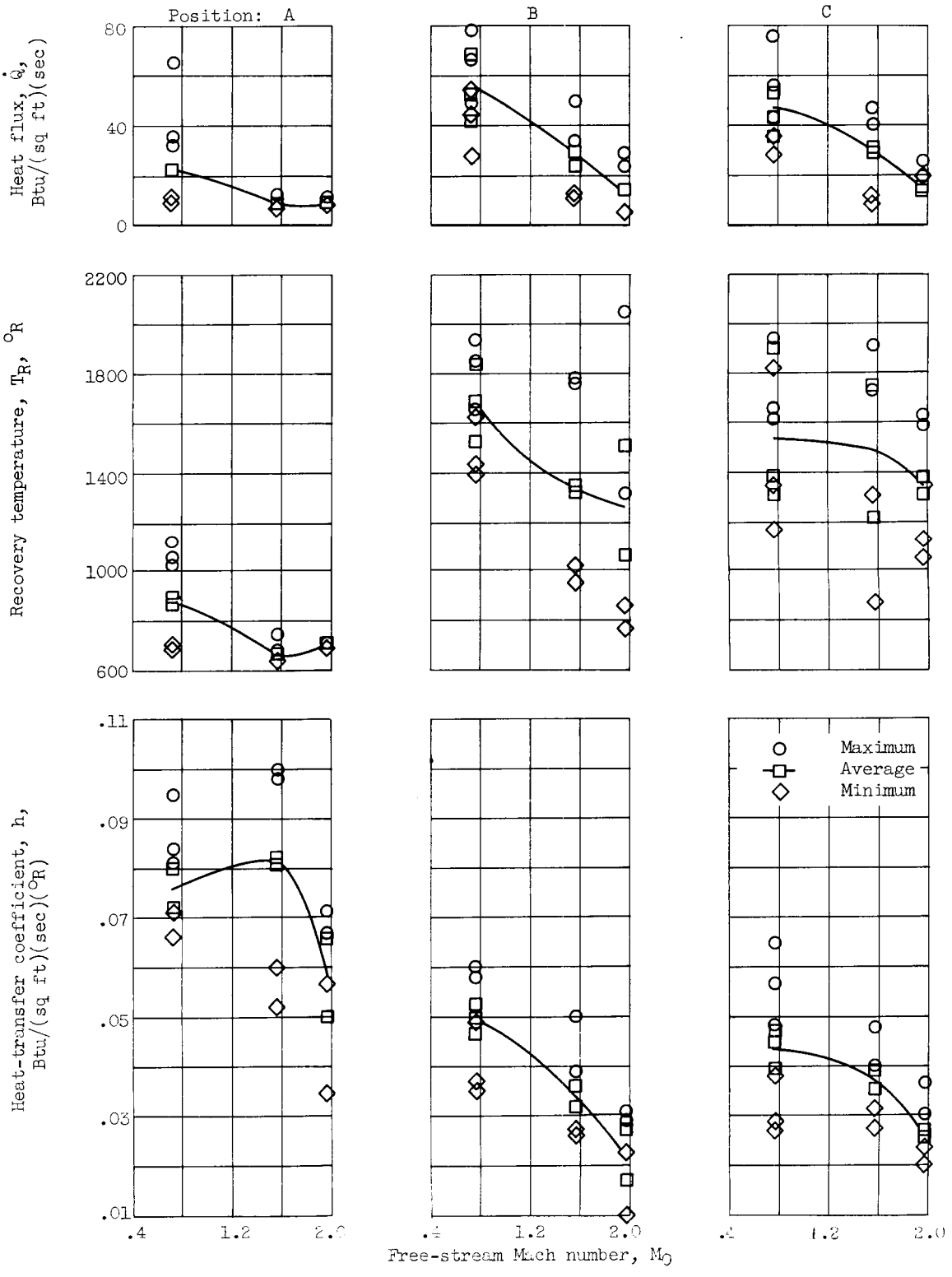

Figure 27. - Basic Saturn configuration with four scoops per shroud, valley flow deflectors, and 1/16-inch turbine-exhaust stacks. Half-rated turbine-exhaust flow.

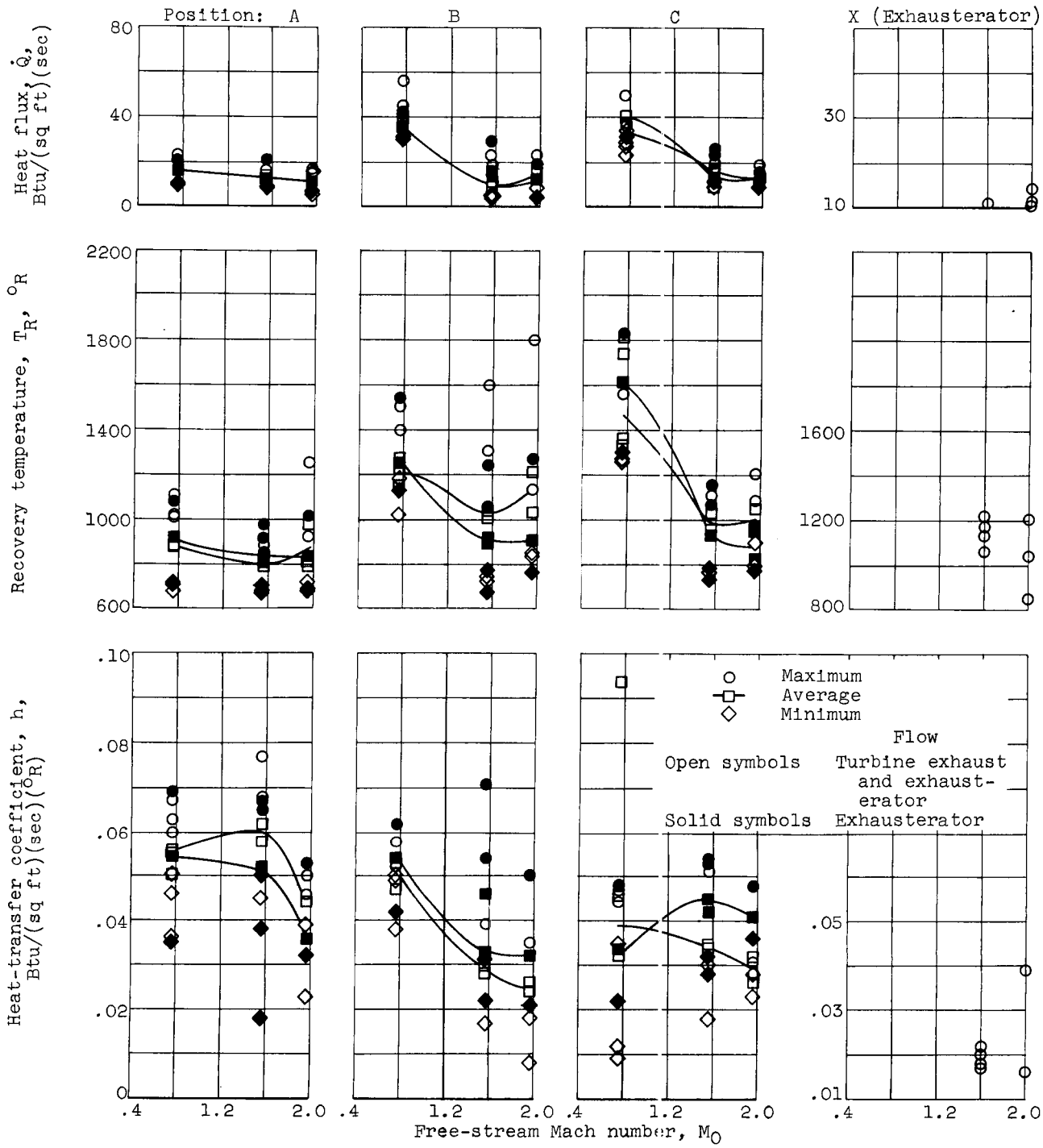

Figure 28. - Basic Saturn configuration with three cooling scoops per shroud, valley flow deflectors, curved turbine-exhaust pipes (SA-1) with Mark I engines. Half-rated flow.

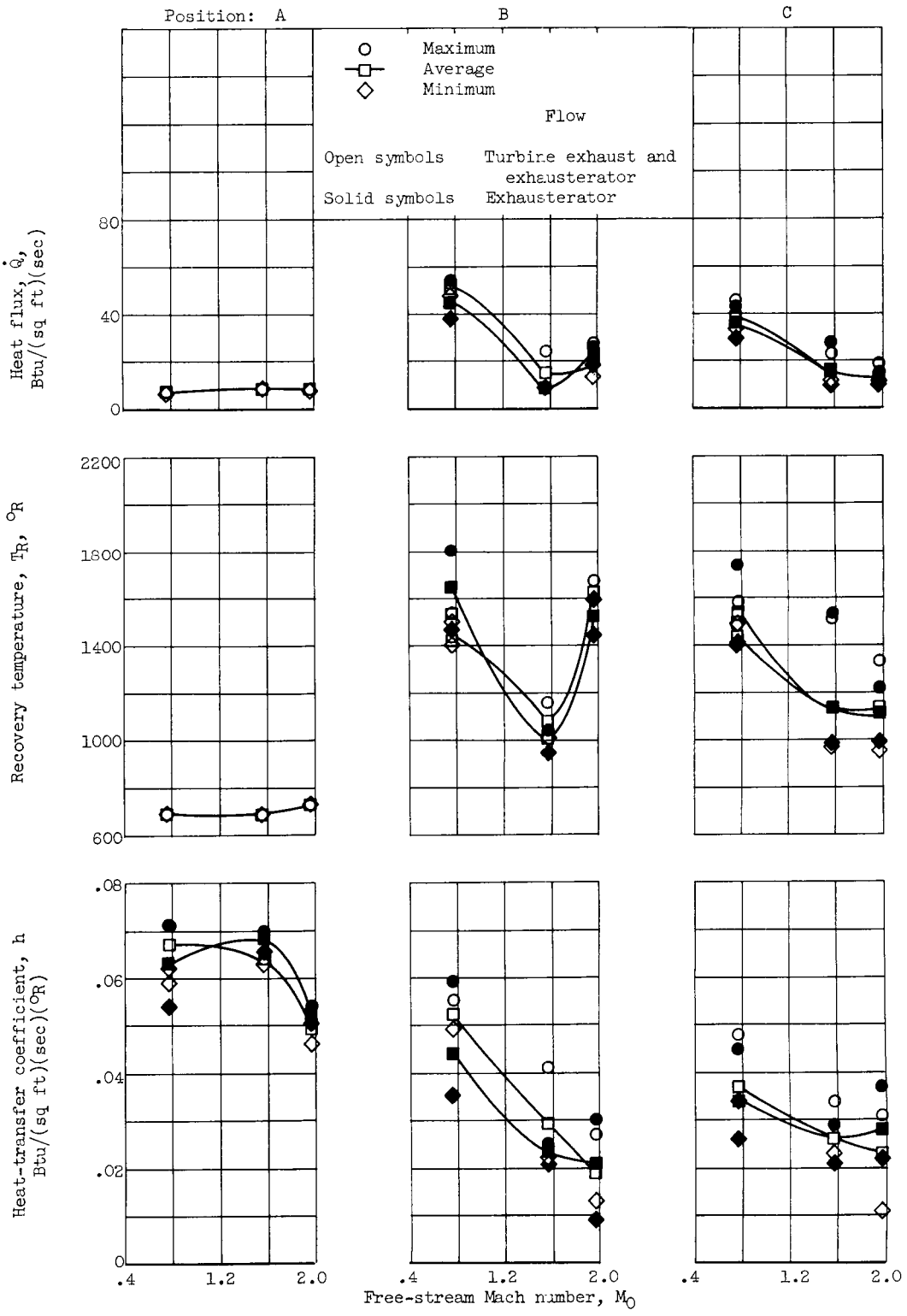

Figure 29. - Basic Saturn configuration with three cooling scoops per shroud, valley flow deflectors, curved turbine-exhaust pipes (SA-1) with Mark II engines. Full-rated flow.

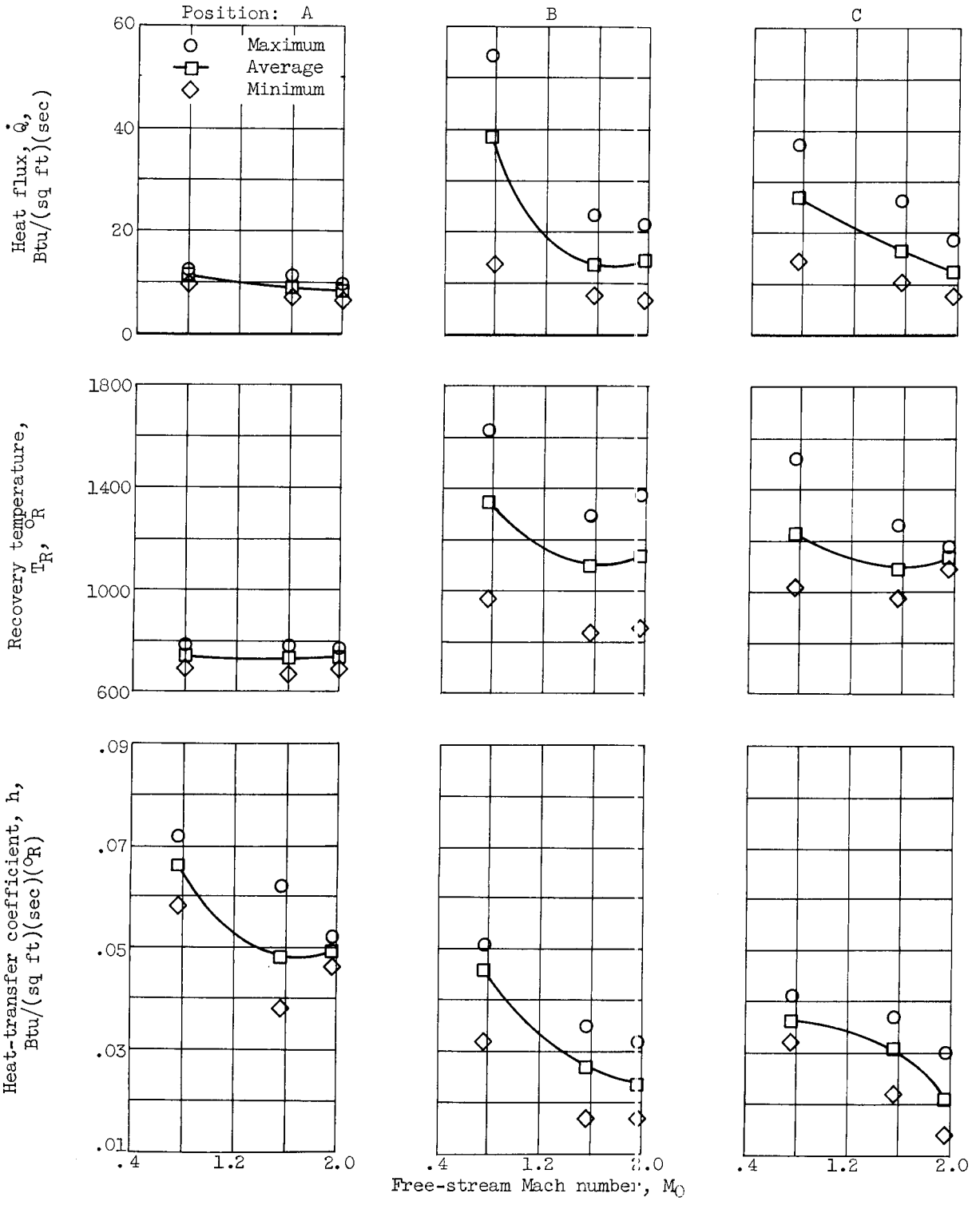

Figure 30. - Basic Saturn configuration with three cooling scoops per shroud, valley flow deflectors, curved turbine-exhaust pipes (SA-1) with Mark II engines. Outboard engine 7 inoperative; full-rated turbine-exhaust and exhausterator flow.

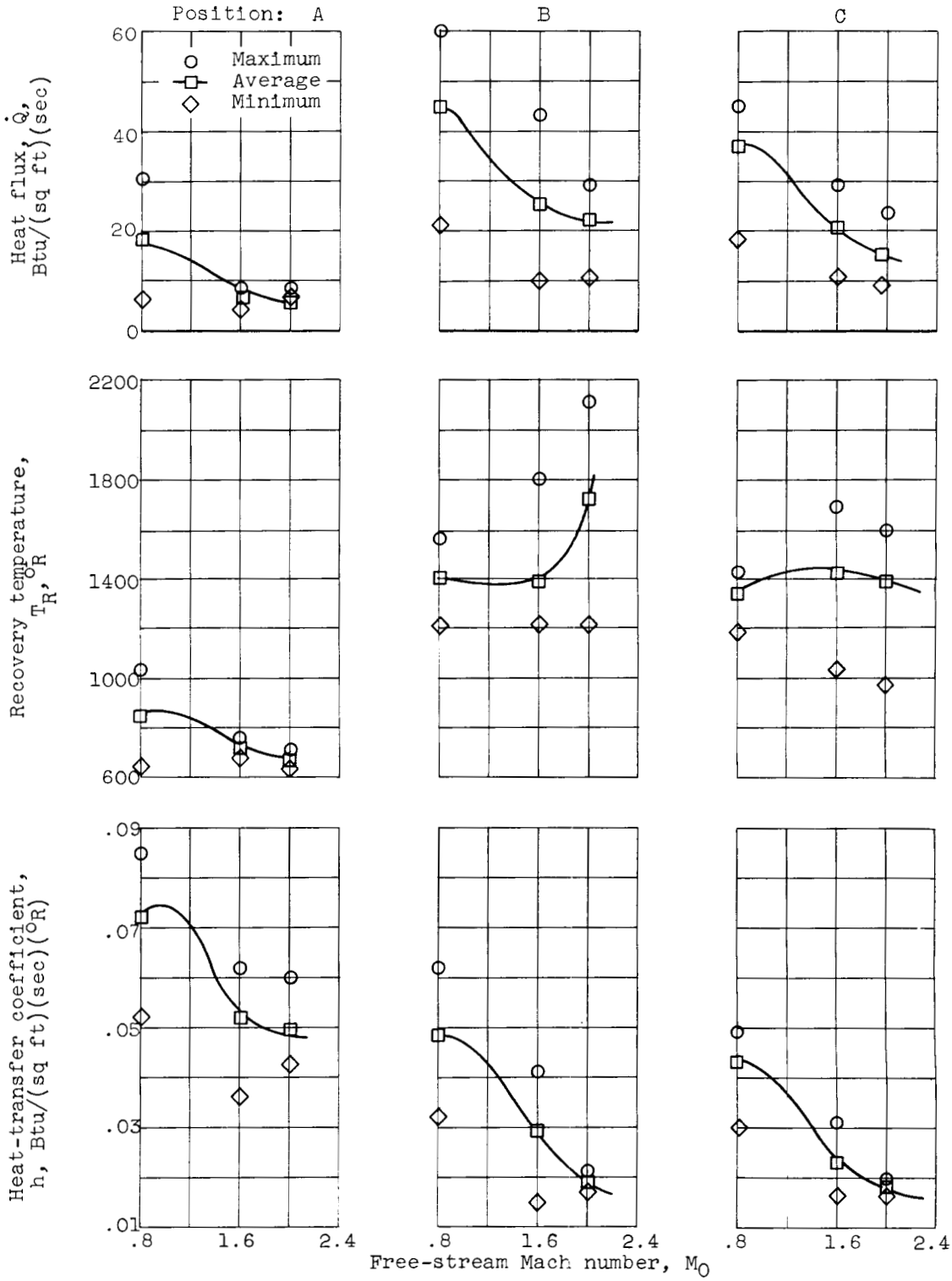

Figure 31. - Basic Saturn configuration with three cooling scoops per shroud, valley flow deflectors, curved turbine-exhaust pipes (SA-1) with Mark II engines. Inboard engine 4 inoperative; full-rated turbine-exhaust and exhausterator flow.

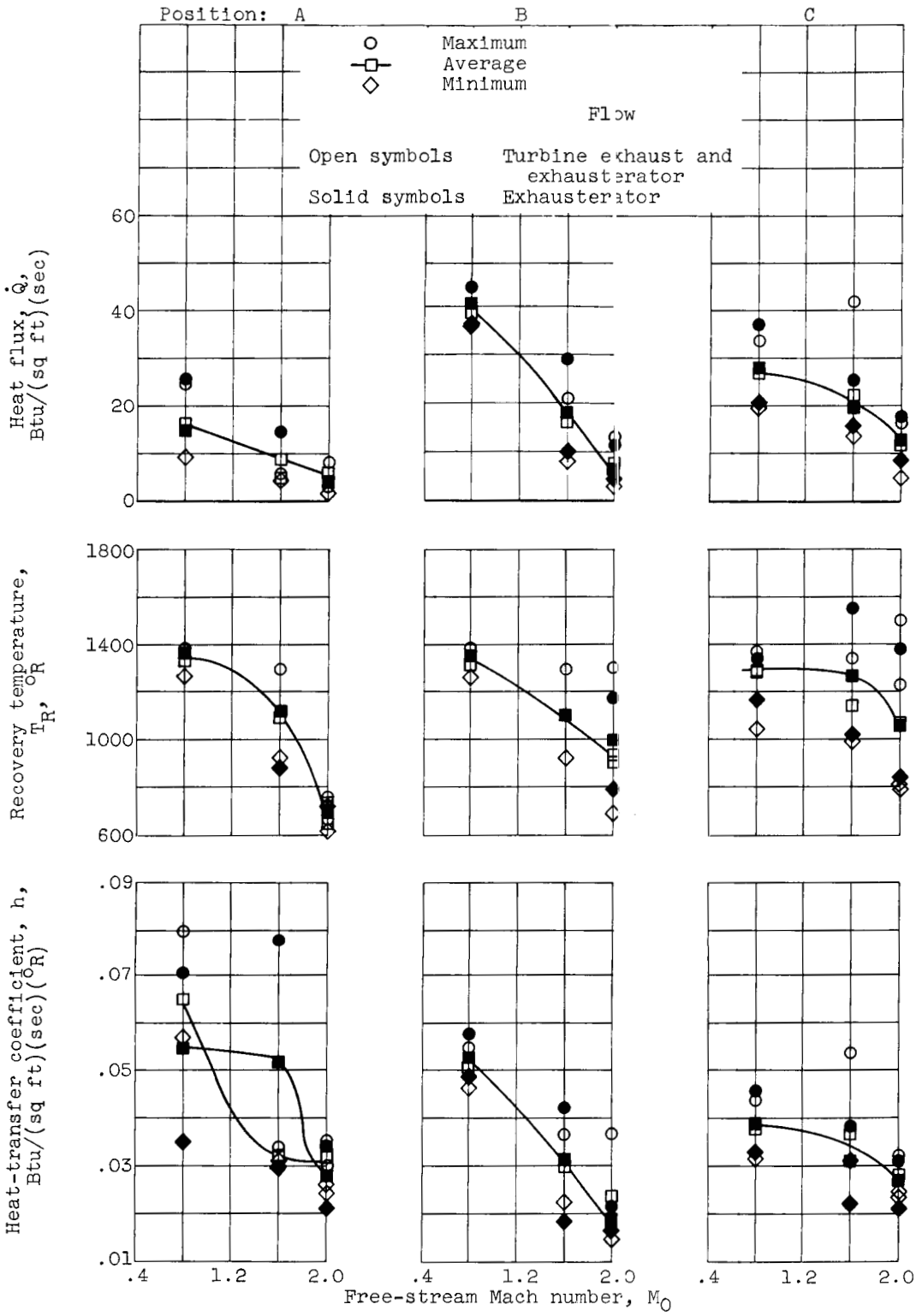

Figure 32. - Basic Saturn configuration with three cooling scoops per shroud, valley flow deflectors, curved turbine-exhaust pipes (SA-1) with Mark II engines. Maximum down gimbal; full-rated flow.

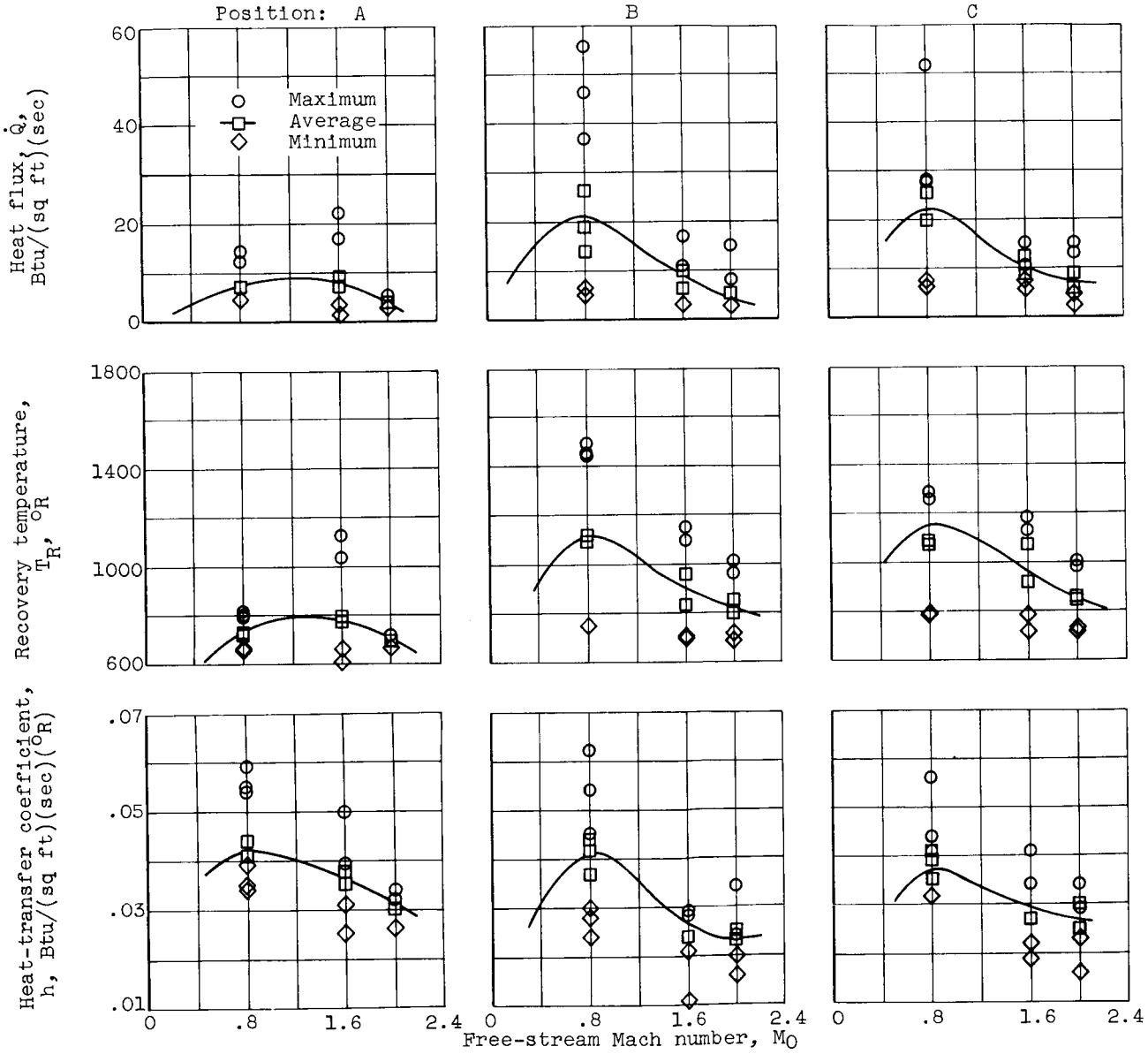

Figure 33. - Basic Saturn configuration with three cooling scoops per shroud, valley flow deflectors, curved turbine-exhaust pipes (SA-1) with Mark II engines. Engine 8 inoperative (corrective gimbal); full-rated turbine-exhaust and exhausterator flow.

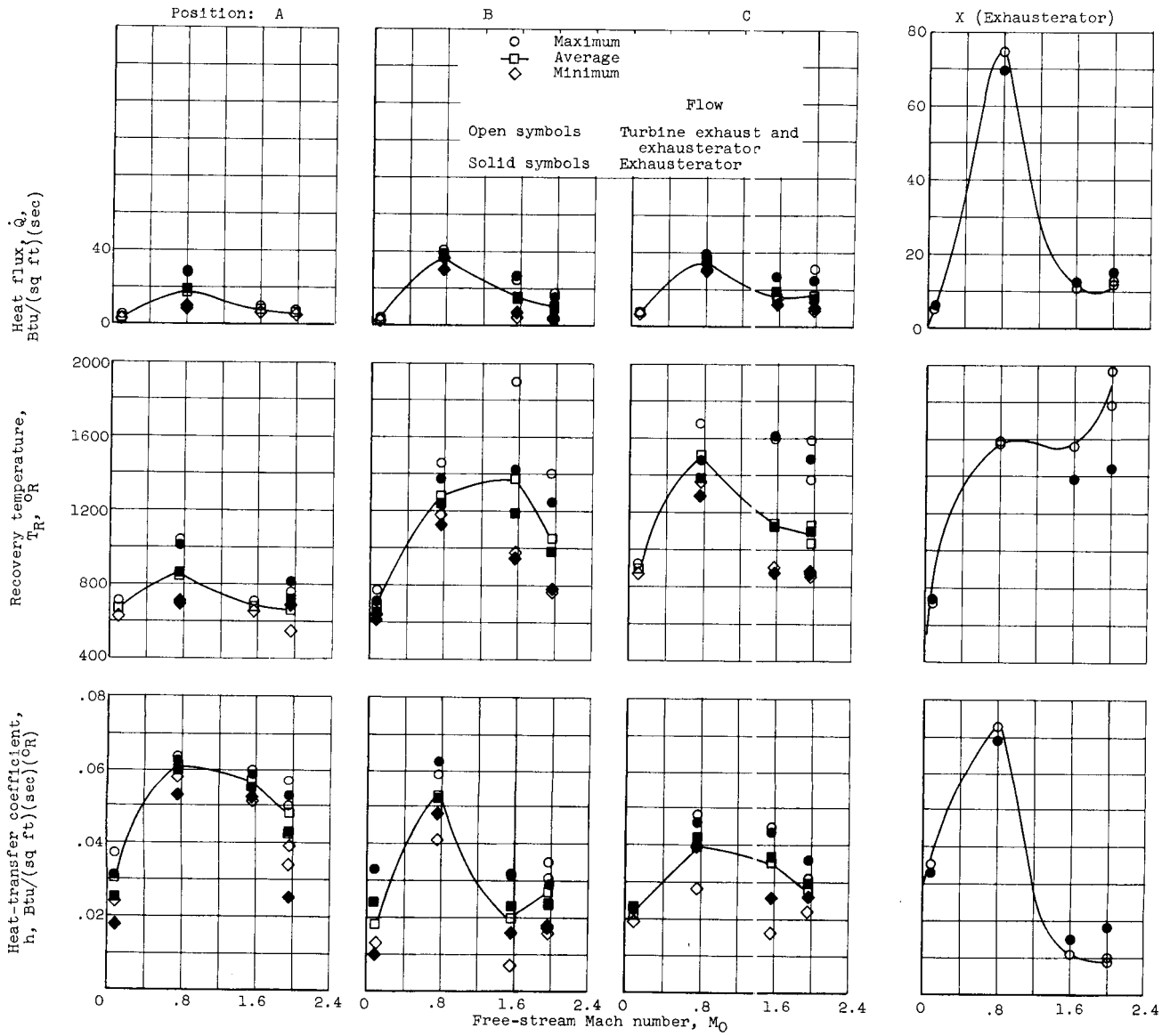

Figure 34. - Basic Saturn configuration with three cooling scoops per shroud, valley flow deflectors, streamlined turbine-exhaust stacks, and half-rated flow.

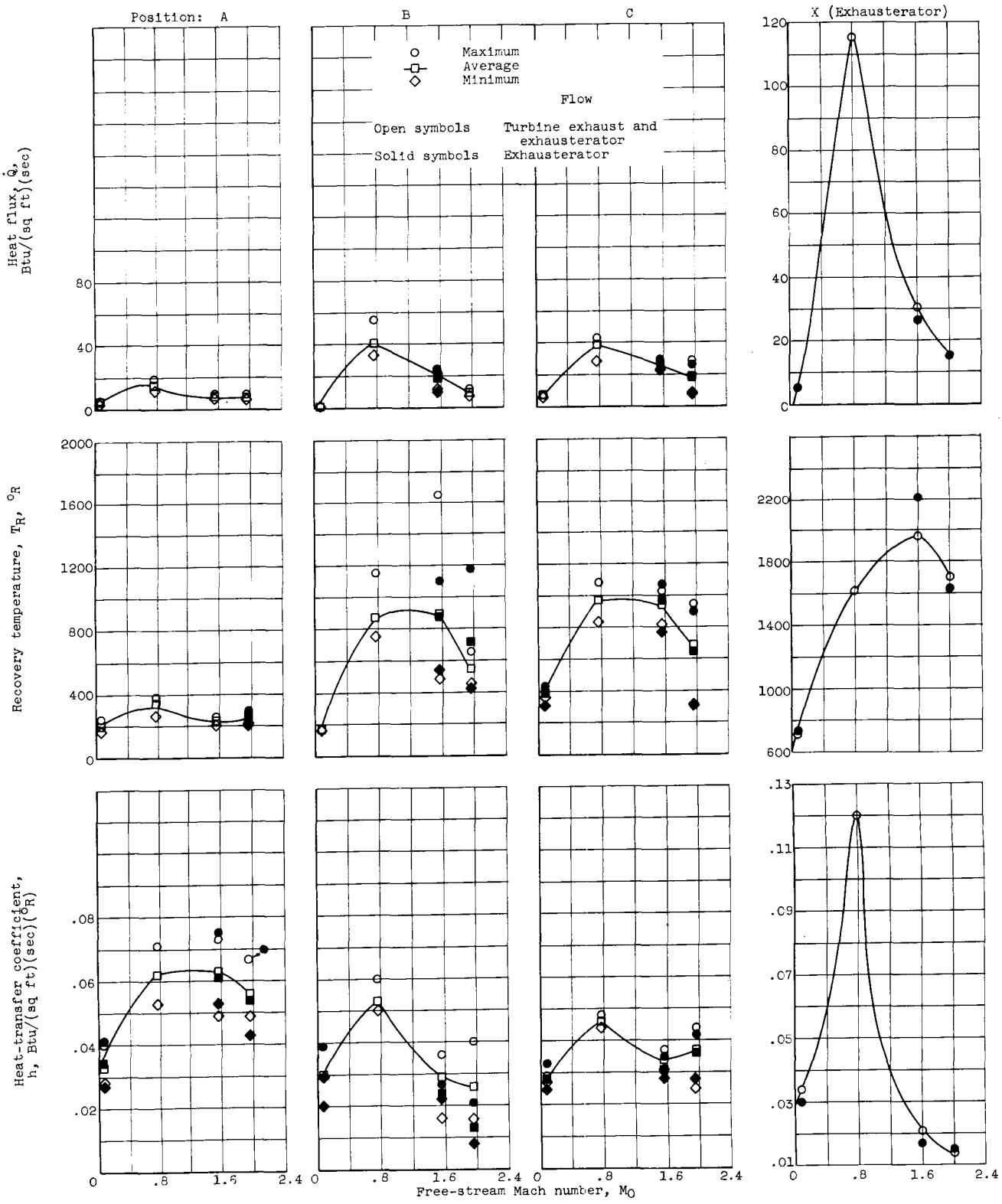

Figure 35. - Basic Saturn configuration with three cooling scoops per shroud, valley flow deflectors, streamlined turbine-exhaust stacks, and full-rated flow.

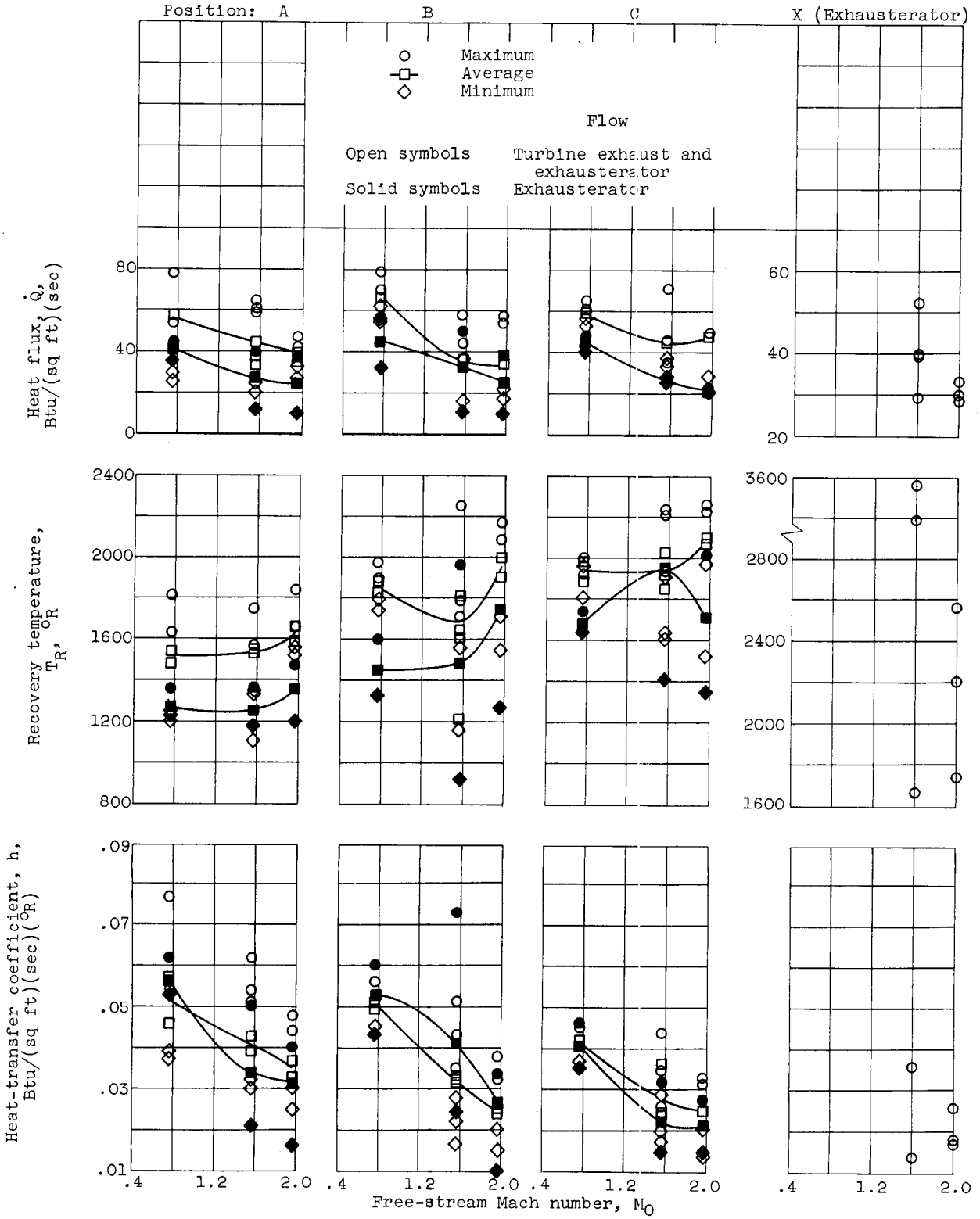

Figure 36. - Basic Saturn configuration without base cooling or outboard engine shrouds but with 3/8-inch turbine-exhaust stacks (flush base) and half-rated flow.

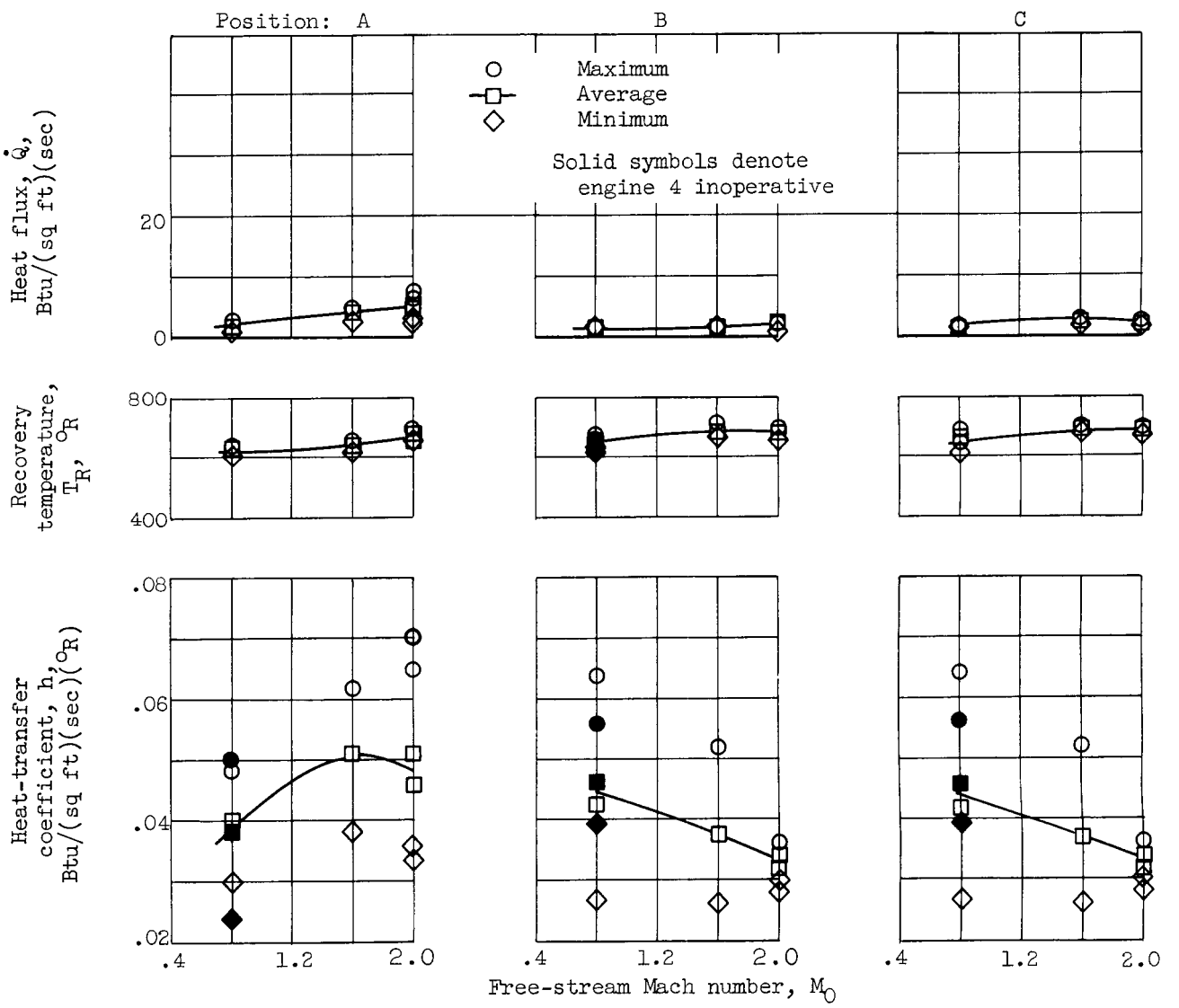

Figure 37. - Recessed-base configuration with shroud and valley cooling scoops, 5/8-inch turbine-exhaust stacks, Mark II engines, and full-rated turbine-exhaust and exhausterator flow.

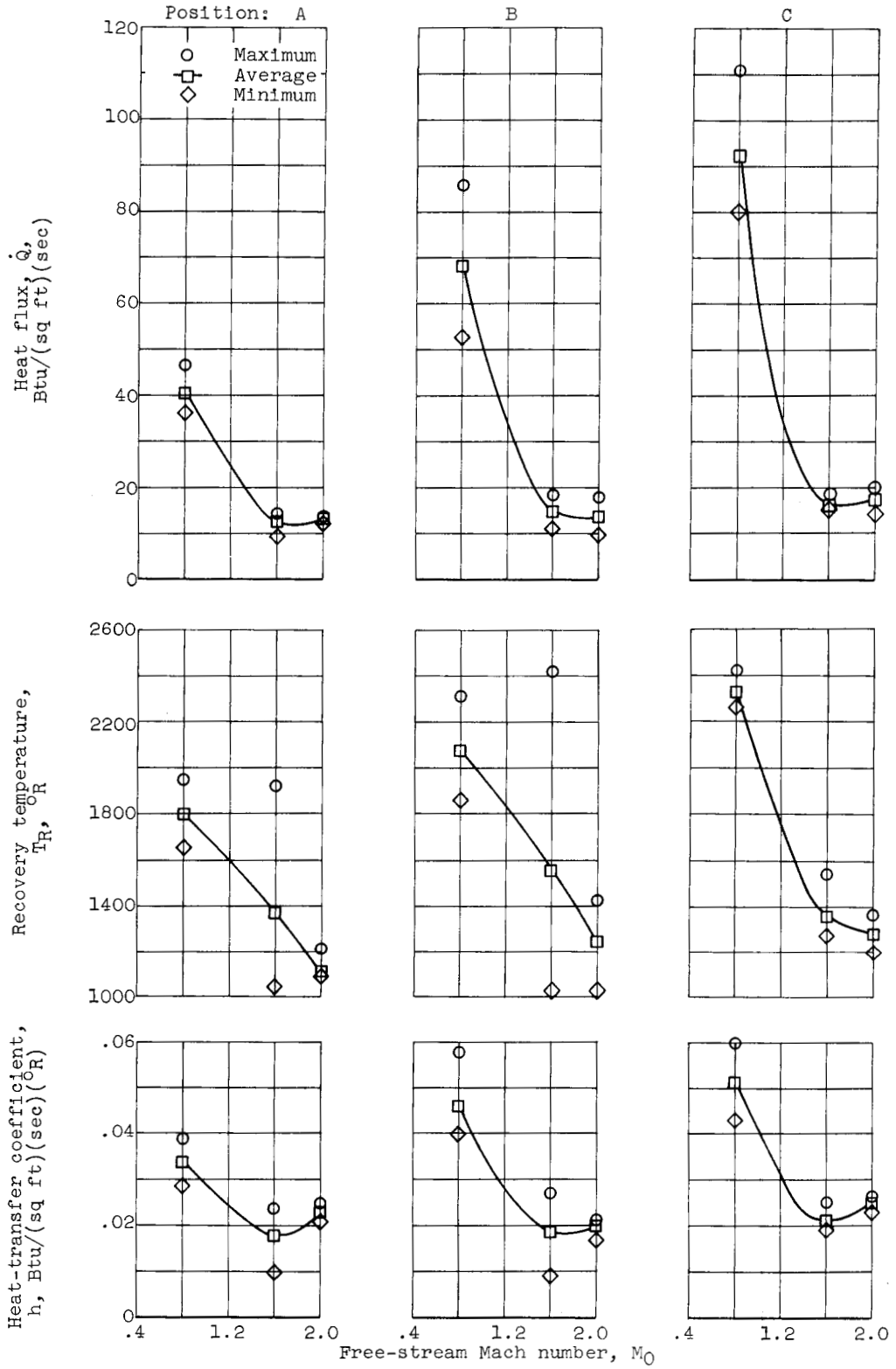

Figure 38. - Circular-base configuration with four-fin, four-stub stabilizer arrangement, streamlined turbine-exhaust stacks, and streamlined upper-stage hydrogen vents on stubs. Full rated turbine-exhaust and exhausterator flow.

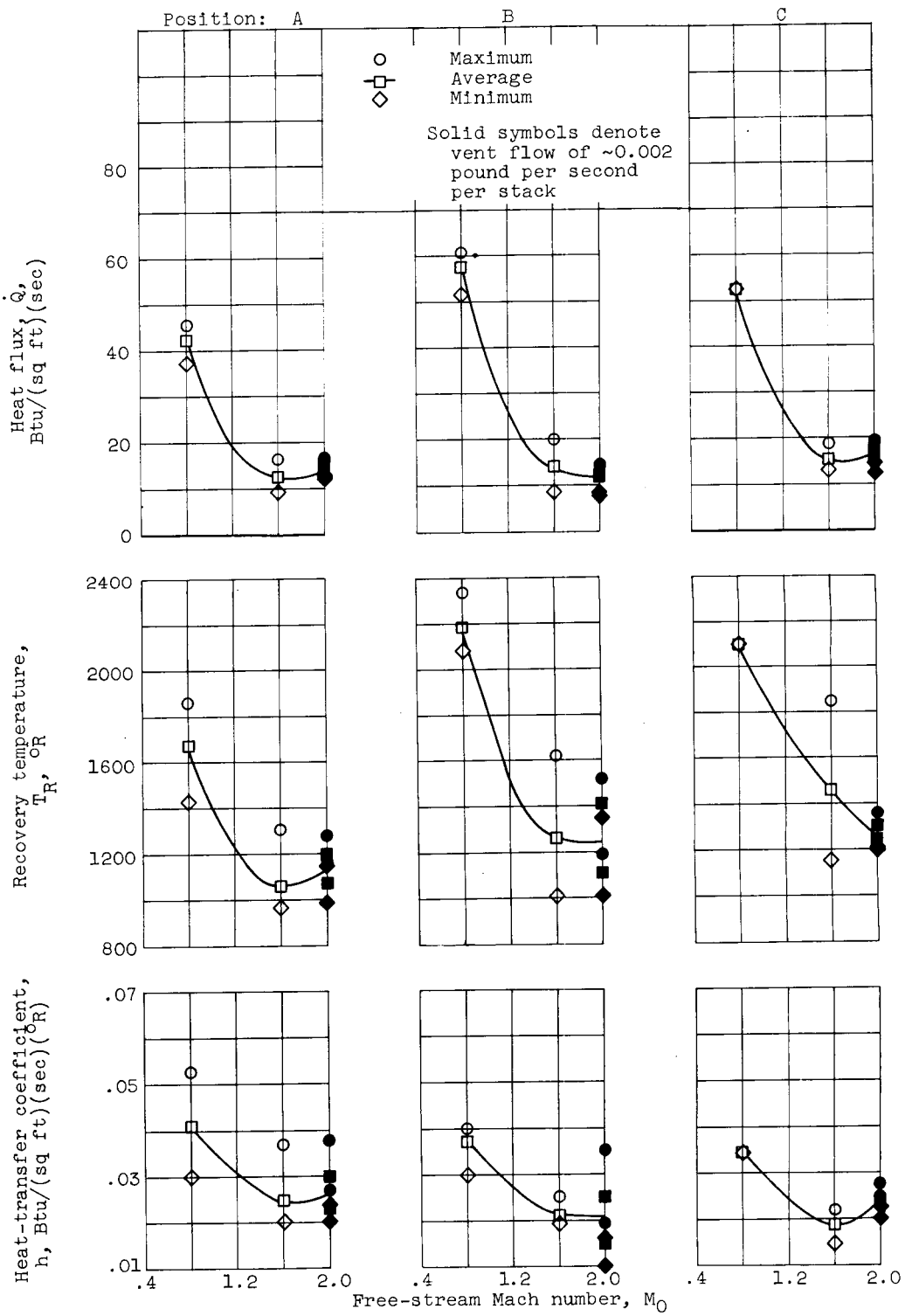

Figure 39. - Circular-base configuration with eight-stub stabilizer arrangement, streamlined turbine-exhaust stacks, and streamlined upper-stage vents on stubs. Full-rated turbine exhaust and exhaust-erator flow.

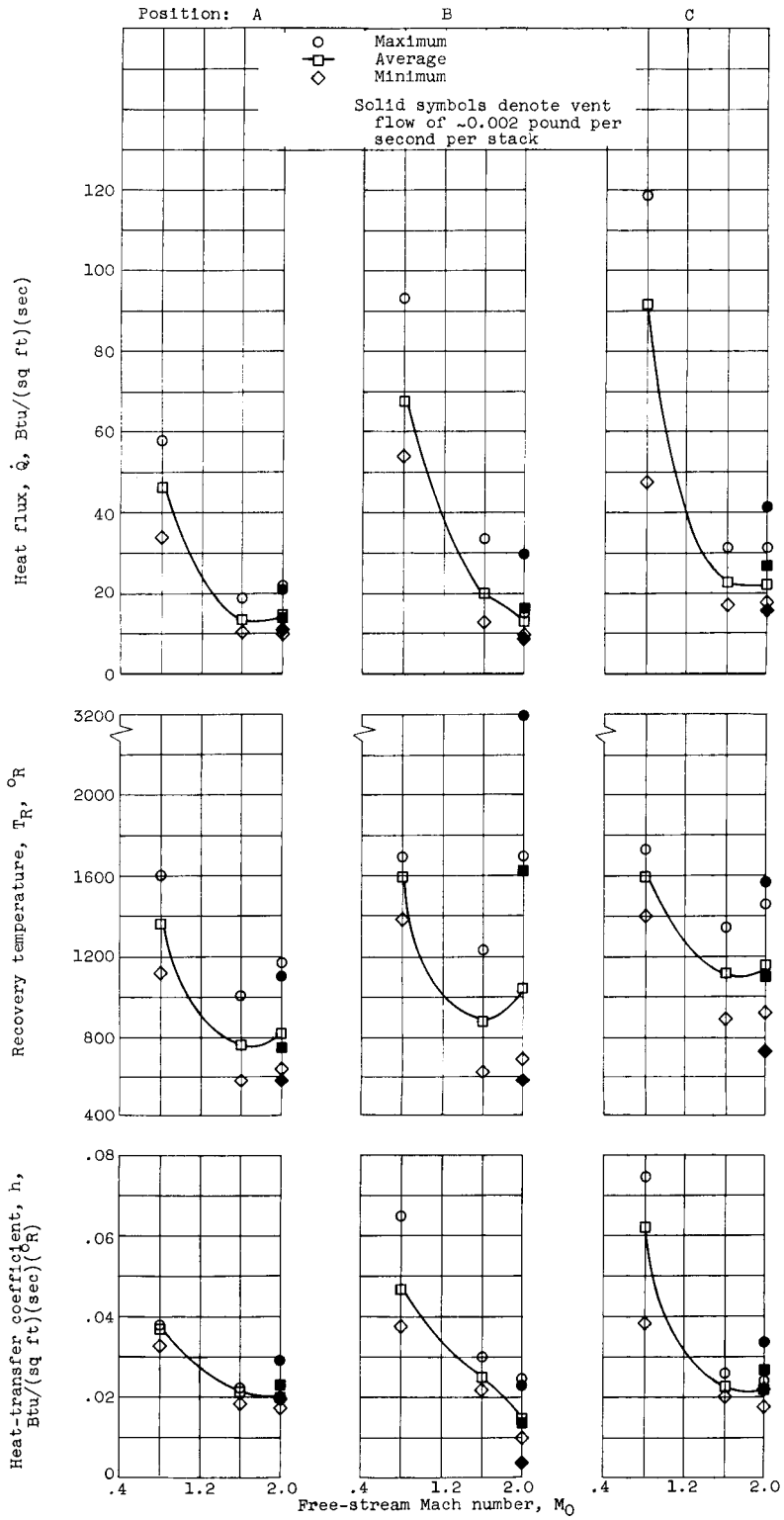

Figure 40. - Circular-base configuration with four-fin, four-stub stabilizer arrangement, streamlined turbine-exhaust stacks, streamlined upper-stage hydrogen vents on stubs, and inboard engine 4 inoperative. Full-rated turbine-exhaust and exhaust-erator flow.